

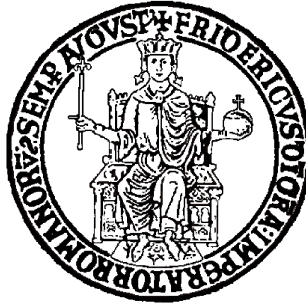


**PON** Ricerca e  
2014- 2020 **Innovazione**



Ministero dell'Istruzione, dell'Università e della Ricerca

UNIVERSITÀ DEGLI STUDI DI NAPOLI FEDERICO II



PhD thesis in Industrial Product and Process Engineering

XXX cycle

***“Applications of gH625 cell-penetrating peptide  
in advanced engineered materials”***

**Pietro Melone**

**Supervisor:**

Prof. Ing. Paolo Antonio Netti

**Coordinator:**

Prof. Ing. Giuseppe Mensitieri

2014-2017



**APPLICATIONS OF gH625  
CELL-PENETRATING PEPTIDE  
IN ADVANCED ENGINEERED MATERIALS**

**A THESIS SUBMITTED IN PARTIAL FULFILLMENT  
OF THE REQUIREMENT FOR THE DEGREE  
OF DOCTOR OF PHILOSOPHY IN**

**INDUSTRIAL PRODUCTS AND PROCESS ENGINEERING**

**AUTHOR**

Melone Pietro

**SUPERVISOR**

Prof. Dr. Paolo A. Netti

**COORDINATOR**

Prof. Dr. Giuseppe Mensitieri



# *TABLE OF CONTENTS*

---

|  |           |
|--|-----------|
| LIST OF FIGURES, SCHEMES AND TABLES  | v         |
| ABSTRACT   | ix        |
| <b>CHAPTER 1</b>   | <b>1</b>  |
| <i>Introduction</i>  |           |
| <b>1.1 CELL-PENETRATING PEPTIDES (CPPS)</b>  | <b>2</b>  |
| <b>1.2 CLASSIFICATION OF CPPS</b>  | <b>3</b>  |
| 1.2.1 CATIONIC CPPS  | 5         |
| 1.2.2 AMPHIPATHIC CPPS   | 6         |
| 1.2.3 HYDROPHOBIC CPPS   | 7         |
| 1.2.4 OTHER CPPS SUBGROUPS   | 7         |
| <b>1.3 CELLULAR INTERNALIZATION MECHANISMS OF CPPS</b>                                     | <b>8</b>  |
| 1.3.1 DIRECT TRANSLOCATION THROUGH THE MEMBRANE BILAYER                                    | 9         |
| 1.3.2 ENDOCYTOSIS-MEDIATE UPTAKE   | 10        |
| 1.3.3 SIGNIFICANT FACTORS THAT INFLUENCE THE MECHANISM OF CPP UPTAKE                       | 11        |
| <b>1.4 UPTAKE PATHWAYS AND ENDOSOMAL ESCAPE MECHANISMS OF CPPS AND CPP-CARGO COMPLEXES</b> | <b>11</b> |
| <b>1.5 BIOMEDICAL AND THERAPEUTIC APPLICATIONS OF CPP</b>                                  | <b>13</b> |
| 1.5.1 EXPLOITING THE SYNERGISTIC EFFECTS OF TARGETING LIGANDS AND CPPS                     | 16        |
| 1.5.2 FUTURE PROSPECTS OF CPPS   | 17        |
| <b>1.6 A CASE STUDY: THE GH625 CELL-PENETRATING PEPTIDE</b>                                | <b>18</b> |
| 1.6.1 GENERAL DESCRIPTION AND MEMBRANE INTERACTIONS  | 19        |
| 1.6.2 DRUG DELIVERY APPLICATION  | 20        |
| 1.6.3 DELIVERY ACROSS THE BLOOD-BRAIN BARRIER  | 22        |
| <b>1.7 AIM AND OUTLINE OF THE THESIS</b>   | <b>23</b> |
| <b>1.8 REFERENCES</b>  | <b>25</b> |

***Substrate-mediate gene delivery platform  
based on functionalized PEI/DNA polyplexes***

|            |  |    |
|------------|--|----|
| <b>2.1</b> | <b>INTRODUCTION</b>  | 38 |
| <b>2.2</b> | <b>EXPERIMENTAL SECTION</b>  | 41 |
|            | 2.2.1 MATERIALS  | 41 |
|            | 2.2.2 AMPLIFICATION AND PURIFICATION OF PLASMID DNA                          | 41 |
|            | 2.2.3 SYNTHESIS OF PEPTIDE   | 42 |
|            | 2.2.4 SYNTHESIS GH625-PEG-PEI CONJUGATE                                      | 43 |
|            | 2.2.5 POLYPLEXES PREPARATION   | 44 |
|            | 2.2.6 CHARACTERIZATION OF DNA COMPLEXES                                      | 44 |
|            | 2.2.7 MODIFICATION OF GLASS SUBSTRATES                                       | 45 |
|            | 2.2.8 WATER CONTACT ANGLE  | 46 |
|            | 2.2.9 BINDING OF PEGYLATED COMPLEXES TO MODIFIED<br>GLASS SUBSTRATE          | 46 |
|            | 2.2.10 COMPLEXES ADSORPTION ON GLASS SUBSTRATES                              | 47 |
|            | 2.2.11 CHARACTERIZATION OF SUBSTRATES  | 48 |
|            | 2.2.12 TRANSFECTION AND CYTOTOXICITY STUDIES                                 | 48 |
|            | 2.2.13 STATISTICAL ANALYSIS  | 49 |
| <b>2.3</b> | <b>RESULTS AND DISCUSSION</b>  | 50 |
|            | 2.3.1 SYNTHESIS AND CHARACTERIZATION OF GH625-PEG-PEI VECTOR                 | 50 |
|            | 2.3.2 POLYPLEXES PHYSICOCHEMICAL AND MORPHOLOGICAL<br>CHARACTERIZATION       | 52 |
|            | 2.3.3 MODIFICATIONS OF GLASS SUBSTRATE AND POLYPLEXES<br>COVALENT ATTACHMENT | 54 |
|            | 2.3.4 SUBSTRATES CHARACTERIZATION  | 57 |
|            | 2.3.5 CELL VIABILITY AND TRANSFECTION STUDIES                                | 58 |
| <b>2.4</b> | <b>CONCLUSIONS</b>   | 62 |
| <b>2.5</b> | <b>REFERENCES</b>  | 63 |

***Size and gH625-functionalization affect  
cytosolic delivery of platinum nanoparticles***

|            |                             |    |
|------------|-----------------------------|----|
| <b>3.1</b> | <b>INTRODUCTION</b>         | 70 |
| <b>3.2</b> | <b>EXPERIMENTAL SECTION</b> | 72 |
|            | 3.2.1 MATERIALS             | 72 |

|            |  |           |
|------------|--|-----------|
| 3.2.2      | PLATINUM NANOPARTICLE SYNTHESIS AND CHARACTERIZATION                     | 72        |
| 3.2.3      | SYNTHESIS OF RHODAMINE-GH625-CYS PEPTIDE                                 | 72        |
| 3.2.4      | PEPTIDE CONJUGATION TO PTNPs   | 73        |
| 3.2.5      | CELL CULTURE   | 74        |
| 3.2.6      | CELL UPTAKE EXPERIMENTS  | 74        |
| 3.2.7      | TRANSMISSION ELECTRON MICROSCOPY   | 75        |
| 3.2.8      | DCF ASSAY  | 75        |
| <b>3.3</b> | <b>RESULTS AND DISCUSSION</b>  | <b>76</b> |
| 3.3.1      | SYNTHESIS AND CHARACTERIZATION OF GH625-FUNCTIONALIZED PTNPs             | 76        |
| 3.3.2      | CELL UPTAKE AND INTRACELLULAR LOCALIZATION OF GH625-FUNCTIONALIZED PTNPs | 78        |
| 3.3.3      | ANTIOXIDANT ACTIVITY OF GH625-FUNCTIONALIZED PTNPs                       | 84        |
| <b>3.4</b> | <b>CONCLUSIONS</b>   | <b>86</b> |
| <b>3.5</b> | <b>REFERENCES</b>  | <b>87</b> |

## CHAPTER 4

93

### *Double peptide functionalization synergistically enhances PLGA-PEG-NPs crossing of the cerebral endothelium*

|            |  |            |
|------------|--|------------|
| <b>4.1</b> | <b>INTRODUCTION</b>                                | <b>94</b>  |
| <b>4.2</b> | <b>EXPERIMENTAL SECTION</b>                        | <b>97</b>  |
| 4.2.1      | MATERIALS  | 97         |
| 4.2.2      | SYNTHESIS OF PEPTIDES                              | 98         |
| 4.2.3      | SYNTHESIS OF COPOLYMERS AND CONJUGATES             | 99         |
| 4.2.4      | NP PREPARATION                                     | 101        |
| 4.2.5      | NP CHARACTERIZATION                                | 102        |
| 4.2.6      | CELL CULTURE                                       | 102        |
| 4.2.7      | CO-LOCALIZATION STUDIES                            | 102        |
| 4.2.8      | PERMEABILITY ASSAY TO NPs IN TRANSWELL SYSTEM      | 103        |
| 4.2.9      | NP ADHESION ASSAY TO BBB BY USING GLYCOTECH SYSTEM | 103        |
| 4.2.10     | STATISTICAL ANALYSIS                               | 104        |
| <b>4.3</b> | <b>RESULTS AND DISCUSSION</b>                      | <b>105</b> |
| 4.3.1      | NPs PRECURSORS SYNTHESIS AND CHARACTERIZATION      | 105        |
| 4.3.2      | NPs CHARACTERIZATION                               | 106        |
| 4.3.3      | CO-LOCALIZATION STUDIES                            | 107        |

|   |     |
|---|-----|
| 4.3.4 NPs TRANSPORT ACROSS <i>IN VITRO</i> MODEL OF THE BBB | 109 |
| 4.3.5 ADHESION ASSAY IN FLOW CONDITION                      | 111 |
| <b>4.4 CONCLUSIONS</b>                                      | 113 |
| <b>4.5 REFERENCES</b>                                       | 114 |

**CHAPTER 5** \_\_\_\_\_ **117**

*Conclusions and future prospective*



# LIST OF FIGURES, SCHEMES AND TABLES

---

- FIGURE 1.1.** HISTOGRAM SHOWING THE INCREASE IN PUBLICATIONS RELATED TO THE KEYWORDS "CELL-PENETRATING PEPTIDE" DURING THE PAST 50 YEARS. PUBMED DATA. 3
- FIGURE 1.2.** MECHANISMS OF CELL-PENETRATING PEPTIDE UPTAKE ACROSS THE CELLULAR MEMBRANE. 9
- FIGURE 1.3.** SCHEMATIC REPRESENTATION OF THE CPPS INTRACELLULAR TRAFFICKING MECHANISMS. 12
- FIGURE 1.4.** SEVERAL APPLICATIONS OF CELL-PENETRATING PEPTIDES AS MOLECULAR DELIVERY VEHICLES FOR A VARIETY OF DRUGS, NUCLEIC ACIDS, PROTEINS, THERAPEUTICS, AND IMAGING AGENTS. 14
- FIGURE 1.5.** (A) HELICAL WHEEL REPRESENTATION AND (B) ENERGY-MINIMIZED STRUCTURE OF THE AMPHIPATHIC  $\alpha$ -HELICAL MODEL OF THE 20-MER GH625 PEPTIDE ILLUSTRATE THE AMPHIPHILIC CHARACTER OF GH625 PEPTIDE. 20
- FIGURE 1.6.** MAJOR APPLICATIONS OF GH625 PEPTIDE TO DRUG DELIVERY. 21
- FIGURE 2.1.** EXPERIMENTAL MODEL OF THE COVALENTLY BONDED GH625-PEG-PEI/DNA POLYPLEXES ON THE SUBSTRATE MEDIATED GENE-DELIVERY PLATFORM. 40
- FIGURE 2.2.**  $^1\text{H-NMR}$  SPECTRA IN  $\text{D}_2\text{O}$  OF PEG-PEI (A) AND GH625-PEG-PEI (B) COPOLYMERS WITH ATTRIBUTION. 52
- FIGURE 2.3.** CONFOCAL IMAGES OF N/P 15 GH625-PEG-PEI COMPLEXES DEMONSTRATE DNA-VECTOR COMPLEXATION BY CO-LOCALIZATION (IMAGE C) OF (A) DNA-HOECHST AND (B) RHODAMINATED GH625-PEG-PEI VECTOR. SCALE BAR:  $25\mu\text{M}$ . 53
- FIGURE 2.4.** EXEMPLIFICATIVE SCANNING ELECTRON MICROSCOPY IMAGES OF GH625-PEG-PEI POLYPLEXES AT DIFFERENT MAGNIFICATIONS. 54

|  |    |
|--|----|
| <b>FIGURE 2.5.</b> SCANNING ELECTRON MICROSCOPY IMAGES OF COVALENT BONDED (A) AND ADSORBED (B) POLYPLEXES ON GLASS SURFACE. SCALE BARS: 200 NM.  | 57 |
| <b>FIGURE 2.6.</b> CLSM AND TRANSMISSION (') IMAGES OF COVALENT BONDED (A) AND ADSORBED (B) POLYPLEXES ON GLASS SURFACE. SCALE BAR: 25 $\mu$ M.  | 58 |
| <b>FIGURE 2.7.</b> CYTOTOXICITY ASSAY OF PEI/DNA AND GH625-PEG-PEI/DNA POLYPLEXES AT DIFFERENT N/P RATIOS IN NIH-3T3 CELLS AFTER 24 H OF INCUBATION.   | 59 |
| <b>FIGURE 2.8.</b> CONFOCAL IMAGES OF NIH-3T3 CELLS TREATED WITH PEI/DNA (A) AND GH625-PEG-PEI/DNA (B) POLYPLEXES AT N/P = 20 IN BOLUS DELIVERY EXPERIMENTS. SCALE BAR: 10 $\mu$ M.  | 60 |
| <b>FIGURE 2.9.</b> TRANSFECTION ASSAY OF PEI/DNA AND GH625-PEG-PEI/DNA POLYPLEXES AT DIFFERENT N/P RATIOS IN NIH-3T3 CELLS AFTER 24 H OF INCUBATION.   | 60 |
| <b>FIGURE 3.1.</b> TEM IMAGES OF BARE PTNPS WITH (A) 2.5, (B) 5 AND (C) 20 NM DIAMETERS. SCALE BAR 50 NM. (D) SIZE DISTRIBUTION OF PT2.5, PT5 AND PT20 NPS CALCULATED BY TEM IMAGE ANALYSIS (N~300) AND REPORTED IN THE CHART. (E) QUANTIFICATION OF PEPTIDE BINDING EFFICIENCY OBTAINED BY USING PEPTIDE/NP RATIOS REPORTED IN TABLE 3.1.     | 76 |
| <b>FIGURE 3.2.</b> CHARACTERIZATION OF RHODAMINE-CONJUGATED GH625 PEPTIDE.   | 77 |
| <b>FIGURE 3.3.</b> QUANTIFICATION OF NPS CELLULAR UPTAKE BY ICP/AES ANALYSIS AFTER 24 H INCUBATION WITH 50 MG/ML NP SUSPENSION IN CELL CULTURE MEDIUM.   | 78 |
| <b>FIGURE 3.4.</b> STEM IMAGES OF ENDO-LYSOSOMAL COMPARTMENTS IN HE <sup>L</sup> A CELLS AFTER 24 H INCUBATION WITH BARE AND GH625-FUNCTIONALIZED PTNPS AT 50 MG/ML PARTICLE CONCENTRATION, INDICATING THE INTRACELLULAR LOCALIZATION OF INTERNALIZED NPS.   | 79 |
| <b>FIGURE 3.5.</b> SEMI-QUANTITATIVE ANALYSIS OF GH625-FUNCTIONALIZED AND BARE PT2.5, PT5 AND PT20 NP DENSITY INTO ENDO-LYSOSOMAL COMPARTMENTS.  | 80 |
| <b>FIGURE 3.6.</b> REPRESENTATIVE STEM IMAGES OF HE <sup>L</sup> A CELLS AFTER 24 H OF INCUBATION WITH GH625-FUNCTIONALIZED PT2.5 NPS (A-C) PT5 NPS (D-E) AT 50 MG/ML PARTICLE CONCENTRATION.  | 81 |
| <b>FIGURE 3.7.</b> (A) STEM IMAGE OF HE <sup>L</sup> A CELLS AFTER 24 H OF INCUBATION WITH GH625-FUNCTIONALIZED PT20 NPS AT 50 MG/ML PARTICLE CONCENTRATION, SHOWING SOME PARTICLE FRAGMENTATION INSIDE AND OUTSIDE THE ENDO-LYSOSOMAL COMPARTMENT. SCALE BAR 100 NM. (B) SIZE RANGE ANALYSIS OF PARTICLE FRAGMENTS WITH A PEAK AROUND 1-2 NM. | 81 |

|  |     |
|--|-----|
| <b>FIGURE 3.8.</b> STEM IMAGES OF GHPT2.5 NPS APPROACHING CELL MEMBRANE.   | 82  |
| <b>FIGURE 3.9.</b> STEM HAADF ELECTRON TOMOGRAPHIES (ET) OF ENDOSOMAL COMPARTMENTS IN HELa CELLS AFTER 24 H INCUBATION WITH GHPT2.5 NPS INDICATING PARTICLE INTRACELLULAR DISTRIBUTION.  | 83  |
| <b>FIGURE 3.10.</b> DCF ASSAY RESULTS INDICATING THE ROS SCAVENGING ACTIVITY OF BARE AND GH625-FUNCTIONALIZED Pt2.5 NPS.   | 85  |
| <b>FIGURE 4.1.</b> TRANSCYTOSIS MECHANISMS OF THE Fe(III) ION AND THE IRON-MIMICKING CRT PEPTIDE ACROSS THE CEREBRAL ENDOTHELIUM.  | 95  |
| <b>FIGURE 4.2.</b> SCHEMATIC SYNTHESIS OF DUAL-FUNCTIONALIZED NPS WITH CRT AND GH625 PEPTIDES FOR THE ACTIVE TARGETING AND CROSSING OF THE CEREBRAL ENDOTHELIUM.   | 97  |
| <b>FIGURE 4.3.</b> A) SCHEMATIC REPRESENTATION OF THE GLYCOTECH FLOW CHAMBER FOR CELLULAR INTERACTION STUDIES. B) PICTURE OF GLYCOTECH SYSTEM.   | 104 |
| <b>FIGURE 4.4.</b> <sup>1</sup> H NMR SPECTRA OF SYNTHESIZED PLGA CONJUGATES SHOWN IN SCHEME 4.1.  | 106 |
| <b>FIGURE 4.5.</b> COLOCALIZATION OF BLANK-NPS (A,D), CRT-NPS (B,E), GH625-NPS (C,F), GH/CRT_33/66-NPS (G,J), GH/CRT_50/50-NPS (H,K) AND GH/CRT_66/33-NPS (I,L) WITH LYSOSOMES AFTER 24 H INCUBATION IN bEND.3 CELLS. RED: NPS; GREEN: LAMP-2. SCALE BAR 50 MM.  | 108 |
| <b>FIGURE 4.6.</b> SCHEMATIC REPRESENTATION OF TRANSWELL® CELL CULTURE INSERTS. NOTE THE POROUS MEMBRANE OF THE INSERT THAT PROVIDES INDEPENDENT ACCESS TO BOTH SIDES OF A CELL MONOLAYER  | 109 |
| <b>FIGURE 4.7.</b> PERMEABILITY OF bEND.3 CELL MONOLAYER TO BLANK, CRT, GH625, GH/CRT_33/66, GH/CRT_50/50 AND GH/CRT_66/33 FUNCTIONALIZED NPS.   | 110 |
| <b>FIGURE 4.8.</b> (A) NP ADHESION ABILITY TO bEND.3 UNDER FLOW CONDITION, $Q = 10$ mL/MIN. $P^* = < 0.05$ ; $P^{**} = < 0.005$ . (B-I) CONFOCAL IMAGES OF NPS IN bEND.3 AFTER THE EXPERIMENTS: (B,F) BLANK-NPS, (C,G) CRT-NPS, (D,H) GH625-NPS AND (E,I) GH/CRT_33/66-NPS. RED: NPS; BLUE: NUCLEI. BAR 50 MM. | 112 |

|  |     |
|--|-----|
| <b>SCHEME 2.1.</b> REACTION OUTLINE FOR THE SYNTHESIS OF GH625-PEG-PEI CONJUGATE: ACTIVATION OF PEI WITH NHS-PEG-ALKYNE FOLLOWED BY THE ADDITION OF THE RHOD-GH625-CYS CPP THROUGH THIOL-YNE “CLICK CHEMISTRY” REACTION. | 50  |
| <b>SCHEME 2.2.</b> SCHEMATIC SYNTHESIS STEPS OF GLASS SURFACE FUNCTIONALIZATION WITH PEI-PEG-GH625 POLYPLEXES.   | 56  |
| <b>SCHEME 4.1.</b> PLGA COPOLYMERS AND CONJUGATES: (A) PLGA-PEG (PELGA) COPOLYMER, (B) PLGA-AMINE, (C) PLGA-RHODAMINE, (D) PLGA-CRT AND (E) PLGA-GH625.  | 105 |
| <b>TABLE 1.1.</b> REPRESENTATIVE CELL-PENETRATING PEPTIDES: SEQUENCE, ORIGIN AND FUNCTION/APPLICATION.   | 4   |
| <b>TABLE 2.1.</b> PARTICLE SIZE AND Z-POTENTIAL VALUES FOR PRODUCED POLYPLEXES. HYDRODYNAMIC DIAMETERS AND SURFACE CHARGES VALUES ARE REPORTED AS MEANS ± STANDARD DEVIATION (SD).                                       | 52  |
| <b>TABLE 2.2.</b> WATER CONTACT ANGLE (WCA) VALUES AND DROP PICTURES ON GLASS COVERSLEIPS AFTER EACH SUBSTRATE MODIFICATION STEP.  | 55  |
| <b>TABLE 3.1.</b> THEORETICAL SURFACE DENSITIES OF GH625 PEPTIDE AS A FUNCTION OF PARTICLE SIZE AND PEPTIDE/NPS RATIOS.  | 73  |
| <b>TABLE 4.1.</b> MASS OF COPOLYMERS USED FOR BLANK-NPS, CRT-NPS, GH625-NPS, GH/CRT_33/66-NPS, GH/CRT_50/50-NPS AND GH/CRT_66/33-NPS PREPARATIONS.   | 101 |
| <b>TABLE 4.2.</b> SIZE, POLYDISPERSITY AND Z-POTENTIAL MEASUREMENTS OF PELGA-NPS AT EACH FUNCTIONALIZATION DEGREES.  | 107 |

## ABSTRACT

---

The membrane bilayer delimits the interior of individual cells and provides them with the ability to survive and function properly. However, the crossing of cellular membranes constitutes the principal impediment to gaining entry into cells, and the potential therapeutic application of many drugs is predominantly dependent on the development of delivery tools that should take the drug to target cells selectively and efficiently with only minimal toxicity. Cell-penetrating peptides (CPPs) act in this context mediating the delivery of various cargoes such as nucleic acids, polymers, liposomes, nanoparticles and low molecular weight drugs. with low cytotoxicity and no restriction with respect to the size or type of cargo.

Among these, peptide gH625 (HGLASTLTRWAHYNALIRAF), was previously identified as a membrane-perturbing domain in the glycoprotein H (gH) of the *Herpes simplex* virus type I. gH625 peptide interacts with biological membranes, contributing to the merging of the viral envelope and the cellular membrane; it is able to traverse the membrane bilayer and to carry cargoes like quantum dots and 100 nm polystyrene NPs inside the cytoplasm in an efficient way. In this context, the aim of this work is to investigate the ability of the gH625 peptide in the construction of novel materials, changing the classical intracellular fate of endocytic pathway and mediating the lysosomal escape of NPs made.

Therefore, firstly, we focus on the combined effects of gH625 peptide and reverse transfection to develop a gene delivery platform based on functionalized polyethylenimine (PEI)/DNA polyplexes. We created PEI based polyplexes in which the gH625 was covalently coupled to 25 kDa PEI through a heterobifunctional polyethylenglycol (PEG) spacer. The obtained polyplexes were tested both in direct and reverse transfection approach, analyzing the cellular behavior in viability and

transfection efficiency assays. Results demonstrate that gH625 CPP functionalization allowed to increase the transfection efficiency of non-viral polymeric carriers, to reduce their own cytotoxicity and mediate an efficient gene transfer with respect to un-functionalized vectors.

In the second part of the work we analyzed the role of particle size in influencing the ability of the gH625 membranotropic peptide to escape the endo-lysosomal pathway and deliver the particles in the cytosol. To this aim, we carried out a systematic assessment of cellular uptake and distribution of monodisperse platinum nanoparticles (PtNPs), having different diameters (2.5, 5 and 20 nm) and citrate capping or gH625 peptide functionalization. Combining the enhanced uptake and partial cytosolic delivery promoted by gH625, we were able to achieve a strong improvement of the antioxidant nanozyme function of 2.5 nm PtNPs, decreasing both the endogenous ROS level and its overproduction following an external oxidative insult.

Finally, in the last chapter, we analyze the behavior of gH625 in dual-functionalized polymeric carrier systems for targeted drug delivery across the blood-brain barrier (BBB), that represent the main obstacle in the treatment of Central-Nervous-System (CNS) diseases. The efficacy of NP functionalized with CRT and gH625 in promoting the translocation across the cerebral endothelium was assessed. Results from co-localization studies, adhesion and permeation assays across *in vitro* brain endothelial model under dynamic conditions establish that the cooperative effect of CRT and gH625 on NPs may change the distribution of NP in the cell and strengthen the BBB crossing of NPs.

# Chapter 1

## Introduction

**Abstract:** Cell-penetrating peptides are short and basic peptides, widely used due to their ability to deliver a cargo across the cell membrane both *in vitro* and *in vivo*. Here we report a general overview about many classes of CPPs, starting from their uptake mechanism, the intracellular trafficking and exploring their uses for many therapeutic applications. In this extensive scenario, a fascinating novel hypothesis is represented by gH625 membranotropic peptides. It can efficiently cross biological membranes (including the blood-brain barrier), *via* local and temporary destabilization and reorganization of the membrane bilayer, and may also be able to enter cells avoiding the endosomal entrapment; in particular, by direct translocation or endosomal escape mechanisms. The role of this sequence is widely described in order to lead the reader through the many applications that are now emerging for this peptide.

## 1.1 Cell-Penetrating Peptides (CPPs)

The hydrophobic nature of phospholipids membrane bilayer represent a selectively permeable barrier of living cells and protects them from the influx of exogenous molecules, including bioactive compounds such as peptides, proteins and oligonucleotides. In order to transport important molecules such as sugars and amino acids across the lipid bilayer, cells use a combination of channels and carrier proteins. Moreover, endocytosis or exocytosis mechanisms are used to transport material in bulk across the membrane. An accurate control of transport is generally helpful for the cell, but then many potential therapeutic drug targets become inaccessible. Thus, cells require entry of drugs in order to be effectively treated. While large macromolecular drugs, such as proteins or nucleic acids, are transported into target cells through both receptor-mediated or non-specific endocytosis, many small therapeutics are believed to go through a combination of carrier-mediated transport and passive diffusion.<sup>1</sup> Regardless of the controversial opinions on which is the predominant mechanism,<sup>2-3</sup> cell entry remains a focus for those working in drug design and discovery.

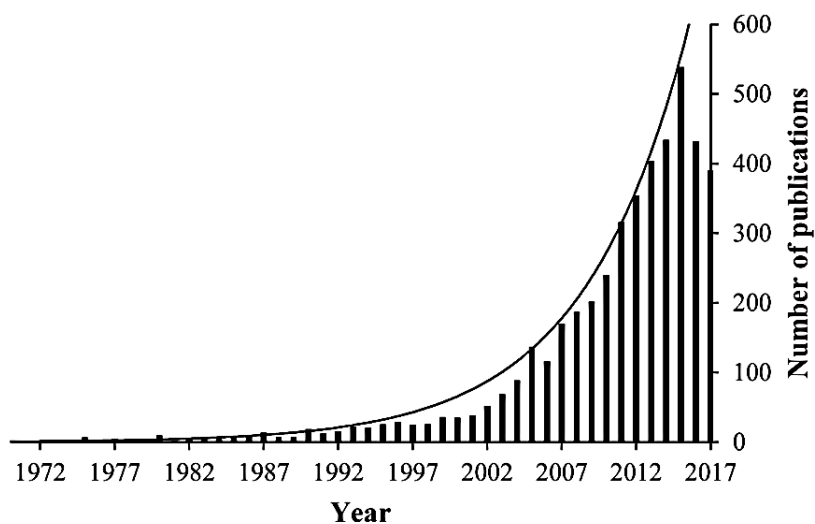
Several strategies have been developed to deliver therapeutic agents across cellular membranes such as microinjection, electroporation, liposome and viral based vectors. However, these methods have shown several drawbacks, including low efficiency, high toxicity, penurious bioavailability and poor specificity. An alternative strategy to overcome the impermeable phospholipid bilayer of the cell membrane emerged in latest '80s, from two different discoveries. Around the same time, first the HIV TAT transactivating factor,<sup>4,5</sup> and then the *Drosophila* Antennapedia transcription factor proteins (later named penetratin)<sup>6</sup> were shown to be able to translocate the cell membranes and enter the cells. After these parallel discoveries, it was demonstrated that short sequences of these proteins exhibited membrane-crossing properties. Thus, TAT and penetratin become the progenitor of a new type of molecular vector able to promote the delivery of a variety of cargoes: the cell-penetrating peptides (CPPs).

In general, CPPs are defined as short, water-soluble and partly hydrophobic and/or polybasic peptides (from 5 up to 30-35 amino acids residues) with a net positive charge at physiological pH.<sup>7</sup> The main feature of CPPs is that they are able to penetrate the cell membrane at low concentrations both *in vivo* and *in vitro* without using any chiral



receptors and without causing significant membrane damage. In addition, and even more important, these peptides are capable of internalizing electrostatically or covalently bound biologically active cargoes such as nucleic acids, polymers, liposomes, nanoparticles and low molecular weight drugs.<sup>8</sup> Further characteristics of the CPPs are low cytotoxicity, their ability to be taken up by a variety of cell types, dose-dependent efficiency and no restriction with respect to the size or type of cargo.<sup>9</sup>

In recent years the number of peptides identified as having cell-penetrating properties have expanded exponentially because they represent a promising tool for biomedical applications. The increasing interest of the scientific community about CPPs topic is due not only for their high internalization ability but also for the potential in variable modification design.



**Figure 1.1.** Histogram showing the increase in publications related to the keywords "cell-penetrating peptide" during the past 50 years. PubMed data.

## 1.2 Classification of CPPs

As regards the classification of CPPs, there are several possible approaches. For example, CPPs can be subdivided into different classes based on their origin or sequence characteristics<sup>10</sup> or otherwise by secondary structure or even their mechanisms of action.

However, a major requirement for most of CPPs is the positively charged sequences of amino acids at physiological pH (primarily arginine and lysine) for the resulting

electrostatic interactions with negatively charged cell surface glycoproteins (before internalization).<sup>11</sup> At physiological pH condition, the guanidine head group of arginine can form hydrogen bonds with the negatively charged phosphates and sulfates on the cell membrane surface and may possibly lead to internalization process. The side chain of the amino acid lysine displays the same net positive charge as arginine, but the absence of the guanidine group results in a less effective penetration of the plasma membrane when acting alone. Consequently, the number and order of amino acids in the peptide sequence, especially arginines, is critical for determining the transduction properties of the CPP.<sup>12</sup> The membranolytic properties of a given CPP can also be governed by its secondary structure, specifically helicity. Indeed, it has been shown that peptides with an  $\alpha$ -helical region can more efficiently enter the cells.<sup>8</sup>

Although CPPs have a great sequence assortment, they can be generally divided into three other classes defined by their physical-chemical properties like peptide sequences and binding properties to the lipids.<sup>13</sup> These classes include cationic, amphipathic and hydrophobic sequences.<sup>14-15</sup>

**Table 1.1.** Representative cell-penetrating peptides: sequence, origin and function/application. Adapted with permission of Ref. <sup>14</sup> Copyright © 2013 Published by Elsevier B.V.

| CPPs                      | Sequence                             | Origin  | Function or application                                      |
|---------------------------|--------------------------------------|---|--|
| <i>Cationic</i>           |                                      |   |  |
| R6H4                      | RRRRRRH HHH                          | Designed  | pH-sensitive delivery  |
| Penetratin                | RQIKIWFAQNRMRKWKK                    | Antennapedia homeodomain                                  | Targeted to human fibroblasts                                |
| (RXR) <sub>4</sub>        | (R-Ahx <sub>8</sub> -R) <sub>4</sub> | Designed  | Targeted to rpoD gene  |
| R9                        | RRRRRRRRR                            | Designed  | Imaging and therapeutic agents delivery                      |
| NLS                       | CGYGPKKKRKVGG<br>PKKKRKV             | SV40 NLS peptide<br>Simian SV40 large tumor antigen       | Nuclear localization<br>Nuclear localization                 |
| KAFAK                     | KAFAKLAARLYRKALARQLGVAA              | Designed  | Anti-inflammatory  |
| hCT(9–32)                 | LGTYTQDFNKFHFTFPQTAIGVGAP            | A hormone secreted by the C cells of the thyroid          | Treatment of diseases, such as hypercalcemia or osteoporosis |
| TAT                       | YGRKKRRQRRR                          | HIV-TAT domain  | Intracellular delivery of peptide-blockers                   |
| DPV3                      | RKKRRRESRKKRRRES                     | Human heparin binding proteins and/or anti-DNA antibodies | Specific subcellular delivery of therapeutic biomolecules    |
| <i>Amphipathic</i>        |                                      |   |  |
| RGD                       | GRGDSY                               | Various circulating proteins                              | Integrin receptors targeting                                 |
| Sweet arrow peptide (SAP) | (VRLPPP) <sub>3</sub>                | N-terminal domain of $\gamma$ -zein                       | Protease-resistance  |

|                    |                                     |  |  |
|--------------------|-------------------------------------|--|--|
| hLF                | KCFQWQRNMRKVRGPPVSCIKR              | Antimicrobial peptides                                 | Antifungal, antimicrobial and antiviral activities                                 |
| MPG                | GALFLGWLGAAGSTMGAPKKKR KV           | HIV glycoprotein 41 protein                            | Nucleic acids delivery   |
| pVEC               | LLIILRRRIRKQAHHSK                   | Murine vascular endothelial-cadherin protein           | Antimicrobial activity   |
| ARF(1–22)          | MVRRFLVTLR IRRACGPPRVV              | p14ARF protein   | Induce cell apoptosis  |
| BPrPp (1–28)       | MVKSKIGSWILVLFVAMWSDVGL CKKRP       | The N-terminus of the unprocessed bovine prion protein | Transport the cargo across the endosomal membrane and into the cytosol and nucleus |
| Bac7               | RRIRPRPRLPRPRPLPFPRPG               | Bactenecin family of antimicrobial peptides            | Antimicrobial activity   |
| MAP                | KLALKLALKALKAAKLKLA                 | Chimeric   | Intracellular delivery of polar bioactive compounds                                |
| DPRSFL             | DPRSFL                              | Proteinase activated receptor 1 (PAR-1)                | Imaging  |
| VP22               | NAATATRGRSAASRPTQRPRAPAR SASRPRRPVQ | Herpes simplex virus (HSV)                             | Nuclear localization   |
| √T5                | DPKGDPKGVTVTVTVTGKGD PKD            | Viral proteins   | Oligonucleotide and oligopeptide delivery  |
| C105Y              | CSIPPEVKFNKPFVYLI                   | aa 359-374 of 1-antitrypsin                            | Enhanced gene expression   |
| CADY               | GLWRALWRLRLSLWRLWRA                 | Designed   | Targeted siRNA delivery  |
| Pep-1              | KETWETWWTEWSQPKKRKV                 | A tryptophan-rich cluster                              | Nucleic acids and peptides delivery  |
| p28                | LSTAADMQGVVTDGMASGLDKD YLKPDD       | Azurin   | Antiproliferative and proapoptotic activity  |
| <i>Hydrophobic</i> |                                     |  |  |
| PFV                | PFVYLI                              | C105Y  | Deliver peptides into cells  |
| SG3                | RLSGMNEVLSFRWL                      | A randomized peptide library                           | Gene delivery  |
| Pep-7              | SDLWEMMMVSLACQY                     | CHL8   | Nucleic acids and peptides delivery  |
| FGF                | PIEVCMYREP                          | Cellular and viral proteins                            | Inhibition radiation induced apoptosis   |

### 1.2.1 Cationic CPPs

Cationic peptides represent the largest class of CPPs. They are characterized by the presence of a high positive net charge and few acidic amino acid residues. Studies suggest that at least eight positive charges are needed for efficient uptake of several cationic CPPs.<sup>16</sup> Because of these electrostatic interactions with negatively charged glycoproteins on the cellular surface, they display a great potential as transmembrane carriers for therapeutic compounds.<sup>17</sup> Cationic CPPs, since TAT (the best-known member of this class) was discovered, were originally considered as ‘Trojan horse’ delivery vehicles that enter the cells without causing a cellular response.<sup>18</sup> On the other hand, cationic CPPs can induce a wide range of side effects, including consequences on membrane integrity and cell

viability, which might be less aggressive than cell death. Typically, R9,<sup>19</sup> pTAT,<sup>20</sup> hLF,<sup>21</sup> (RXR)<sup>422</sup> and nuclear localization sequences (NLSs) also belong to this class.

### 1.2.2 Amphipathic CPPs

The term amphipathicity generally refers to molecules with both hydrophilic and hydrophobic faces.<sup>23</sup> Peptides can be amphipathic in their primary or secondary structure. Peptides, such as MPG,<sup>24</sup> penetratin<sup>25</sup> and CADY<sup>26</sup> which contain both polar and nonpolar regions are defined as amphipathic peptides, based on their primary structure. Other primary amphipathic peptides, defined as chimeric peptides, correspond to the sequential assembly of hydrophobic and hydrophilic domains divided by a certain number of residues that acts as spacer. Chimeric peptides are also obtained by covalently attaching a NLS to a cell membrane targeting domain. For example, MPG (GALFLGWLGAAGSTM-GAPKKKRKV) is based on the SV40-NLS PKKRKV and the hydrophobic domain derived from the fusion sequence of the HIV glycoprotein 41, separated from the NLS through a linker (WSQP). Several other primary amphipathic CPPs are fully derived from natural proteins, such as pVEC,<sup>27</sup> ARF (1–22)<sup>28</sup> and BPrPr (1-28).<sup>29</sup>

Secondary amphipathic peptides are generated by the conformational state which allows positioning of hydrophobic and hydrophilic residues on opposite sides of the same molecule.<sup>30</sup> Amphipathic  $\alpha$ -helical CPPs have a highly hydrophobic patch on one face, whereas the other face can be cationic, anionic, or polar. The amphipathicity of  $\beta$ -sheet structures are due one hydrophobic and one hydrophilic stretch of amino acids exposed to the solvent, such as vT5.<sup>31</sup> In most cases, this structural organization of the amino acid residues occurs upon interaction with the phospholipid membrane, facilitating the peptide interaction and insertion into the bilayer.<sup>32</sup> Conformational polymorphism also plays a key role: in fact, the ability to shift from random to  $\alpha/\beta$  conformations as a consequence of membrane composition and peptide concentration has emerged as a common structural pattern for this class of peptides.<sup>32</sup>

### 1.2.3 Hydrophobic CPPs

Hydrophobic peptides mostly contain apolar residues; they include stapled peptides,<sup>33</sup> prenylated peptides<sup>34</sup> and pepducins.<sup>35</sup> So far, only a few hydrophobic CPP sequences have been discovered, such as the signal sequences from integrin  $\beta 3$  (VTVLALGALAGVGVG) and Kaposi fibroblast growth factor (AAVALLPAVLLALLAP).<sup>36</sup> Hydrophobic amino acids are also present in amphipathic CPPs, for example MAP,<sup>37</sup> and in other longer chimeric CPPs, together with additional cationic residues for enhancing uptake and delivery capacity.<sup>38</sup>

### 1.2.4 Other CPPs subgroups

In addition to this ‘bulky’ CPP classification, additional CPP subgroups should be mentioned. A particularly interesting class of CPPs is proline-rich and poly-proline amphipathic sequences, which have been reported in diverse families that differ in sequence and structure. However, they all contain a proline pyrrolidine template.<sup>39</sup> Among all, the permeation ability of the sweet arrow peptide (SAP), which is a sequence with 50% proline content in addition to three arginine residues that is derived from a storage protein in maize, has been reported.<sup>40</sup>

Even if proline has a hydrophobic nature, proline-rich peptides are unexpectedly soluble in water as well as a broad range of organic solvents.  $\gamma$ -Amino-L-proline has an extra amino group (in the  $\gamma$  position of the proline) that allows even higher water solubility. Thanks to the use of two orthogonal protecting groups for both the amino functionalities, the  $\gamma$ -amino group is used in the peptide bond formation while the  $\alpha$ -amino group may be properly functionalized in a following step. Therefore,  $\gamma$ -amino-L-proline has been used as a very convenient building block for the preparation of cell-penetrating  $\gamma$ -peptides, which can be considered special amphipathic peptides as a result of their backbone and their charged side chain linkages.<sup>41-42</sup>

As more CPPs emerged, synthetic peptides have been developed using prediction programs, rational design strategies, or even trial and error procedures. In addition, research groups started to include non-primary and even unnatural amino acids<sup>41</sup> and other modifications in order to create new CPPs or improve existing ones.

For instance, substitution of a lysine residue with an ornithine residue leads to a better peptide resistance to cellular degradation.<sup>43-44</sup> The peptide degradation prevention, with consequent increase of cargo delivery efficiency, can also be improved by changing the structure of the peptide itself (e.g. dendrimers<sup>45-51</sup> or cyclic peptides<sup>52</sup>).

Finally, antimicrobial peptides (AMPs) share molecular similarities with CPPs; they are cationic and may serve as potential structures for future drug delivery systems.<sup>40</sup> These antimicrobial peptides, such as LL-37, S413-PV and Buforin 2, are able to damage bacterial membranes during cell entry and possess microbicidal properties.

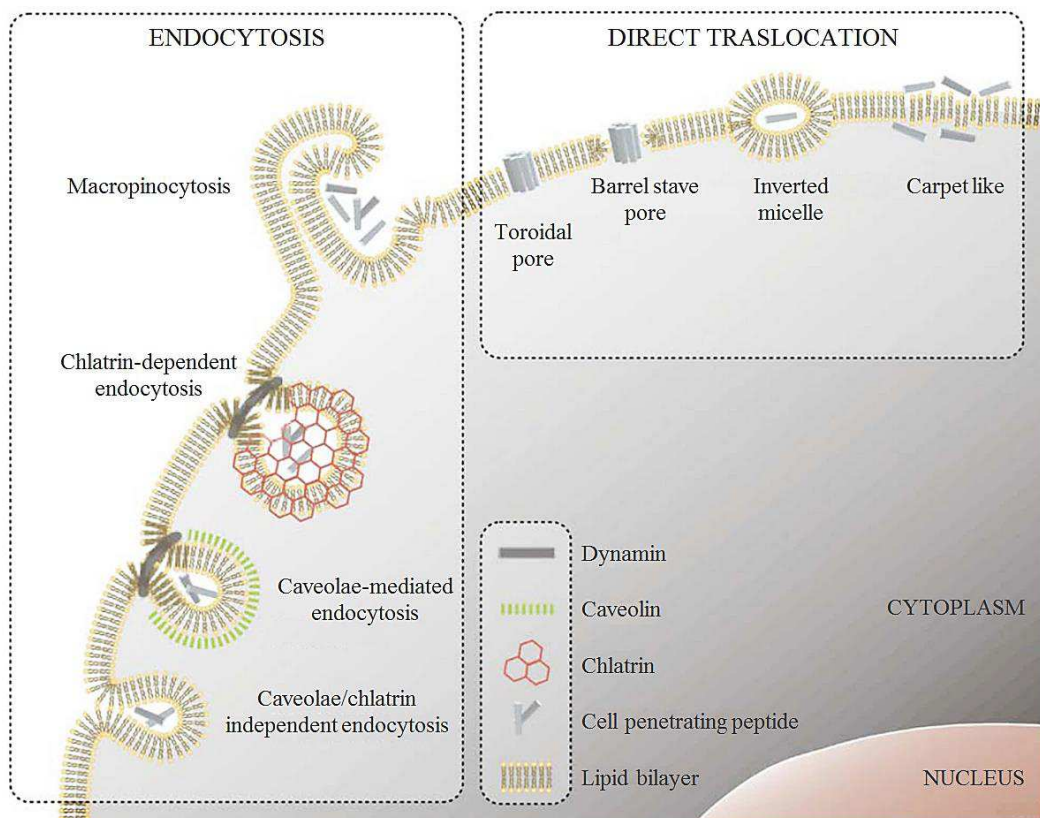
### **1.3 Cellular internalization mechanisms of CPPs**

From the beginning there has been considerable interest in investigate how CPPs penetrate the cells. Although numerous studies about the uptake mechanism of CPPs across the plasma membrane have been reported, the pathways through which CPPs enter the cells have not been absolutely resolved yet.<sup>53</sup>

CPPs are translocated into cells by several independent mechanisms but that can occur simultaneously. While direct translocation across the cell membrane occurs in some cases, it is generally accepted that the majority of CPPs and CPP-cargo complexes enter cells through an endocytic pathway.<sup>54</sup>

The protein or peptide from which CPPs derive can often provide information about the mechanism of internalization. Mainly short, positively charged, arginine-rich CPPs interact with the negatively charged lipid membrane and activate permeabilization of the cell membrane through a receptor independent pathway, which results in endocytosis of the cargo, including macropinocytosis, clathrin mediated endocytosis and caveolae/lipid raft-mediated endocytosis.<sup>55</sup>

On the other hand, CPPs can cross the membranes through an energy-independent way known as the direct translocation pathway. In this case a spontaneous peptide-membrane interaction occurs and a translocation mechanism happens involving direct membrane penetration. This interaction is explained through different mechanisms such as the inverted micelle formation, pore formation, the carpet-like model and the membrane-thinning model.<sup>13, 56-57</sup>



**Figure 1.2.** Mechanisms of cell-penetrating peptide uptake across the cellular membrane. They include endocytic energy-dependent pathways, based on vesicle formation, and direct translocation or cell penetration models, involving the formation of hydrophilic pores or achieving local destabilization of the lipid bilayer. Adapted with permission from Ref. <sup>57</sup>.

### 1.3.1 Direct translocation through the membrane bilayer

All of the hypothesized direct translocation mechanisms can be clustered into four pathways (Figure 1.2):<sup>57</sup> (i) inverted micelle formation,<sup>54</sup> (ii) pore formation,<sup>58</sup> (iii) the carpet-like model<sup>59</sup> and (iv) the membrane thinning model.<sup>60</sup> All these routes start with the interaction between the positively charged CPP and the negatively charged components of membrane such as the phospholipid bilayer as well as the heparan sulfate (HS). This interaction causes the folding of the peptide into the membrane with a subsequent destabilization of the lipid membrane.<sup>61-62</sup> Generally, high CPP concentrations and primary amphipathic CPPs lead to a direct penetration following an internalization mechanism that depends on the peptide concentration, peptide sequence and lipid composition in each model membrane study.<sup>63-65</sup>

The “inverted micelle” is a suggested model for the direct penetration of penetratin.<sup>66</sup> It is characterized by an additional interaction between hydrophobic peptide residues and the hydrophobic part of the membrane. Thus, this mechanism is not probable for the highly cationic CPPs, such as TAT.

Pore formation can be described by the barrel stave model and the toroidal model.<sup>57-58</sup> In the first one, helical CPPs form a barrel by which hydrophobic residues are close to the lipid chains and hydrophilic residues form the central pore. In the toroidal model, lipids bend in a way that the CPP is always close to the head group and both CPP and lipids form a pore. Both mechanisms depend on the overcoming of a certain peptide concentration threshold, which is different for different peptides.

Lastly, in the carpet-like model<sup>59</sup> and membrane thinning model,<sup>60</sup> interactions between phospholipids and CPPs result in a carpeting and thinning of the membrane, respectively. Also in this case, translocation of the CPP is achieved when CPP concentration is above a limit value.

### **1.3.2 Endocytosis-mediate uptake**

Endocytosis is a natural, energy-dependent, cellular process that starts with electrostatic interactions with proteoglycans at the cellular surface or by direct destabilization interactions across the lipid bilayer.<sup>56</sup> Endocytosis of CPPs or CPP-cargoes (Figure 1.2) includes several pathways: phagocytosis for the uptake of large particles and pinocytosis for solute uptake. Pinocytosis is categorized as macropinocytosis and clathrin or caveolin dependent (or independent) endocytosis.<sup>67-68</sup>

Macropinocytosis is associated with the inward folding of the outer surface of the plasma membrane, which results in the formation of vesicles called macropinosomes. Dynamin protein is required for membrane invagination. The resulting macropinosomes are surrounded by a membrane similar to the cell membrane.

In receptor-mediated endocytosis, clathrin or caveolin are involved in the mechanism of uptake. They are required for invagination of the membrane and help to form the vesicles after the extracellular molecule binding to the membrane receptor.<sup>67-68</sup>



### **1.3.3 Significant factors that influence the mechanism of CPP uptake**

As mentioned above, the mechanisms of CPPs entries into cells have not been entirely clarified yet.<sup>69</sup> Despite the similarities among CPPs, the mechanisms of their uptake considerably may vary due to several factors. The most important issue is represented by the CPP concentration as it can lead the activation of different uptake pathways.<sup>24, 70</sup> At low CPP concentrations, endocytosis is believed to be the main common uptake mechanism. Indeed, for many cationic CPPs, rapid cytosolic uptake is observed above a concentration threshold, which leads to direct translocation, while at lower concentrations the uptake is primarily endocytic.<sup>71-72</sup> However, for primary hydrophobic CPPs at high concentrations, direct penetration is more probable.

The concentration threshold for direct penetration differs among different CPPs, cell lines and the type and the size of the cargo. TAT attached to a large cargo is mostly entrapped in the endosomal vesicles; however, it redistributes throughout the cell cytosol or even deeper into the nucleus when attached to a small one.<sup>73-74</sup> Furthermore, labeling a peptide with different fluorophores may also influence the uptake mechanism, intracellular distribution and cytotoxicity of the peptide.<sup>75-76</sup> Other important experimental factors for the uptake mechanisms are, for example, cell type, temperature and incubation time.

Despite all the debates about the route of entry, some consensual features are now privileged, hoping that further work could clear the variables affecting the modes of internalization.

## **1.4 Uptake pathways and endosomal escape mechanisms of CPPs and CPP-Cargo complexes**

While the mechanism of CPP-mediated cell entry has been the subject of many studies, more work is needed to provide clarifications about the mechanisms of cellular uptake and internalization pathways of CPP-cargo complexes.<sup>53, 77</sup>

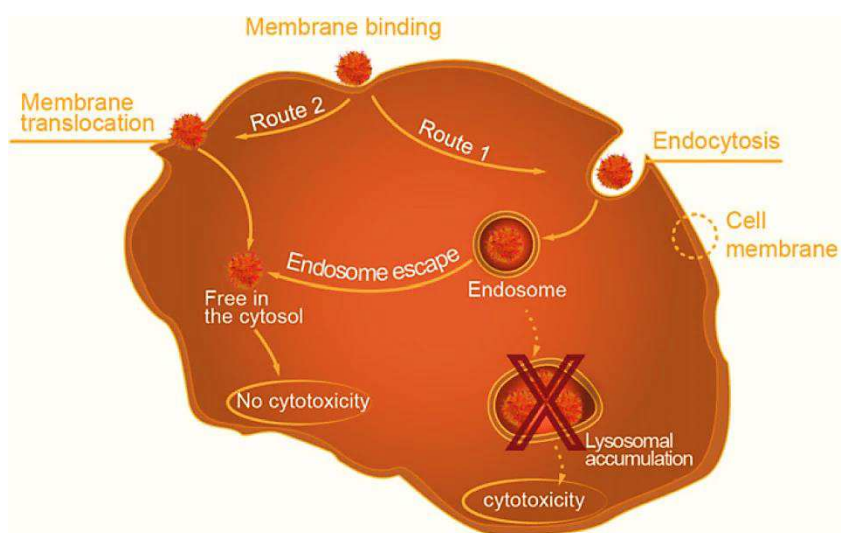
The entry of a CPP-cargo complex into the cell could be influenced by several factors, including the physicochemical properties of CPPs (such as molecule length, charge delocalization, hydrophobicity), the nature of the attached cargo (type, size, surface

potential), differences in the cell line being utilized and the concentration of CPP. Depending on the size of the cargo, several internalization routes may act simultaneously.

Generally, most cell-penetrating peptides or CPP-cargoes are taken up through endocytosis processes and they are immediately transported into the endocytic vesicles.

Initially, the pH value in early endosome drops from neutral to around pH 6.<sup>44</sup>

Then, early endosomes can follow two different pathways: (i) they may fuse with sorting endosomes and the internalized content can be transported out of the cell by exocytosis. More often, (ii) the delivery systems are trafficked to late endosomes which are rapidly acidified to pH 5-6 by the action of the ATPase proton-pump. Subsequently, the fusion with lysosomes (which contains various degradative enzymes) causes a further pH reduction to approximately pH 4.5 that facilitates substrate denaturation and helps lysosomal hydrolases, most of which operate optimally in the range of pH 4.5-5.5.<sup>78</sup>



**Figure 1.3.** Schematic representation of the intracellular trafficking mechanisms. CPPs and/or CPP-cargoes are able to reach cytoplasm through a direct translocation mechanisms across cell membrane (route 2), or, when endocytosis takes place, *via* endosomal escape (route 1). The ability of CPPs to avoid accumulation into lysosomes is strictly related with the reduction of cytotoxicity. Adapted by permission from Ref <sup>79</sup> © 2015 IOP Publishing Ltd.

CPP-cargoes that fail to be released from these acidic vesicles will ultimately be degraded. This accumulation leads to two important consequences: (i) a low efficiency for a successful delivery<sup>80-81</sup> and (ii) an increase of NP toxicological effects due to the very degradative environment in the lysosomes.<sup>82-83</sup>

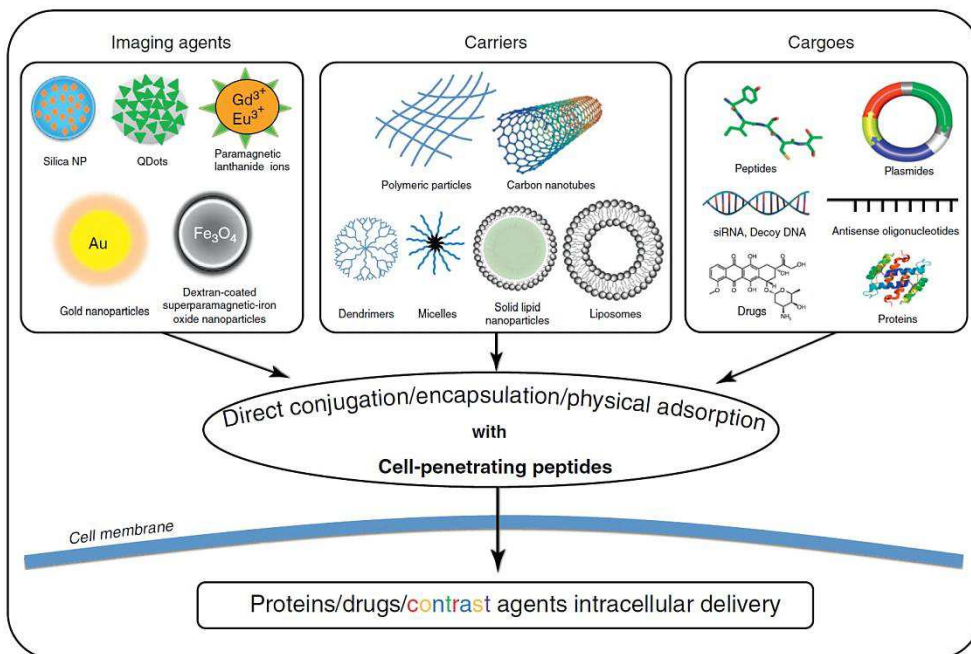
Ideal CPP-cargoes should be released from these acidic compartments at an early stage in order to explicate their function and prevent the fate of lysosomal destruction. Therefore, CPPs have a second chance to exemplify their function inducing endosomolytic activity and promote endosomal escape following the same direct membrane translocation mechanisms described above (1.3.1). Furthermore, during the acidification of the endosomes, the imidazole groups of histidine residues could also be protonated and the peptide increases its net positive charge, intensifying its interaction with the anionic lipids in the endosomal membrane. Thus, membrane destabilization occurs, followed by the release of the construct into the cytosol.<sup>84</sup>

Pore formation is another mechanism that explains the endosomal escape of peptide-based delivery systems. In addition, multiple mechanisms may be accounted for the enhancement of transfection efficiency, including structural changes of the peptide at low pH values, facilitation of nucleic acid dissociation from the lipoplexes and the flip-flop mechanism.<sup>85</sup>

## **1.5 Biomedical and therapeutic applications of CPP**

There is now convincing evidence that CPPs have a therapeutic potential and, indeed, they have been efficaciously used to facilitate the intracellular delivery of several molecules of pharmacological interest in different cell lines. It has already been proven that they have the potential to improve intracellular delivery of a large arsenal of biologically active agents.<sup>86-88</sup> Since their discovery, CPPs have been conjugated to cargoes with a large number of different sizes, transporting them both in *in vitro* and *in vivo* experiments. Cargo examples are peptides, proteins, nanoparticles, nucleic acids (oligonucleotides, cDNA, RNA, siRNA), fluorochromes, antibodies, lipid-based formulations, quantum dots, viruses, contrast agents for magnetic resonance imaging and drugs (Figure 1.4).<sup>10, 57, 87-89</sup>

In this paragraph, some of the numerous instances where CPPs have been used to deliver therapeutics are highlighted. As concern *in vivo* delivery, many of the examples are limited to small animals and application of CPPs to human therapeutics has yet to prove effective.



**Figure 1.4.** Several applications of Cell-penetrating peptides as molecular delivery vehicles for a variety of drugs, nucleic acids, proteins, therapeutics, and imaging agents. Reprinted with permission of Ref. <sup>10</sup> Copyright © 2012 Elsevier Ltd.

### *Nucleic acid delivery*

One of the first biomedical applications of CPPs was the delivery of nucleic acids into cells. Generally, plasmids DNA are not able to reach the cell nuclei because of both nuclease enzymatic degradation processes and inefficient capacity of passing through the cell membrane. To improve the delivery of nucleic acids, plasmid DNA has been complexed with cationic polymers, liposomes or cationic CPPs, which condense DNA into particles capable of entering the cells through endocytosis.<sup>90</sup>

CPPs have been used also to functionalize existing synthetic gene vectors. For instance, polyarginine functionalized lipoplexes efficiently silenced genes in a mouse liver.<sup>91</sup> Furthermore, an unexpected and interesting finding was that CPPs seem to be able to improve the long-term gene expression from vectors. For example, PEI coupling with TAT CPP extend the gene expression period from about 1 month to almost 7 months compared to TAT or PEI alone.<sup>92</sup>

### *Peptides, proteins and enzymes*

As with gene delivery, proteins are typically unable to passively enter the cells. CPPs make it possible to transport enzymes and other therapeutic targets, which can lead to treatments for a wide range of diseases. Enzymes that prevent oxidative damage, used for treatments against ischemic injury, are just one of several types of protein of interest for intracellular delivery. For example, TAT CPP was combined with glyoxalase to prevent oxidative damage of neuronal cells.<sup>93</sup> Moreover, TAT was used to improve cell delivery of antioxidant enzymes catalase and superoxide dismutase, which protected the cells from oxidative stress.<sup>94-95</sup>

### *Small molecules & cancer treatment*

Small hydrophilic molecules have difficulties in traversing the hydrophobic cell membrane. Additionally, diseases, such as cancer, can also preclude an effective transport of small molecules across the lipid bilayer and these kinds of drugs are sometimes toxic and expensive. Therefore, new strategies to develop modalities to cure cancer are needed. Anticancer drugs affect cell growth, vascularization and metastatic spread by preventing effective DNA replication, by damaging the mechanisms of cell division or by blocking the paths implicated in cell growth.<sup>96</sup> Small chemotherapeutic drugs such as doxorubicin, methotrexate, cyclosporine A, paclitaxel, properly developed with CPPs, represent a very promising tool for the treatment of critical tissues such as tumors, heart, etc.<sup>97</sup> Thanks to a better interaction with glycosaminoglycans, the cationic CPP polyarginine can drive doxorubicin to the inhibition of tumor growth *in vivo* with fewer side effects compared to doxorubicin alone.<sup>98</sup> Moreover, doxorubicin was loaded in cancer cell by means of PFV CPP functionalized liposomes with significant reduction in tumor volume and fewer side effects compared to an unmodified liposome.<sup>99</sup>

### *CPPs in imaging*

Imaging is a growing field in the detection and monitoring of disease markers, which can lead to a more effective disease management. CPPs have been coupled with contrast agents, fluorophores, quantum dots and other readily detectable molecules in order to improve their permeability<sup>53</sup> and visualize the intracellular environment, as well as for

specific cells in a tissue. The high efficiency characteristic of CPPs makes them promising tools in the imaging field such as proteases detection,<sup>100-101</sup> optical imaging of cancers<sup>102-103</sup> and molecular imaging analyses<sup>104</sup> providing novel and powerful tools in the development of new imaging agents.

#### *CPPs with nuclear localization sequences (NLSs) to improve nuclear import efficiency*

To improve nuclear import efficiency, CPPs have been attached with nuclear localization sequences (NLSs) to DNA or gene carriers.<sup>105</sup> As mentioned in paragraph 1.2.1, NLSs are special cases of cationic CPPs, characterized by the presence of lysine-, arginine- or proline-rich motifs that can be recognized by members of the Importin super family of nuclear transport proteins. Thus, NLS promote the overcoming of the nuclear membrane barrier in nuclear translocation processes.<sup>106</sup> The most extensively studied NLS sequence for gene therapy is derived from the large tumor antigen of the simian virus 40 (SV40).<sup>107</sup>

#### *CPPs-modified pH-sensitive delivery*

Acidic pH is another feature that influences the cytoplasmic delivery of cargo molecules performed with CPPs.<sup>19, 62, 73, 76, 108-109</sup> Because of the pH gradient between the lysosomal or tumor milieu and the physiological environment, triggered exposure mechanisms of CPPs-cargo can be activated.

Exposure mechanisms include acid-degradable cross-links,<sup>73, 76, 109</sup> removal or enzyme degradation of protective coat<sup>21, 108</sup> and so on. These selective deliveries through triggered work mechanisms enhance the therapeutic efficiency of nanocarriers and decrease toxicity.

### **1.5.1 Exploiting the synergistic effects of targeting ligands and CPPs**

Cell-penetrating peptide (CPP)-based delivery systems represent a strategy that facilitates pharmaceutical import efficiently into cells<sup>110</sup> In many cases, this approach occurs with some lack of specificity that implies lower efficacy and safety during the whole process. As a result, this issue is probably one of the major drawbacks for the use of CPPs as delivery vehicles *in vivo*.<sup>69</sup> Novel approaches to improve the targeted delivery of biomolecules combined with CPPs, such as conjugation with targeting ligand in order to elicit cell surface binding and receptor-mediated endocytosis, have been developed.

In order to achieve a synergetic effect of targeting ligands and CPPs to improve cancer-cell selectivity, several research groups have focused the attention on the CPP-TPP (Tumor Targeting Peptide) conjugates in anticancer drug delivery for site specific transport of therapeutics. Conjugation of TTPs with CPPs facilitates the translocation of the conjugate unit to target tumor sites with enhanced specificity and selectivity.<sup>111</sup>

Furthermore, modifying anticancer agents with CPPs, for example, conjugating a TAT-derived CPP with an anti-Her-2/neu peptide mimetic,<sup>112</sup> AHNP, could selectively make this mimetic binds target to ErbB2, an epidermal growth factor receptor over-expressed in 30% of breast cancers.<sup>113</sup>

Synergistic effects of targeting ligands and CPPs can also be accomplished by employing a natural ligand (or a truncated version thereof) which can bind a receptor expressed on the target organ or tumor and penetrate cell membrane through endocytosis.<sup>114</sup> Additionally, exploiting bioinformatic design of a peptide library solves crystal structures can identify potential ligands for receptor targets These approaches bypass the need for screening and synthesizing large peptide libraries.<sup>115</sup> Moreover, direct targeting design can offer a good basis for the development of targeting tools.<sup>14</sup>

### **1.5.2 Future prospects of CPPs**

It is without doubt that from their first serendipitous discovery to the present day, CPPs have opened many doors to a wealth of biomedical and therapeutic opportunities both *in vitro* and *in vivo*. However, many features are still a matter of debate and open several scenarios for the future CPPs developments. *In vitro* CPP tracking demonstrated that a single mechanism could not explain the intracellular pathway of CPPs.<sup>13</sup>

Several differences in experimental conditions, for example the CPP concentration, the cell type, the conditions of incubation, the type and size of the cargo as well as the binding methodology, lead to the observation of contradictory results. There is still a major need to compare different CPP-mediated delivery systems in the same cell model. Recent attempts have been made to compare the effects of the cargo, but it is still impossible to define precise guidelines that might clarify all the observed divergences.

Moreover, the lack of cell specificity of CPPs along with their weakness to proteolytic cleavage under physiological conditions has led to the design of so-called ‘smart’ delivery

platforms, exploiting peculiar physiological or micro-environmental features related to the targeted tissue or cell type. CPP-modified nanocarriers should be designed in such a way so that during the first phase of their delivery surface CPP moieties are sterically shielded. After reaching their target (passively or actively), CPPs should be exposed under unique local conditions to enhance a penetration of the carrier through the cell membrane followed by intracellular delivery of its bioactive cargo. With these perspective, cancer cells metabolism and additional pathological conditions can be used as triggers for CPP exposure for an effective intracellular drug delivery.<sup>10</sup> Chemical modifications of the structure of known CPPs or logical design of novel CPPs represent also a new effective rationale that could improve CPPs efficiency as regards as specificity and resistance to proteolytic degradation in cellular environment.<sup>8</sup>

Finally, the abundance of drug-discovery data and now a growing mass of *in vivo* applications, also considering the current inefficiency of traditional drug-discovery programs, require the use of CPP technologies as biomedical tools and molecular therapeutics further into drug development and clinical setting.<sup>116</sup>

## **1.6 A case study: the gH625 cell-penetrating peptide**

The use and the study of the sequence “gH625” have been revolutionary in understanding the role of hydrophobic viral peptides. gH625 derives from glycoprotein H (gH) of *Herpes simplex virus type I*. *Herpes simplex virus* (HSV) is a well-known human pathogen with high range of worldwide morbidity and mortality and its complex multi-component entry technology has been widely studied because of its highest fusion capability.

It is not yet well understood the role of the other membranotropic sequences, in particular by the glycoprotein H. Nevertheless, it is now widely accepted that several regions are involved in the local destabilization of the membrane bilayer which tops in the fusion of the viral envelope with the host cell membrane.

gH625 was first selected and characterized in 2005,<sup>117</sup> and was initially identified using the WWIH (Wimley-White interfacial hydrophobicity) scale. Following works allowed to determine the many uses of this sequence (thanks to its fusion capability), from membrane fusion to viral inhibition and drug delivery.<sup>118-120</sup>



### 1.6.1 General description and membrane interactions

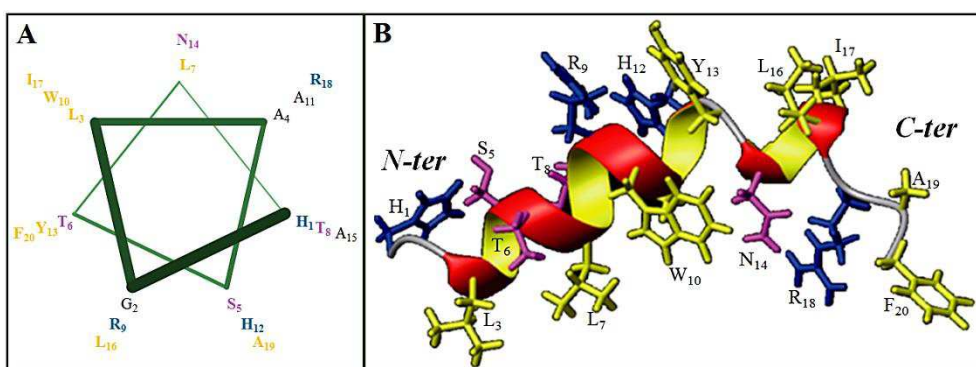
The twenty residue peptide gH625 (Figure 1.5 – HGLASTLTRWAHYNALIRAF – from aa 625 to aa 644) is rich in hydrophobic residues including glycines, leucines, alanines and aromatic residues like tryptophan and tyrosines, which are favorably located at the membrane interface. The peptide-lipid interactions starts with the action of the arginine residue (R<sub>18</sub>) located at the C-terminus, indeed the mutation of arginine strongly weakens the fusogenic properties of the peptide.<sup>121-124</sup>

The hydrophobic domain is also critical for the insertion of the peptide into the membrane and supports the opinion that hydrophobic interactions between cell membrane phospholipids and fusion proteins initiate membrane perturbation at the initial stages of viral fusion. The numerous biophysical experiments made on gH625 demonstrated that the peptide interacts with model membranes, enters the bilayer from its N-terminal side, has a tryptophan residue hidden inside the bilayer and adopts a helical conformation with its hydrophobic residues on one face of the helix and polar or charged residues on the opposite face (Figure 1.5 A).<sup>117, 122-123</sup>

The analysis of peptides with longer and shorter sequences resultant from this region and of their interactions with membranes demonstrated that the activity of this region depends on the amino acid sequence and on its length. The histidine residue at the N-terminus of the native sequence is also responsible to the increase fusion activity, since it helps both the initial interactions with the membrane and the oligomerization process:<sup>122</sup> this hypothesis is additionally supported by the fact that the histidine is placed at the N-terminus and the correct configuration of peptide appears to be crucial for the fusogenic function of several fusion proteins as well as its location in the membrane core after peptide-bilayer interaction. This histidine residue is sufficient to make the peptide approximately 8-fold more active.

gH625 powerfully interacts and naturally penetrates the lipid-phase and inserts into membranes with a  $\alpha$ -helical structure.<sup>122, 125-126</sup> Both the tryptophan and tyrosine are on the same side of the helix in the three-dimensional structure forming an amphiphilic helix, which on one side is constituted by aromatic and hydrophobic residues and on the other one is formed by hydrophilic or small residues (Figure 1.5 B).

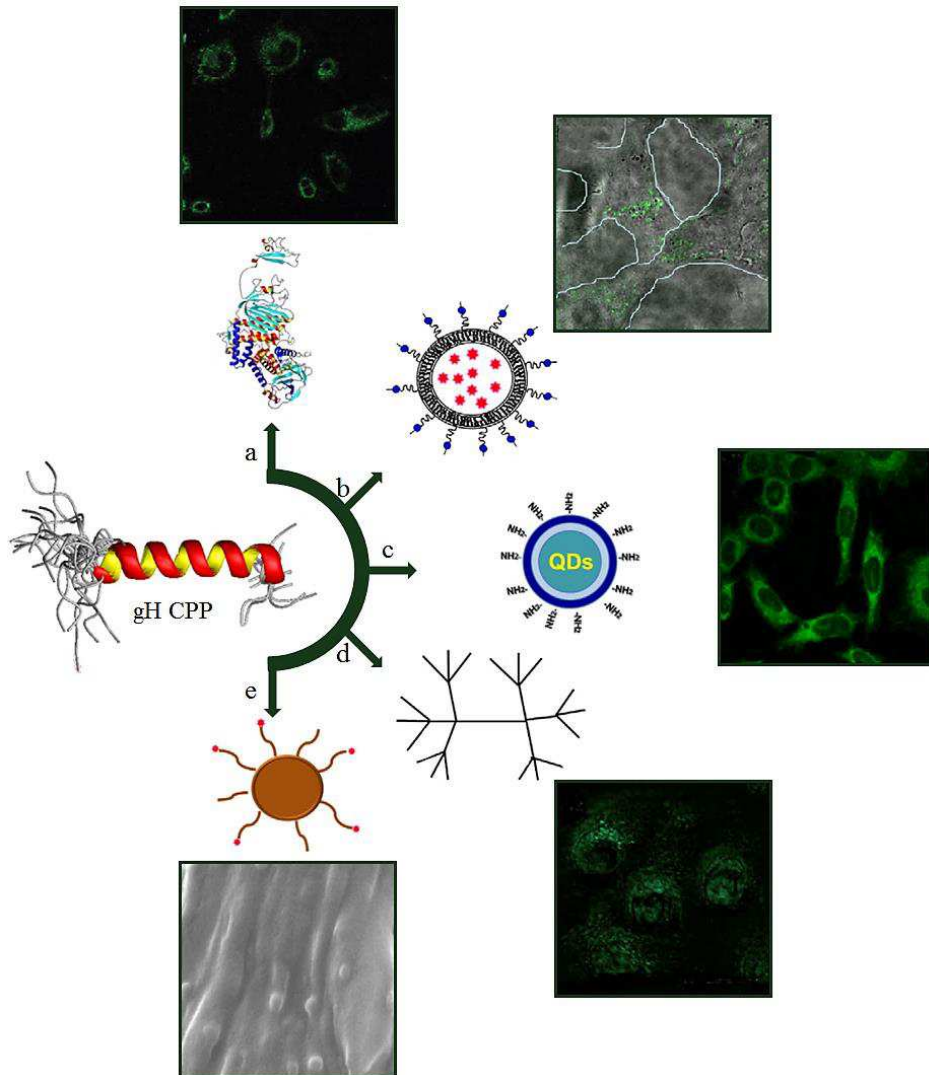
During the contact with the membrane the interaction between the aromatic ring of the tryptophan and the side chain of the tyrosine is fundamental for the structural stability. An amphipathic  $\alpha$ -helix of membranotropic peptides play a crucial role for mediating lipid-protein interactions during the binding of proteins to membranes; once bound, the hydrophobic face of the amphipathic peptide would allow the peptide to enter the membrane interior triggering local fusion of the membrane leaflets, transient pore formation, cracks and membrane fusion.<sup>30</sup> gH625 has the ability to penetrate deep into the bilayer as a helix without causing significant bilayer perturbations. This feature may help explaining its ability to perform various roles.



**Figure 1.5.** (A) Helical wheel representation and (B) energy-minimized structure of the amphipathic  $\alpha$ -helical model of the 20-mer gH625 peptide illustrate the amphiphilic character of gH625 peptide. All the hydrophobic residue side chain (yellow) fall on one face of the helix while the charged (blue) and the polar (violet) residues stays on the hydrophilic side of the helix. Adapted with permission of Ref. <sup>125</sup> © 2012 American Chemical Society.

## 1.6.2 Drug delivery application

The ability of gH625 to traverse the membrane bilayer has been recently validated, it also has the ability to transport several compounds into the cytosol, such as QDs,<sup>127-128</sup> liposomes,<sup>129</sup> NPs,<sup>130-132</sup> dendrimers<sup>133</sup> and proteins.<sup>134</sup> Examples of using gH625 as an intracellular delivery enhancer are described as follow (Figure 1.6).<sup>135</sup>



**Figure 1.6.** Major applications of gH625 peptide to drug delivery. Confocal microscopy images showing the internalization of gH625 functionalized: (a) proteins;<sup>134</sup> (b) liposomes;<sup>129</sup> (c) Quantum dots;<sup>127</sup> (d) dendrimers.<sup>133</sup> (e) Scanning electron microscopy images of functionalized polystyrene nanoparticles.<sup>131</sup> Adapted with permission of Ref. <sup>135</sup> © 2014 Elsevier B.V.

gH625-QD internalization was demonstrated to be highly successful and to implicate only to a minor degree the endocytic pathway.<sup>127</sup> Liposomes with gH625 and loaded with doxorubicin<sup>129</sup> were able to enter inside living HeLa cells; the results suggest that the functionalization of liposomes with gH625 could affect the uptake mechanism of liposomes and their intracellular distribution, and doxorubicin release. This information could be useful in the design of carriers for a controlled delivery and release of doxorubicin in order to avoid side effects associated to doxorubicin itself.

Dendrimers<sup>136-137</sup> also represent a very powerful instrument for drug delivery, combining the ideal size as *in vivo* carriers and multivalency of nanoparticles, the low cost, the tunable properties and biocompatibility of polymeric materials plus the monodispersity and detailed control of small molecules.<sup>137-138</sup> Their surface modification, by means of conjugation or adsorption of a biospecific ligand, may allow their delivery to specific sites and modulations of drug release minimizing toxic effects and increasing intracellular bioavailability.<sup>139</sup> The attachment of gH625 to dendrimer allows the conjugate to enter into the cellular matrix, whereas the un-functionalized dendrimer is omitted from translocation. The peptide-functionalized dendrimer is rapidly taken into the cells mainly through a non-active translocation mechanism.<sup>133</sup> The combination of the benefits of dendrimers and peptide chemistry could be useful for the development of a selective carrier, which could cross the membrane and be proficiently internalized into the cellular targets.

### **1.6.3 Delivery across the blood-brain barrier**

The blood-brain barrier (BBB) protects the brain and excludes many therapeutic drugs from entering.<sup>140</sup> Most of the strategies to transport drugs inside the central nervous system (CNS) cause disruption of the anatomical texture of the BBB, impairing its natural function; therefore, effective delivery approaches should be thoughtfully evaluated considering their effect on the function of the BBB.<sup>141-142</sup> Targeted delivery of a therapeutic cargo appears to be one of the most auspicious non-invasive approaches to overcome the BBB, combining the advantages of brain targeting, high incorporation capacity, reduction of side effects and circumvention of the multidrug efflux system.<sup>143-145</sup> Polystyrene nanoparticles (NPs) decorated on their surface by gH625 showed that the uptake of NPs by brain endothelial cells was superior than that of the NPs without the peptide, functionalized NPs were also free to move intracellularly.<sup>131</sup> Above all, gH625 decreased NP intracellular accumulation as large aggregates and improved the NP-BBB crossing with low toxicity.<sup>79</sup>

The ability of gH625 to cross the BBB *in vivo* was recently estimated.<sup>146</sup> gH625 was administered *in vivo* to rats and its presence in the liver and in the brain was detected within 3.5 h in proximity of cell neurites. gH625 has no toxic effect *in vivo*, since it does not affect brain maximal oxidative capacity and mitochondrial respiration rate.

gH625 constructs represents an innovative nanocarrier system for drug delivery to the central nervous system for its ability to cross the BBB. These results open new possibilities for direct delivery of drugs and might address the treatment of several human diseases.

gH625 is the first viral membranotropic peptide which can be used as delivery system for macromolecules *in vivo*; these results coupled with previous *in vitro* data support the view that gH625 enters the BBB without involving endocytic processes and damaging it. Hence, the eventual cargo may be immediately and completely available.<sup>146</sup> The use of such peptide-based ligand for targeted drug delivery *in vivo* may be restricted by the presence of several metabolic barriers. gH625 starts to degrade after 1 h of incubation but the intact peptide is still present after 3.5 h of incubation and thus could extend the brain targeting efficiency.<sup>146</sup>

## **1.7 Aim and Outline of the Thesis**

Intracellular delivery of potentially diagnostic or therapeutic molecules is one of the key problems in drug delivery because of the presence of the plasma membrane of cells. It represents an effective semi-permeable barrier that is essential to cell integrity and survival. Up to now, multiple and only partially successful attempts have been done to bring various drugs and drug-loaded pharmaceutical carriers directly into the cell cytoplasm bypassing the endocytic pathway, in order to protect cargoes from the lysosomal degradation. The discovery of cell-penetrating peptides (CPPs) launched a novel field in molecular delivery based on these non-invasive vectors. These peptides are able to cross cellular membranes and efficiently transport various biologically active molecules inside living cells and thus are considered promising devices for medical and biotechnological developments. Among this, gH625 CPP has shown exceptional vector properties. In fact, it is able to efficiently deliver a range of cargoes also by a non-endocytic pathway, avoiding endosomal entrapment producing the desired biochemical effect in the expected cellular localizations.

At the moment, researchers are focusing on the enhancement of CPPs cell specificity and the exploitation of novel technical strategies for pharmaceutical development of viable

CPP-carriers for drug delivery and numerous other applications. For these reasons, in this work, different gH625-based materials were designed in order to exploit the CPP properties in many field of nanomedicine. Moreover, in each Chapter an original biological application is proposed, where gH625 functionalization show considerable advantages in increasing the overall nanomaterial performances, such as changing their classical intracellular fate of endocytic pathway and mediating lysosomal escape. Following, the outline of the thesis is reported with a brief description of each chapter.

The **Chapter 1** of this thesis presents an introduction on Cell-Penetrating Peptides with an overview of their classification, cellular interaction and applications in biomedical field. Then, an outline of the “gH625” CPP is exposed, highlighting the potential application of this peptide in nanomedicine. In **Chapter 2** we focused on the combined effects of gH625 peptide and reverse transfection to develop a gene delivery platform based on functionalized polyethylenimine (PEI)/DNA polyplexes. We created a PEI based vector in which the gH625 was covalently coupled to 25 kDa PEI through a heterobifunctional polyethyleneglycol (PEG) spacer. Transfection and cell viability assays were carried out using adsorbed or covalent bonded complexes on glass surface. In **Chapter 3** we analyzed the role of particle size in influencing the ability of the gH625 membranotropic peptide to escape the endo-lysosomal pathway and deliver the particles in the cytosol. To this aim, we carried out a systematic assessment of cellular uptake and distribution of monodisperse platinum nanoparticles (PtNPs), having different diameters (2.5, 5 and 20 nm) and citrate capping or gH625 peptide functionalization.

Moreover, gH625 also demonstrated the ability to penetrate the Blood Brain Barrier (BBB) both *in vitro* and *in vivo*. In **Chapter 4**, this feature was exploited analyzing the behavior of gH625 in dual-functionalized polymeric carrier systems for targeted drug delivery across the BBB. The specificity of the nanomaterial in targeting the BBB is given by the peptide CRTIGPSVC (CRT), which functionally mimics the endogenous iron and promotes the crossing. Finally, in **Chapter 5**, a summary about the main results achieved in this thesis is presented and future applications are proposed.

## 1.8 References

1. Sugano, K.; Kansy, M.; Artursson, P.; Avdeef, A.; Bendels, S.; Di, L.; Ecker, G. F.; Faller, B.; Fischer, H.; Gerebtzoff, G., Coexistence of passive and carrier-mediated processes in drug transport. *Nature reviews. Drug discovery* **2010**, *9* (8), 597.
2. Kell, D. B.; Dobson, P. D.; Oliver, S. G., Pharmaceutical drug transport: the issues and the implications that it is essentially carrier-mediated only. *Drug discovery today* **2011**, *16* (15), 704-714.
3. Di, L.; Artursson, P.; Avdeef, A.; Ecker, G. F.; Faller, B.; Fischer, H.; Houston, J. B.; Kansy, M.; Kerns, E. H.; Krämer, S. D., Evidence-based approach to assess passive diffusion and carrier-mediated drug transport. *Drug discovery today* **2012**, *17* (15), 905-912.
4. Frankel, A. D.; Pabo, C. O., Cellular uptake of the tat protein from human immunodeficiency virus. *Cell* **1988**, *55* (6), 1189-1193.
5. Green, M.; Loewenstein, P. M., Autonomous functional domains of chemically synthesized human immunodeficiency virus tat trans-activator protein. *Cell* **1988**, *55* (6), 1179-1188.
6. Derossi, D.; Joliot, A. H.; Chassaing, G.; Prochiantz, A., The third helix of the Antennapedia homeodomain translocates through biological membranes. *Journal of Biological Chemistry* **1994**, *269* (14), 10444-10450.
7. Järver, P.; Langel, Ü., Cell-penetrating peptides—a brief introduction. *Biochimica et Biophysica Acta (BBA)-Biomembranes* **2006**, *1758* (3), 260-263.
8. Copolovici, D. M.; Langel, K.; Eriste, E.; Langel, U., Cell-penetrating peptides: design, synthesis, and applications. *ACS nano* **2014**, *8* (3), 1972-1994.
9. Heitz, F.; Morris, M. C.; Divita, G., Twenty years of cell-penetrating peptides: from molecular mechanisms to therapeutics. *British journal of pharmacology* **2009**, *157* (2), 195-206.
10. Koren, E.; Torchilin, V. P., Cell-penetrating peptides: breaking through to the other side. *Trends in molecular medicine* **2012**, *18* (7), 385-393.
11. Mitchell, D. J.; Steinman, L.; Kim, D.; Fathman, C.; Rothbard, J., Polyarginine enters cells more efficiently than other polycationic homopolymers. *Chemical Biology & Drug Design* **2000**, *56* (5), 318-325.
12. Lindgren, M.; Langel, Ü., Classes and prediction of cell-penetrating peptides. *Cell-penetrating peptides: Methods and protocols* **2011**, 3-19.
13. Madani, F.; Lindberg, S.; Langel, Ü.; Futaki, S.; Gräslund, A., Mechanisms of cellular uptake of cell-penetrating peptides. *Journal of Biophysics* **2011**, *2011*.
14. Wang, F.; Wang, Y.; Zhang, X.; Zhang, W.; Guo, S.; Jin, F., Recent progress of cell-penetrating peptides as new carriers for intracellular cargo delivery. *Journal of Controlled Release* **2014**, *174*, 126-136.
15. Ziegler, A., Thermodynamic studies and binding mechanisms of cell-penetrating peptides with lipids and glycosaminoglycans. *Advanced drug delivery reviews* **2008**, *60* (4), 580-597.

16. El-Sayed, A.; Futaki, S.; Harashima, H., Delivery of macromolecules using arginine-rich cell-penetrating peptides: ways to overcome endosomal entrapment. *The AAPS journal* **2009**, *11* (1), 13-22.
17. Foged, C.; Nielsen, H. M., Cell-penetrating peptides for drug delivery across membrane barriers. *Expert opinion on drug delivery* **2008**, *5* (1), 105-117.
18. Verdurmen, W. P.; Brock, R., Biological responses towards cationic peptides and drug carriers. *Trends in pharmacological sciences* **2011**, *32* (2), 116-124.
19. Kale, A. A.; Torchilin, V. P., Enhanced transfection of tumor cells in vivo using “Smart” pH-sensitive TAT-modified pegylated liposomes. *Journal of drug targeting* **2007**, *15* (7-8), 538-545.
20. Maiolo, J. R.; Ferrer, M.; Ottinger, E. A., Effects of cargo molecules on the cellular uptake of arginine-rich cell-penetrating peptides. *Biochimica et Biophysica Acta (BBA)-Biomembranes* **2005**, *1712* (2), 161-172.
21. Kale, A. A.; Torchilin, V. P., “Smart” drug carriers: PEGylated TATp-modified pH-sensitive liposomes. *Journal of liposome research* **2007**, *17* (3-4), 197-203.
22. Abes, R.; Moulton, H. M.; Clair, P.; Yang, S.-T.; Abes, S.; Melikov, K.; Prevot, P.; Youngblood, D. S.; Iversen, P. L.; Chernomordik, L. V., Delivery of steric block morpholino oligomers by (RXR) 4 peptides: structure–activity studies. *Nucleic acids research* **2008**, *36* (20), 6343-6354.
23. Harris, F.; Wallace, J.; Phoenix, D., Use of hydrophobic moment plot methodology to aid the identification of oblique orientated  $\alpha$ -helices. *Molecular membrane biology* **2000**, *17* (4), 201-207.
24. Deshayes, S.; Plénat, T.; Aldrian-Herrada, G.; Divita, G.; Le Grimellec, C.; Heitz, F., Primary amphipathic cell-penetrating peptides: structural requirements and interactions with model membranes. *Biochemistry* **2004**, *43* (24), 7698-7706.
25. Lundberg, P.; Magzoub, M.; Lindberg, M.; Hällbrink, M.; Jarvet, J.; Eriksson, L.; Langel, Ü.; Gräslund, A., Cell membrane translocation of the N-terminal (1–28) part of the prion protein. *Biochemical and biophysical research communications* **2002**, *299* (1), 85-90.
26. Rydström, A.; Deshayes, S.; Konate, K.; Crombez, L.; Padari, K.; Boukhaddaoui, H.; Aldrian, G.; Pooga, M.; Divita, G., Direct translocation as major cellular uptake for CADY self-assembling peptide-based nanoparticles. *PloS one* **2011**, *6* (10), e25924.
27. Nan, Y. H.; Park, I. S.; Hahm, K. S.; Shin, S. Y., Antimicrobial activity, bactericidal mechanism and LPS-neutralizing activity of the cell-penetrating peptide pVEC and its analogs. *Journal of Peptide Science* **2011**, *17* (12), 812-817.
28. Johansson, H. J.; El-Andaloussi, S.; Holm, T.; Mäe, M.; Jänes, J.; Maimets, T.; Langel, Ü., Characterization of a novel Cytotoxic cell-penetrating Peptide Derived from p14ARF protein. *Molecular Therapy* **2008**, *16* (1), 115-123.
29. Magzoub, M.; Sandgren, S.; Lundberg, P.; Oglęcka, K.; Lilja, J.; Witttrup, A.; Eriksson, L. G.; Langel, Ü.; Belting, M.; Gräslund, A., N-terminal peptides from unprocessed prion proteins enter cells by macropinocytosis. *Biochemical and biophysical research communications* **2006**, *348* (2), 379-385.



30. Beevers, A. J.; Dixon, A. M., Helical membrane peptides to modulate cell function. *Chemical Society Reviews* **2010**, *39* (6), 2146-2157.
31. Eguchi, A.; Dowdy, S. F., siRNA delivery using peptide transduction domains. *Trends in pharmacological sciences* **2009**, *30* (7), 341-345.
32. Joanne, P.; Nicolas, P.; El Amri, C., Antimicrobial peptides and viral fusion peptides: how different they are? *Protein and peptide letters* **2009**, *16* (7), 743-750.
33. Schafmeister, C. E.; Po, J.; Verdine, G. L., An all-hydrocarbon cross-linking system for enhancing the helicity and metabolic stability of peptides. *Journal of the American Chemical Society* **2000**, *122* (24), 5891-5892.
34. Ochocki, J. D.; Mullen, D. G.; Wattenberg, E. V.; Distefano, M. D., Evaluation of a cell penetrating prenylated peptide lacking an intrinsic fluorophore via in situ click reaction. *Bioorganic & medicinal chemistry letters* **2011**, *21* (17), 4998-5001.
35. Covic, L.; Gresser, A. L.; Talavera, J.; Swift, S.; Kuliopulos, A., Activation and inhibition of G protein-coupled receptors by cell-penetrating membrane-tethered peptides. *Proceedings of the National Academy of Sciences* **2002**, *99* (2), 643-648.
36. Watkins, C. L.; Brennan, P.; Fegan, C.; Takayama, K.; Nakase, I.; Futaki, S.; Jones, A. T., Cellular uptake, distribution and cytotoxicity of the hydrophobic cell penetrating peptide sequence PFVYLI linked to the proapoptotic domain peptide PAD. *Journal of Controlled Release* **2009**, *140* (3), 237-244.
37. Fernández-Carneado, J.; Kogan, M. J.; Pujals, S.; Giralt, E., Amphipathic peptides and drug delivery. *Peptide Science* **2004**, *76* (2), 196-203.
38. Deshayes, S.; Morris, M.; Heitz, F.; Divita, G., Delivery of proteins and nucleic acids using a non-covalent peptide-based strategy. *Advanced drug delivery reviews* **2008**, *60* (4), 537-547.
39. Pujals, S.; Giralt, E., Proline-rich, amphipathic cell-penetrating peptides. *Advanced drug delivery reviews* **2008**, *60* (4), 473-484.
40. Pujals, S.; Sabido, E.; Tarrago, T.; Giralt, E., all-D proline-rich cell-penetrating peptides: a preliminary in vivo internalization study. Portland Press Limited: 2007.
41. Farrera-Sinfreu, J.; Giralt, E.; Castel, S.; Albericio, F.; Royo, M., Cell-penetrating cis- $\gamma$ -amino-l-proline-derived peptides. *Journal of the American Chemical Society* **2005**, *127* (26), 9459-9468.
42. Cavalli, S.; Carbajo, D.; Acosta, M.; Lope-Piedrafita, S.; Candiota, A. P.; Arus, C.; Royo, M.; Albericio, F., Efficient  $\gamma$ -amino-proline-derived cell penetrating peptide–superparamagnetic iron oxide nanoparticle conjugates via aniline-catalyzed oxime chemistry as bimodal imaging nanoagents. *Chemical Communications* **2012**, *48* (43), 5322-5324.
43. Ezzat, K.; EL Andaloussi, S.; Zaghoul, E. M.; Lehto, T.; Lindberg, S.; Moreno, P. M.; Viola, J. R.; Magdy, T.; Abdo, R.; Guterstam, P., PepFect 14, a novel cell-penetrating peptide for oligonucleotide delivery in solution and as solid formulation. *Nucleic acids research* **2011**, *39* (12), 5284-5298.
44. Patel, L. N.; Zaro, J. L.; Shen, W.-C., Cell penetrating peptides: intracellular pathways and pharmaceutical perspectives. *Pharmaceutical research* **2007**, *24* (11), 1977-1992.

45. Angeles-Boza, A. M.; Erazo-Oliveras, A.; Lee, Y.-J.; Pellois, J.-P., Generation of endosomolytic reagents by branching of cell-penetrating peptides: tools for the delivery of bioactive compounds to live cells in cis or trans. *Bioconjugate chemistry* **2010**, *21* (12), 2164-2167.
46. Bode, S. A.; Wallbrecher, R.; Brock, R.; van Hest, J. C.; Löwik, D. W., Activation of cell-penetrating peptides by disulfide bridge formation of truncated precursors. *Chemical Communications* **2014**, *50* (4), 415-417.
47. Farrera-Sinfreu, J.; Giralt, E.; Royo, M.; Albericio, F., Cell-penetrating proline-rich peptidomimetics. *Peptide Characterization and Application Protocols* **2007**, 241-267.
48. Hoyer, J.; Neundorf, I., Knockdown of a G protein-coupled receptor through efficient peptide-mediated siRNA delivery. *Journal of controlled release* **2012**, *161* (3), 826-834.
49. Hoyer, J.; Schatzschneider, U.; Schulz-Siegmund, M.; Neundorf, I., Dimerization of a cell-penetrating peptide leads to enhanced cellular uptake and drug delivery. *Beilstein journal of organic chemistry* **2012**, *8*, 1788.
50. Lempens, E. H.; Merckx, M.; Tirrell, M.; Meijer, E., Dendrimer display of tumor-homing peptides. *Bioconjugate chemistry* **2011**, *22* (3), 397-405.
51. Saleh, A. F.; Arzumanov, A.; Abes, R.; Owen, D.; Lebleu, B.; Gait, M. J., Synthesis and splice-redirecting activity of branched, arginine-rich peptide dendrimer conjugates of peptide nucleic acid oligonucleotides. *Bioconjugate chemistry* **2010**, *21* (10), 1902-1911.
52. Mandal, D.; Nasrolahi Shirazi, A.; Parang, K., Cell-Penetrating Homochiral Cyclic Peptides as Nuclear-Targeting Molecular Transporters. *Angewandte Chemie International Edition* **2011**, *50* (41), 9633-9637.
53. Fonseca, S. B.; Pereira, M. P.; Kelley, S. O., Recent advances in the use of cell-penetrating peptides for medical and biological applications. *Advanced drug delivery reviews* **2009**, *61* (11), 953-964.
54. Derossi, D.; Calvet, S.; Trembleau, A.; Brunissen, A.; Chassaing, G.; Prochiantz, A., Cell internalization of the third helix of the Antennapedia homeodomain is receptor-independent. *Journal of Biological Chemistry* **1996**, *271* (30), 18188-18193.
55. Conner, S. D.; Schmid, S. L., Regulated portals of entry into the cell. *Nature* **2003**, *422* (6927), 37.
56. Bechara, C.; Sagan, S., Cell-penetrating peptides: 20 years later, where do we stand? *FEBS letters* **2013**, *587* (12), 1693-1702.
57. Trabulo, S.; Cardoso, A. L.; Mano, M.; De Lima, M. C. P., Cell-penetrating peptides—mechanisms of cellular uptake and generation of delivery systems. *Pharmaceuticals* **2010**, *3* (4), 961-993.
58. Matsuzaki, K.; Yoneyama, S.; Murase, O.; Miyajima, K., Transbilayer transport of ions and lipids coupled with mastoparan X translocation. *Biochemistry* **1996**, *35* (25), 8450-8456.
59. Pouny, Y.; Rapaport, D.; Mor, A.; Nicolas, P.; Shai, Y., Interaction of antimicrobial dermaseptin and its fluorescently labeled analogs with phospholipid membranes. *Biochemistry* **1992**, *31* (49), 12416-12423.

60. Lee, M.-T.; Hung, W.-C.; Chen, F.-Y.; Huang, H. W., Many-body effect of antimicrobial peptides: on the correlation between lipid's spontaneous curvature and pore formation. *Biophysical journal* **2005**, *89* (6), 4006-4016.
61. Wadia, J. S.; Stan, R. V.; Dowdy, S. F., Transducible TAT-HA fusogenic peptide enhances escape of TAT-fusion proteins after lipid raft macropinocytosis. *Nature medicine* **2004**, *10* (3), 310.
62. Rothbard, J. B.; Jessop, T. C.; Lewis, R. S.; Murray, B. A.; Wender, P. A., Role of membrane potential and hydrogen bonding in the mechanism of translocation of guanidinium-rich peptides into cells. *Journal of the American Chemical Society* **2004**, *126* (31), 9506-9507.
63. Duchardt, F.; Fotin-Mleczek, M.; Schwarz, H.; Fischer, R.; Brock, R., A comprehensive model for the cellular uptake of cationic cell-penetrating peptides. *Traffic* **2007**, *8* (7), 848-866.
64. Kosuge, M.; Takeuchi, T.; Nakase, I.; Jones, A. T.; Futaki, S., Cellular internalization and distribution of arginine-rich peptides as a function of extracellular peptide concentration, serum, and plasma membrane associated proteoglycans. *Bioconjugate chemistry* **2008**, *19* (3), 656-664.
65. Deshayes, S.; Morris, M. C.; Divita, G.; Heitz, F., Interactions of amphipathic CPPs with model membranes. *Biochimica et Biophysica Acta (BBA)-Biomembranes* **2006**, *1758* (3), 328-335.
66. Derossi, D.; Chassaing, G.; Prochiantz, A., Trojan peptides: the penetratin system for intracellular delivery. *Trends in cell biology* **1998**, *8* (2), 84-87.
67. Jones, A. T., Macropinocytosis: searching for an endocytic identity and role in the uptake of cell penetrating peptides. *Journal of cellular and molecular medicine* **2007**, *11* (4), 670-684.
68. Mayor, S.; Pagano, R. E., Pathways of clathrin-independent endocytosis. *Nature reviews Molecular cell biology* **2007**, *8* (8), 603-612.
69. Vivès, E.; Schmidt, J.; Pèlegri, A., Cell-penetrating and cell-targeting peptides in drug delivery. *Biochimica et Biophysica Acta (BBA)-Reviews on Cancer* **2008**, *1786* (2), 126-138.
70. Brock, R., The uptake of arginine-rich cell-penetrating peptides: putting the puzzle together. *Bioconjugate chemistry* **2014**, *25* (5), 863-868.
71. Nakase, I.; Tanaka, G.; Futaki, S., Cell-penetrating peptides (CPPs) as a vector for the delivery of siRNAs into cells. *Molecular BioSystems* **2013**, *9* (5), 855-861.
72. Padari, K.; Koppel, K.; Lorents, A.; Hällbrink, M.; Mano, M.; Pedroso de Lima, M. C.; Pooga, M., S413-PV cell-penetrating peptide forms nanoparticle-like structures to gain entry into cells. *Bioconjugate chemistry* **2010**, *21* (4), 774-783.
73. Tünnemann, G.; Martin, R. M.; Haupt, S.; Patsch, C.; Edenhofer, F.; Cardoso, M. C., Cargo-dependent mode of uptake and bioavailability of TAT-containing proteins and peptides in living cells. *The FASEB journal* **2006**, *20* (11), 1775-1784.
74. de la Fuente, J. M.; Berry, C. C., Tat peptide as an efficient molecule to translocate gold nanoparticles into the cell nucleus. *Bioconjugate chemistry* **2005**, *16* (5), 1176-1180.

75. Fischer, R.; Waizenegger, T.; Köhler, K.; Brock, R., A quantitative validation of fluorophore-labelled cell-permeable peptide conjugates: fluorophore and cargo dependence of import. *Biochimica et Biophysica Acta (BBA)-Biomembranes* **2002**, *1564* (2), 365-374.
76. Lundberg, P.; El-Andaloussi, S.; Sütlü, T.; Johansson, H.; Langel, Ü., Delivery of short interfering RNA using endosomolytic cell-penetrating peptides. *The FASEB Journal* **2007**, *21* (11), 2664-2671.
77. Mäe, M.; Langel, Ü., Cell-penetrating peptides as vectors for peptide, protein and oligonucleotide delivery. *Current opinion in pharmacology* **2006**, *6* (5), 509-514.
78. Mellman, I.; Fuchs, R.; Helenius, A., Acidification of the endocytic and exocytic pathways. *Annual review of biochemistry* **1986**, *55* (1), 663-700.
79. Guarnieri, D.; Muscetti, O.; Falanga, A.; Fusco, S.; Belli, V.; Perillo, E.; Battista, E.; Panzetta, V.; Galdiero, S.; Netti, P., Surface decoration with gH625-membranotropic peptides as a method to escape the endo-lysosomal compartment and reduce nanoparticle toxicity. *Nanotechnology* **2015**, *26* (41), 415101.
80. Whitehead, K. A.; Langer, R.; Anderson, D. G., Knocking down barriers: advances in siRNA delivery. *Nature reviews. Drug discovery* **2009**, *8* (2), 129.
81. Özel, R. E.; Alkasir, R. S.; Ray, K.; Wallace, K. N.; Andreescu, S., Comparative evaluation of intestinal nitric oxide in embryonic zebrafish exposed to metal oxide nanoparticles. *Small* **2013**, *9* (24), 4250-4261.
82. Wu, X.; Tan, Y.; Mao, H.; Zhang, M., Toxic effects of iron oxide nanoparticles on human umbilical vein endothelial cells. *International journal of nanomedicine* **2010**, *5*, 385.
83. Bacchetta, R.; Santo, N.; Fascio, U.; Moschini, E.; Freddi, S.; Chirico, G.; Camatini, M.; Mantecca, P., Nano-sized CuO, TiO<sub>2</sub> and ZnO affect *Xenopus laevis* development. *Nanotoxicology* **2012**, *6* (4), 381-398.
84. Kichler, A.; Mason, A. J.; Bechinger, B., Cationic amphipathic histidine-rich peptides for gene delivery. *Biochimica et Biophysica Acta (BBA)-Biomembranes* **2006**, *1758* (3), 301-307.
85. Liang, W.; Lam, J. K., Endosomal escape pathways for non-viral nucleic acid delivery systems. In *Molecular regulation of endocytosis*, InTech: 2012.
86. Gupta, B.; Levchenko, T. S.; Torchilin, V. P., Intracellular delivery of large molecules and small particles by cell-penetrating proteins and peptides. *Advanced drug delivery reviews* **2005**, *57* (4), 637-651.
87. Torchilin, V. P., Cell penetrating peptide-modified pharmaceutical nanocarriers for intracellular drug and gene delivery. *Peptide Science* **2008**, *90* (5), 604-610.
88. Lindberg, S.; Copolovici, D. M.; Langel, Ü., Therapeutic delivery opportunities, obstacles and applications for cell-penetrating peptides. *Therapeutic delivery* **2011**, *2* (1), 71-82.
89. Langel, Ü., Handbook of Cell-Penetrating Peptides:(Eds.: U. Langel) CRC Taylor & Francis. *Boca Raton* **2007**.
90. Segura, T.; Shea, L. D., Materials for non-viral gene delivery. *Annual Review of Materials Research* **2001**, *31* (1), 25-46.

91. Hayashi, Y.; Yamauchi, J.; Khalil, I. A.; Kajimoto, K.; Akita, H.; Harashima, H., Cell penetrating peptide-mediated systemic siRNA delivery to the liver. *International journal of pharmaceutics* **2011**, *419* (1), 308-313.
92. Yamano, S.; Dai, J.; Hanatani, S.; Haku, K.; Yamanaka, T.; Ishioka, M.; Takayama, T.; Yuvienco, C.; Khapli, S.; Moursi, A. M., Long-term efficient gene delivery using polyethylenimine with modified Tat peptide. *Biomaterials* **2014**, *35* (5), 1705-1715.
93. Shin, M. J.; Kim, D. W.; Lee, Y. P.; Ahn, E. H.; Jo, H. S.; Kim, D.-S.; Kwon, O.-S.; Kang, T.-C.; Cho, Y.-J.; Park, J., Tat-glyoxalase protein inhibits against ischemic neuronal cell damage and ameliorates ischemic injury. *Free Radical Biology and Medicine* **2014**, *67*, 195-210.
94. Kwon, H. Y.; Eum, W. S.; Jang, H. W.; Kang, J. H.; Ryu, J.; Ryong Lee, B.; Jin, L. H.; Park, J.; Choi, S. Y., Transduction of Cu, Zn-superoxide dismutase mediated by an HIV-1 Tat protein basic domain into mammalian cells. *FEBS letters* **2000**, *485* (2-3), 163-167.
95. Jin, L. H.; Bahn, J. H.; Eum, W. S.; Kwon, H. Y.; Jang, S. H.; Han, K. H.; Kang, T.-C.; Won, M. H.; Kang, J. H.; Cho, S.-W., Transduction of human catalase mediated by an HIV-1 TAT protein basic domain and arginine-rich peptides into mammalian cells. *Free Radical Biology and Medicine* **2001**, *31* (11), 1509-1519.
96. Tobias, J. S.; Hochhauser, D.; Tobias, J., *Cancer and its management*. John Wiley & Sons: 2014.
97. Stewart, K. M.; Horton, K. L.; Kelley, S. O., Cell-penetrating peptides as delivery vehicles for biology and medicine. *Organic & biomolecular chemistry* **2008**, *6* (13), 2242-2255.
98. Nakase, I.; Konishi, Y.; Ueda, M.; Saji, H.; Futaki, S., Accumulation of arginine-rich cell-penetrating peptides in tumors and the potential for anticancer drug delivery in vivo. *Journal of controlled release* **2012**, *159* (2), 181-188.
99. Cai, D.; Gao, W.; He, B.; Dai, W.; Zhang, H.; Wang, X.; Wang, J.; Zhang, X.; Zhang, Q., Hydrophobic penetrating peptide PFVYLI-modified stealth liposomes for doxorubicin delivery in breast cancer therapy. *Biomaterials* **2014**, *35* (7), 2283-2294.
100. Olson, E. S.; Whitney, M. A.; Friedman, B.; Aguilera, T. A.; Crisp, J. L.; Baik, F. M.; Jiang, T.; Baird, S. M.; Tsimikas, S.; Tsien, R. Y., In vivo fluorescence imaging of atherosclerotic plaques with activatable cell-penetrating peptides targeting thrombin activity. *Integrative Biology* **2012**, *4* (6), 595-605.
101. Barnett, E. M.; Zhang, X.; Maxwell, D.; Chang, Q.; Piwnica-Worms, D., Single-cell imaging of retinal ganglion cell apoptosis with a cell-penetrating, activatable peptide probe in an in vivo glaucoma model. *Proceedings of the National Academy of Sciences* **2009**, *106* (23), 9391-9396.
102. Huang, C.-W.; Li, Z.; Conti, P. S., In Vivo Near-Infrared Fluorescence Imaging of Integrin  $\alpha 2\beta 1$  in Prostate Cancer with Cell-Penetrating Peptide-Conjugated DGEA Probe. *Journal of Nuclear Medicine* **2011**, *52* (12), 1979-1986.

103. Olson, E. S.; Jiang, T.; Aguilera, T. A.; Nguyen, Q. T.; Ellies, L. G.; Scadeng, M.; Tsien, R. Y., Activatable cell penetrating peptides linked to nanoparticles as dual probes for in vivo fluorescence and MR imaging of proteases. *Proceedings of the National Academy of Sciences* **2010**, *107* (9), 4311-4316.
104. Kamei, N.; Morishita, M.; Kanayama, Y.; Hasegawa, K.; Nishimura, M.; Hayashinaka, E.; Wada, Y.; Watanabe, Y.; Takayama, K., Molecular imaging analysis of intestinal insulin absorption boosted by cell-penetrating peptides by using positron emission tomography. *Journal of Controlled Release* **2010**, *146* (1), 16-22.
105. Wang, H.-Y.; Chen, J.-X.; Sun, Y.-X.; Deng, J.-Z.; Li, C.; Zhang, X.-Z.; Zhuo, R.-X., Construction of cell penetrating peptide vectors with N-terminal stearylated nuclear localization signal for targeted delivery of DNA into the cell nuclei. *Journal of controlled release* **2011**, *155* (1), 26-33.
106. Milletti, F., Cell-penetrating peptides: classes, origin, and current landscape. *Drug discovery today* **2012**, *17* (15), 850-860.
107. Bolhassani, A., Potential efficacy of cell-penetrating peptides for nucleic acid and drug delivery in cancer. *Biochimica et Biophysica Acta (BBA)-Reviews on Cancer* **2011**, *1816* (2), 232-246.
108. Jiang, T.; Zhang, Z.; Zhang, Y.; Lv, H.; Zhou, J.; Li, C.; Hou, L.; Zhang, Q., Dual-functional liposomes based on pH-responsive cell-penetrating peptide and hyaluronic acid for tumor-targeted anticancer drug delivery. *Biomaterials* **2012**, *33* (36), 9246-9258.
109. Lorents, A.; Kodavali, P. K.; Oskolkov, N.; Langel, Ü.; Hällbrink, M.; Pooga, M., Cell-penetrating peptides split into two groups based on modulation of intracellular calcium concentration. *Journal of Biological Chemistry* **2012**, *287* (20), 16880-16889.
110. Govindarajan, S.; Sivakumar, J.; Garimidi, P.; Rangaraj, N.; Kumar, J. M.; Rao, N. M.; Gopal, V., Targeting human epidermal growth factor receptor 2 by a cell-penetrating peptide–affibody bioconjugate. *Biomaterials* **2012**, *33* (8), 2570-2582.
111. Regberg, J.; Srimanee, A.; Langel, Ü., Applications of cell-penetrating peptides for tumor targeting and future cancer therapies. *Pharmaceuticals* **2012**, *5* (9), 991-1007.
112. Tan, M.; Lan, K.-H.; Yao, J.; Lu, C.-H.; Sun, M.; Neal, C. L.; Lu, J.; Yu, D., Selective inhibition of ErbB2-overexpressing breast cancer in vivo by a novel TAT-based ErbB2-targeting signal transducers and activators of transcription 3–blocking peptide. *Cancer research* **2006**, *66* (7), 3764-3772.
113. Tan, M.; Yao, J.; Yu, D., Overexpression of the c-erbB-2 gene enhanced intrinsic metastasis potential in human breast cancer cells without increasing their transformation abilities. *Cancer Research* **1997**, *57* (6), 1199-1205.
114. Park, B.-W.; Hong-Tao, Z.; Wu, C.; Berezov, A.; Zhang, X.; Dua, R.; Wang, Q.; Kao, G.; O'Rourke, D. M.; Greene, M. I., Rationally designed anti-HER2/neu peptide mimetic disables P185HER2/neu tyrosine kinases in vitro and in vivo. *Nature biotechnology* **2000**, *18* (2), 194.
115. Svensen, N.; Walton, J. G.; Bradley, M., Peptides for cell-selective drug delivery. *Trends in pharmacological sciences* **2012**, *33* (4), 186-192.

116. Howl, J.; Nicholl, I. D.; Jones, S., The many futures for cell-penetrating peptides: how soon is now? Portland Press Limited: 2007.
117. Galdiero, S.; Falanga, A.; Vitiello, M.; Browne, H.; Pedone, C.; Galdiero, M., Fusogenic domains in herpes simplex virus type 1 glycoprotein H. *Journal of Biological Chemistry* **2005**, *280* (31), 28632-28643.
118. Galdiero, S.; Falanga, A.; Vitiello, M.; Grieco, P.; Caraglia, M.; Morelli, G.; Galdiero, M., Exploitation of viral properties for intracellular delivery. *Journal of Peptide Science* **2014**, *20* (7), 468-478.
119. Galdiero, S.; Falanga, A.; Tarallo, R.; Russo, L.; Galdiero, E.; Cantisani, M.; Morelli, G.; Galdiero, M., Peptide inhibitors against herpes simplex virus infections. *Journal of Peptide Science* **2013**, *19* (3), 148-158.
120. Vitiello, G.; Falanga, A.; Galdiero, M.; Marsh, D.; Galdiero, S.; D'Errico, G., Lipid composition modulates the interaction of peptides deriving from herpes simplex virus type I glycoproteins B and H with biomembranes. *Biochimica et Biophysica Acta (BBA)-Biomembranes* **2011**, *1808* (10), 2517-2526.
121. Galdiero, S.; Falanga, A.; Vitiello, M.; D'Isanto, M.; Cantisani, M.; Kampanaraki, A.; Benedetti, E.; Browne, H.; Galdiero, M., Peptides containing membrane-interacting motifs inhibit herpes simplex virus type 1 infectivity. *Peptides* **2008**, *29* (9), 1461-1471.
122. Galdiero, S.; Falanga, A.; Vitiello, M.; Raiola, L.; Russo, L.; Pedone, C.; Isernia, C.; Galdiero, M., The presence of a single N-terminal histidine residue enhances the fusogenic properties of a membranotropic peptide derived from herpes simplex virus type 1 glycoprotein H. *Journal of Biological Chemistry* **2010**, *285* (22), 17123-17136.
123. Galdiero, S.; Falanga, A.; Vitiello, M.; Raiola, L.; Fattorusso, R.; Browne, H.; Pedone, C.; Isernia, C.; Galdiero, M., Analysis of a membrane interacting region of herpes simplex virus type 1 glycoprotein H. *Journal of Biological Chemistry* **2008**, *283* (44), 29993-30009.
124. Badani, H.; Garry, R. F.; Wimley, W. C., Peptide entry inhibitors of enveloped viruses: the importance of interfacial hydrophobicity. *Biochimica et Biophysica Acta (BBA)-Biomembranes* **2014**, *1838* (9), 2180-2197.
125. Galdiero, S.; Russo, L.; Falanga, A.; Cantisani, M.; Vitiello, M.; Fattorusso, R.; Malgieri, G.; Galdiero, M.; Isernia, C., Structure and orientation of the gH625-644 membrane interacting region of herpes simplex virus type 1 in a membrane mimetic system. *Biochemistry* **2012**, *51* (14), 3121-3128.
126. Galdiero, S.; Falanga, A.; Vitiello, G.; Vitiello, M.; Pedone, C.; D'Errico, G.; Galdiero, M., Role of membranotropic sequences from herpes simplex virus type I glycoproteins B and H in the fusion process. *Biochimica et Biophysica Acta (BBA)-Biomembranes* **2010**, *1798* (3), 579-591.
127. Falanga, A.; Vitiello, M. T.; Cantisani, M.; Tarallo, R.; Guarnieri, D.; Mignogna, E.; Netti, P.; Pedone, C.; Galdiero, M.; Galdiero, S., A peptide derived from herpes simplex virus type 1 glycoprotein H: membrane translocation and applications to the delivery of quantum dots. *Nanomedicine: Nanotechnology, Biology and Medicine* **2011**, *7* (6), 925-934.

128. Galdiero, E.; Falanga, A.; Siciliano, A.; Maselli, V.; Guida, M.; Carotenuto, R.; Tussellino, M.; Lombardi, L.; Benvenuto, G.; Galdiero, S., Daphnia magna and Xenopus laevis as in vivo models to probe toxicity and uptake of quantum dots functionalized with gh625. *International journal of nanomedicine* **2017**, *12*, 2717.
129. Tarallo, R.; Accardo, A.; Falanga, A.; Guarnieri, D.; Vitiello, G.; Netti, P.; D'Errico, G.; Morelli, G.; Galdiero, S., Clickable functionalization of liposomes with the gH625 peptide from Herpes simplex virus type I for intracellular drug delivery. *Chemistry-a European Journal* **2011**, *17* (45), 12659-12668.
130. Guarnieri, D.; **Melone, P.**; Moglianetti, M.; Marotta, R.; Netti, P. A.; Pompa, P. P., Particle size affects the cytosolic delivery of membranotropic peptide-functionalized platinum nanozymes. *Nanoscale* **2017**, *9* (31), 11288-11296.
131. Guarnieri, D.; Falanga, A.; Muscetti, O.; Tarallo, R.; Fusco, S.; Galdiero, M.; Galdiero, S.; Netti, P. A., Shuttle-Mediated Nanoparticle Delivery to the Blood–Brain Barrier. *Small* **2013**, *9* (6), 853-862.
132. Perillo, E.; Hervé-Aubert, K.; Allard-Vannier, E.; Falanga, A.; Galdiero, S.; Chourpa, I., Synthesis and in vitro evaluation of fluorescent and magnetic nanoparticles functionalized with a cell penetrating peptide for cancer theranosis. *Journal of Colloid and Interface Science* **2017**, *499*, 209-217.
133. Carberry, T. P.; Tarallo, R.; Falanga, A.; Finamore, E.; Galdiero, M.; Weck, M.; Galdiero, S., Dendrimer Functionalization with a Membrane-Interacting Domain of Herpes Simplex Virus Type 1: Towards Intracellular Delivery. *Chemistry-A European Journal* **2012**, *18* (43), 13678-13685.
134. Smaldone, G.; Falanga, A.; Capasso, D.; Guarnieri, D.; Correale, S.; Galdiero, M.; Netti, P. A.; Zollo, M.; Galdiero, S.; Di Gaetano, S., gH625 is a viral derived peptide for effective delivery of intrinsically disordered proteins. *International journal of nanomedicine* **2013**, *8*, 2555.
135. Galdiero, S.; Falanga, A.; Morelli, G.; Galdiero, M., gH625: A milestone in understanding the many roles of membranotropic peptides. *Biochimica et Biophysica Acta (BBA)-Biomembranes* **2015**, *1848* (1), 16-25.
136. Newkome, G. R.; Moorefield, C. N.; Vögtle, F.; Vögtle, F.; Vögtle, F.; Chemist, G., *Dendrimers and dendrons: concepts, syntheses, applications*. Wiley Online Library: 2001; Vol. 623.
137. Lee, C. C.; MacKay, J. A.; Fréchet, J. M.; Szoka, F. C., Designing dendrimers for biological applications. *Nature biotechnology* **2005**, *23* (12), 1517.
138. Gillies, E. R.; Fréchet, J. M., Dendrimers and dendritic polymers in drug delivery. *Drug discovery today* **2005**, *10* (1), 35-43.
139. Gunaseelan, S.; Gunaseelan, K.; Deshmukh, M.; Zhang, X.; Sinko, P. J., Surface modifications of nanocarriers for effective intracellular delivery of anti-HIV drugs. *Advanced drug delivery reviews* **2010**, *62* (4), 518-531.
140. Lu, C.-T.; Zhao, Y.-Z.; Wong, H. L.; Cai, J.; Peng, L.; Tian, X.-Q., Current approaches to enhance CNS delivery of drugs across the brain barriers. *International journal of nanomedicine* **2014**, *9*, 2241.
141. Abbott, N. J.; Rönnbäck, L.; Hansson, E., Astrocyte-endothelial interactions at the blood-brain barrier. *Nature reviews. Neuroscience* **2006**, *7* (1), 41.



142. Malakoutikhah, M.; Teixidó, M.; Giralt, E., Shuttle-Mediated Drug Delivery to the Brain. *Angewandte Chemie International Edition* **2011**, *50* (35), 7998-8014.
143. Sánchez-Navarro, M.; Giralt, E.; Teixidó, M., Blood–brain barrier peptide shuttles. *Current Opinion in Chemical Biology* **2017**, *38*, 134-140.
144. Mahajan, S. D.; Law, W.-C.; Aalinkeel, R.; Reynolds, J.; Nair, B. B.; Yong, K.-T.; Roy, I.; Prasad, P. N.; Schwartz, S. A., 3 Nanoparticle-Mediated Targeted Delivery of Antiretrovirals to the Brain. *Methods in enzymology* **2012**, *509*, 41.
145. Qiao, R.; Jia, Q.; Hüwel, S.; Xia, R.; Liu, T.; Gao, F.; Galla, H.-J.; Gao, M., Receptor-mediated delivery of magnetic nanoparticles across the blood–brain barrier. *Acs Nano* **2012**, *6* (4), 3304-3310.
146. Valiante, S.; Falanga, A.; Cigliano, L.; Iachetta, G.; Busiello, R. A.; La Marca, V.; Galdiero, M.; Lombardi, A.; Galdiero, S., Peptide gH625 enters into neuron and astrocyte cell lines and crosses the blood–brain barrier in rats. *International journal of nanomedicine* **2015**, *10*, 1885.



## Chapter 2

# Substrate-mediate gene delivery platform based on functionalized PEI/DNA polyplexes

**Abstract.** In this study, we describe a new modification of PEI, in which the gH625 cell-penetrating peptide was covalently coupled to 25 kDa PEI through a heterobifunctional polyethylenglycol (PEG) spacer resulting in a gH625-PEG-PEI conjugate. The new vector and the obtained polyplexes were widely characterized by <sup>1</sup>H-NMR spectroscopy and confocal and electronic microscopy, respectively. Furthermore, transfection efficiency and cytotoxicity of both PEI and gH625-PEG-PEI polyplexes with DNA were evaluated under *in vitro* conditions (NIH-3T3 cell line) using both direct and reverse transfection methodologies. In all cases, improved cell viability and DNA reporter gene complexation and delivery were observed for gH625-polyplexes. Finally, a new strategy to covalently bound functionalized polyplexes on a silanized glass substrate has been developed in order to explore the potential advantages coming from this technique.

## 1.1 Introduction

Plasmid DNA complexation with vectors sustain the cell internalization and the transfection activity, although a high efficiency and duration of gene expression are not always guaranteed. Gene vectors can facilitate intracellular trafficking which includes endosomal escape, cytoplasmic transport, nuclear entry and the dissociation from the DNA to allow gene expression.<sup>1-2</sup> In particular, non-viral vectors are safer and easier to prepare than viral vectors, but typically have lower efficiency and shorter duration of gene expression.<sup>3</sup> Regarding the more traditional delivery methods, controlled delivery systems have the potential to overcome extracellular barriers, as well as enhance gene delivery.<sup>4</sup>

In recent years, the development of systems capable of controlled and efficient gene transfer has been widely investigated in *in vitro* research and in diagnostic applications.<sup>5</sup> In particular, gene delivery from surfaces is the basis of many screening systems to examine the cell response to the altered gene expression within a more representative biological context.<sup>5-6</sup> Cell-based array technology permits simultaneous detection of several different activities located at the surfaces or inside cells, allowing the complex characterization of cells with an amount of information that is hardly assessed by any other technique<sup>7</sup> such as cell arrays for studies in functional genomics<sup>8-10</sup> or patterned gene delivery for models of tissue growth.<sup>11-12</sup>

Substrate-mediated gene transfer, also known as reverse transfection, immobilizes the DNA to a substrate that supports cell adhesion, placing the vector directly in the cellular microenvironment, reducing mass transport limitations and localizes delivery.<sup>4, 13-14</sup> The retention or release of DNA from surface can be dictated by the strength and specificity of the molecular interactions between the vector and substrate.<sup>15-17</sup> The immobilization of vectors provides many advantages as regards transfection efficiency, although a correct balance between the binding to the substrate and the vehicle release ability is necessary.

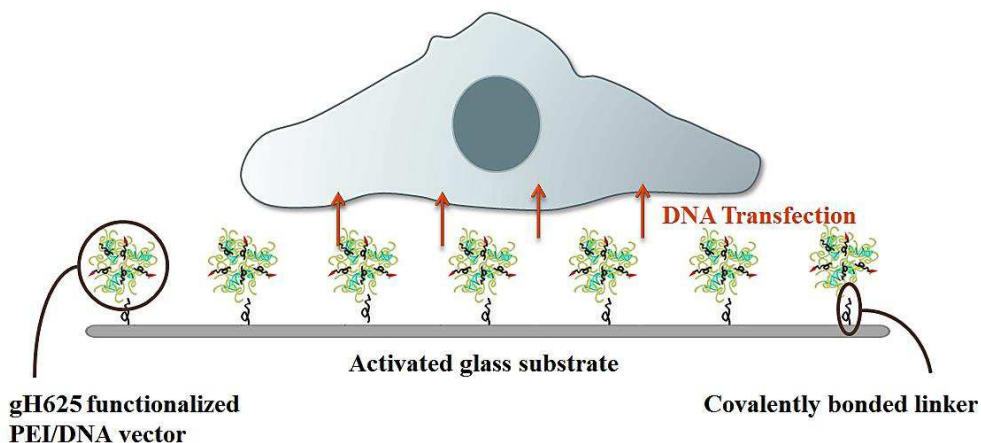
Moreover, some other limiting factors have to be considered in non-viral gene delivery.

- (i) The concentration of DNA at the cell surface<sup>14</sup> leads to mass transport issues such as aggregation effects in case of excessive high density of the complexes on substrate.
- (ii) The chemistry of substrate itself (size and shape) affects the immobilization and

expression of non-viral vectors. For instance, the inclusion of PEG-like moieties influence the surface properties of PEI polyplexes adsorbed to monolayers of carboxylic end groups, increasing their transfection efficiency.<sup>13</sup> (iii) Non-viral gene vectors have to overcome a series of barriers to transport DNA from the cytoplasm to the nucleus. In particular, the accumulation in lysosome compartment decreases the transfection ability and causes cytotoxic effects due to the low pH and the degradative environment.<sup>18</sup> Generally, positively charged vectors entrapped in endosomes<sup>19</sup> are able to escape *via* the “proton sponge effect,” in which the buffering capacity of the cationic polymer leads to an osmotic pressure increase when the endosomal pH drops, ultimately causing the endosome rupture and releasing the polyplexes into the cytosol.<sup>20</sup> However, this proton sponge effect is apparently not sufficient to release the majority of PEI particles from the vesicles, especially with small PEI polyplexes at low concentrations.<sup>21</sup>

A promising approach to further increase cell uptake and endosomal escape of polyplexes is represented by the use of cell-penetrating peptides (CPPs), whose membranotropic action has been shown to significantly favor the uptake of a variety of molecules and cargoes even reducing their own cytotoxicity.<sup>22</sup> For example, TAT-derived PEI mediated cell uptake of DNA, increase DNA condensation and polyplex stability. Moreover, peptide functionalization significantly reduced the cytotoxicity and demonstrated higher transfection efficiency than PEI.

As a matter of fact, in order to overcome the gene delivery limitation previously described, the aim of this study was to combine favorable characteristics of PEG-grafted PEI, cell-penetrating peptides and reverse transfection approach in order to create a substrate mediate gene delivery platform with functionalized vectors capable of mediating efficient transfection. In addition, the new vector should be able to mediate gene transfer and exhibit a lower toxicity with respect of PEI. Experimental model of the gene delivery platform is showed in Figure 2.1.



**Figure 2.1.** Experimental model of the covalently bonded gH625-PEG-PEI/DNA polyplexes on the substrate mediated gene-delivery platform.

In this chapter we report the synthesis, characterization and cell transfection behavior of polymer conjugates in which a CPP, namely gH625, modified by a C-terminal cysteine residue is covalently coupled to linear PEI (25 kDa) using a hetero-bifunctional PEG based linker. The peptide gH625 belongs to the glycoprotein H of *Herpes simplex virus* type I (HSV-1) and is a membranotropic domain which contributes to the fusing of the vires with the cell membranes.<sup>23-24</sup> This peptide exhibit exceptional vector properties and has been shown to be principally internalized by a direct translocation mechanism, avoiding endosomal entrapment. Therefore, gH625 is a very good delivery vector and its coupling to nanocarriers may be exploited to change their internalization mechanism and to avoid or reduce their toxicity.<sup>25-32</sup>

Additionally, immobilization of bioactive compounds on a surface can be used to extend its half-life and stability or prevent its metabolism. Besides the conventional adsorption method, the new approach developed in this work is based on a covalent attachment of polyplexes on a functionalized glass surface through PEG spacer. Tethering the complexes to a solid substrate *via* a spacer molecule can also improve bioactivity by reducing steric constraints and shielding them from surface induced denaturation.

## 1.2 Experimental section

### 2.1.1 Materials

Linear Polyethylenimine (L-PEI, av. MW 25 kDa) was purchased from Polysciences (Warrington, PA). Tetramethylrhodamine-conjugated linear PEI (JetPEI-fluoR) was purchased from Polyplus-transfection SA (7mM ammine content, Illkirch, France). All Fmoc-aminoacids and  $\alpha$ -Succinimidyl ester- $\omega$ -propargylacetamido poly(ethylene glycol) (NHS-PEG-Alkyne, MW 3.3 kDa) were purchased from IRIS Biotech GmbH (Germany). 3-bromopropyl trimetoxysilane (BPTMS), Sodium azide, 2-(N-Morpholino)ethanesulfonic acid hemisodium salt (MES buffer), 1-ethyl-3(3-dimethylamino-propyl)-carbodiimide hydrochloride (EDC), 2-Hydroxy-2-methylpropiophenone (DAROCUR 1173), N-hydroxysuccinimide (NHS) Sodium ascorbate, Copper sulfate pentahydrate ( $\text{CuSO}_4 \cdot 5\text{H}_2\text{O}$ ), N,N-diisopropylethylamine (DIPEA), O-benzotriazole-N,N,N',N'-tetramethyluronium-hexafluoro-phosphate (HBTU), Ethyl (hydroxyimino)cianoacetate (Oxyma Pure<sup>®</sup>), anhydrous N,N-dimethyl-formamide (DMF), Acetonitrile (ACN), Rhodamine B, Dichloromethane (DCM), Methanol, Ethanol, Acetone, Piperidine, Toluene, Trifluoroacetic acid (TFA), Triisopropylsilane (TIS), Acetic Anhydride, HPLC-grade water, 2,2,2-trifluoroethanol (TFE) and all buffer solutions were purchased from Sigma-Aldrich (USA). Hoechst 33342 trihydrochloride trihydrate was purchased from Invitrogen (USA). Dialysis bag MWCO 6000-8000 Da were purchased from Spectrum Laboratories, Inc. (Netherlands). Distilled and deionized water used Millipore Milli-RO 10 Plus (Millipore, USA) at 18 M $\Omega$  resistance. Amicon<sup>®</sup> Ultra-4 centrifugal filters were purchased from Millipore Merck.

### 2.1.2 Amplification and purification of plasmid DNA

Plasmid DNA, pTagGFP2-actin (Evrogen, Russia), containing a reporter gene encoding for green fluorescent protein (GFP) (bright green fluorescence with ex/em maxima at 483 and 506 nm, respectively), was used for fluorescent labeling of  $\beta$ -actin intransfection studies. The chemically competent DH5 $\alpha$ TM bacterial strain (*Escherichia coli* species) was transformed with pTagGFP2 using heat shock method. Plasmid DNA in the transformed

culture was then expanded in *E. coli* in Lennox L Broth (LB Broth) supplemented with 50 mg/L kanamycin overnight at 37 °C in an incubator, shook at 300 rpm. Plasmid DNA was extracted and purified from bacterial culture using an Invitrogen PureLink™ HiPure plasmid filter midprep kit according to the manufacturer's specifications. The concentration (adjusted to 0.5 µg/µL) and the purity of plasmid DNA solution were determined using a UV-Vis Spectrophotometer by measuring the sample absorbance at 260 nm and the 260/280 absorbance ratio, respectively.

### 2.1.3 Synthesis of peptide

The peptide gH625-Cys [Ac-HGLASTLTRWAHYNALIRAFK(Mtt)GGGC-NH<sub>2</sub>] was synthesized using standard solid-phase-9-fluorenyl methoxy carbonyl (Fmoc) method, Rink Amide resin on a fully automated multichannel peptide synthesizer Biotage® Syro Wave™. As concern rhodamine functionalization, Mtt group was removed from lysine amino group using DCM/TIS/TFA (95/4/1) solution; Kaiser test was used to confirm the complete removal of Mtt groups. Conjugation of rhodamine (rhod) to gH625 peptide was performed on solid-phase by a standard coupling procedure in order to bind the lysine side chain amine and the rhodamine carboxylic group. The mixture of peptide (1 eq), HBTU (3 eq), Oxyma Pure® (3 eq), DIPEA (6 eq) and Rhodamine-B (2.5 eq) in anhydrous DMF reacted for 2 h at room temperature under continuous stirring. Then, resin was washed several times with DMF, DCM and methanol before. Cleavage of peptide from resin was performed by standard TFA/TIS/water (95/2.5/2.5) solution, followed by precipitation in cold ethyl ether. The reaction product was verified by analytical LC-MS analysis and then purified by RP-HPLC using a 20/80 (v/v) ACN/ 0.1% v/v TFA. MS for rhod-gH625-Cys peptide: calculated for [M+H]<sup>+</sup> = 3167.73 m/z; found (ESI) [M+3H]<sup>3+</sup> = 1056.58 m/z, [M+4H]<sup>4+</sup> = 792.68 m/z, [M+5H]<sup>5+</sup> = 634.35 m/z, [M+6H]<sup>6+</sup> = 528.69 m/z.

In order to verify the secondary structure of gH625-Cys peptide, circular dichroism (CD) spectra were recorded using a JASCO J1500 CD spectrometer in a 0.1 cm quartz cell at room temperature. The spectra were an average of 15 consecutive scans from 260 to 190 nm, recorded with a band width of 1 nm, a data pitch of 0.2 nm and a scan rate of 100 nm/min. Spectra were recorded and corrected for the blank sample. MS and CD spectra are subsequently showed and debated within Chapter 3 (Figure 3.2).



#### 2.1.4 Synthesis gH625-PEG-PEI conjugate

gH625-PEG-PEI copolymer was synthesized in two steps. First, NHS-functionalized carboxylic group of glutamic acid residue of PEG 3.3 kDa and secondary amines of PEI polymer chain reacted in order to obtain 2 % PEG branched PEI. Polymer functionalization degree is expressed as percentage of PEI monomeric units that reacted with PEG considering that, for a 25 kDa PEI chain consist on ~ 580 [-CH<sub>2</sub>CH<sub>2</sub>NH-] monomeric units. Briefly, 5 mL of a 2 mg/mL PEI solution in MES buffer, pH 5.5 (corresponding to 10 mg/0.400 μmol PEI; 232 μmol total amine), were added to 15.58 mg (4.7 μmol) of NHS-PEG-Alkyne, previously weighted in a round bottom flask. The reaction was carried out for 5 h at room temperature under vigorous magnetic stirring. The adducts were purified from unreacted reagents using dialysis bags (MWCO 6-8 kDa) against pure water and lyophilized. The reaction products were verified by <sup>1</sup>H-NMR spectroscopy using deuterated water (D<sub>2</sub>O) as solvent. The degree of PEG substitution was determined by comparing the integral values obtained from the number of [-CH<sub>2</sub>CH<sub>2</sub>O-] protons of PEG and [-CH<sub>2</sub>CH<sub>2</sub>NH-] protons of PEI.<sup>33-35</sup> PEG-PEI copolymer <sup>1</sup>H NMR (600 MHz, D<sub>2</sub>O) attribution refers to Figure 2.2 A: δ ppm 3.93 (t, **i**); 3.90-3.50 (**h**); 3.46 (t, **g**); 3.13 (**a**); 2.99 (**b**); 2.58-2.48 (m, **e+j**); 2.44 (s, **l**); 2.26 (t, **k**); 1.90 (m, **g**); 1.25 and 1.14 (t, **c+c'**).

As regards peptide coupling, 10 mg of the PEG-PEI copolymer (MW ~ 63 kDa), that correspond to 1.84 μmol of alkyne functional groups, 1.30 μmol of rhod-gH625-Cys and 0.13 μmol of DAROCUR 1173 (used as photoinitiator) were dissolved in 10 mM citrate buffer. Thiol-yne reaction were performed by illumination of the solution with an UV lamp (λ = 365 nm) for 10 minutes in static condition. After that, magnetic stirring was activated and the mixture reacted for additional 50 minutes. The amount of peptide has been chosen in order to obtain a resulting peptide degree of functionalization of about 1 % of the total PEI amine content (verified by NMR spectroscopy). Again, the adducts were purified from unreacted reagents using dialysis bags (MWCO 6-8 kDa) against pure water and lyophilized. The reaction products were verified by <sup>1</sup>H-NMR spectroscopy. Considering the final stoichiometry of the copolymer (gH625/PEG/PEI 5.8/11.6/1), MW of the construct was estimate to be ~ 82 kDa.

gH625-PEG-PEI copolymer  $^1\text{H}$  NMR (600 MHz,  $\text{D}_2\text{O}$ ) attribution refers to Figure 2.2 B:  $\delta$  ppm 8.10-7.50 (peptide amide backbone, \*); 3.93 (t, **i**); 3.90-3.50 (**h**); 3.46 (t, **g**); 3.13 (**a**); 3.00 (**b**); 2.58-2.48 (m, **e+j**); 2.45 (s, **l**); 2.27 (t, **k**); 1.90 (m, **g**); 1.25 and 1.14 (t, **c+c'**).

### 2.1.5 Polyplexes preparation

DNA complexes were formed by addition of cationic polymer (PEI) to plasmid resulting in self-assembled colloidal particles.<sup>20</sup> For gH625-PEG-PEI/DNA and PEI/DNA complexes formation, stock solution (11.6 mM of amine, corresponding to 500  $\mu\text{g}/\text{mL}$  of PEI 25 kDa) of gH625-PEG-PEI copolymer or only PEI were prepared. As regards PEI stock solution, 10 % of total amines were provided by jetPEI-fluoR in order to realize fluorescent polyplexes useful for the following characterization.

Proper amount of both polymers and plasmid DNA (3  $\mu\text{g}$ ) solutions were diluted in 50  $\mu\text{L}$  of 150 mM NaCl water solution, gently vortexed and spun down. After 10 minutes, PEI solution were added to DNA solutions, rapidly mixed by pipetting up and down and incubated for 20 minutes at room temperature to allow complex formation between the positively charged PEI (amine groups) and the negatively charged DNA (phosphate groups).<sup>36-37</sup>

In order to optimize the complexes formulation, in terms of best transfection efficiency and lower cytotoxicity, complexes were generated using different N (nitrogen) to P (phosphate) ratios (N/P = 5, 10, 15, 20 and 30). This represents the molar ratio of amine groups of PEI to phosphate groups in DNA backbone (usually 3 nmol of P for  $\mu\text{g}$  of DNA). Polyplexes were created setting the DNA concentration and suitably changing the polymer amount.

### 2.1.6 Characterization of DNA complexes

Obtained gH625-PEG-PEI/DNA and PEI/DNA complexes were physicochemically and morphologically characterized. The particle size and zeta-potential were measured by dynamic light scattering (DLS) using a Zetasizer Nano-ZS (Malvern Instruments, Worcestershire, UK). All measurements were done in triplicate, the mean value was recorded as the average of three different runs.

Thus, confocal laser scanning microscopy (CLSM) was used to effectively verify the complexes formation through the detection of plasmid DNA labelled with Hoechst 33342 staining and rhodaminated polymeric vectors. Polyplexes solution were dropped on a glass microscope slide and observed by a Leica Microsystem (Germany) TCS SP5 II SMD confocal/multiphoton microscope, equipped with a HCX IRAPO L 25 X/0.95 water immersion objective was used to acquire. Emitted light was detected with two photomultipliers. Excitation of rhodamine-labeled PEI, was achieved using the 543 nm HeNe excitation line, with the resulting fluorescent wavelengths observed in 560-610 nm and excitation of DNA-Hoechst 33342 was achieved with the multiphoton Chameleon Ultra II Ti/Sapphire NIR femtosecond 80 MHz pulsed laser (Coherent Inc., USA) at 700 nm excitation line, with the resulting fluorescence observed at 400-480 nm. Confocal images were acquired with pinhole aperture of 1AU (Airy Units) corresponding to a section thickness of 1.4  $\mu\text{m}$ , with a frame size of 1024 $\times$ 1024 pixels (equivalent to a field of view of 630 $\times$ 630  $\mu\text{m}^2$ ).

Finally, complex characterization was evaluated using scanning electron microscopy (SEM). Prior to imaging, dried samples were mounted to microscope stub and coated with 7 nm of platinum-palladium under argon atmosphere using a SEM sputter coating system (Cressington, 208 HR, UK). Samples surface morphology was then observed using a scanning electron microscope (Zeiss, FEG Ultraplus, Germany) with an accelerating voltage of 8 kV and variable magnifications.

### **2.1.7 Modification of glass substrates**

Glass coverslips of 12 mm  $\varnothing$  (Knittel glass, Germany) were used to covalently bind gH625-PEG-PEI complexes. In order to provide bonding sites for alkyne-azide click chemistry reaction for the polyplexes onto the glass surface, 12 mm diameter glass coverslips were firstly treated with 3-bromopropyl trimethoxy silane (BPTMS). BPTMS was immobilized to the substrate by silane condensation.

Prior modification, the glass coverslips were cleaned carefully by immersion in acetone and ultra-sonication for 10 min (3 times) and then dried in a nitrogen flow. Subsequently, the activation of substrates was carried out immersing the glass coverslips in a 0.1 M NaOH solution for 3 minutes, followed by several water and ethanol washes.

Then, coverslips were placed in a petri dish and covered with 4 % toluene solution of BPTMS (~ 0.5 mL for each coverslip), overnight, slightly agitated on an orbital shaker. After the silane treatment, glass coverslips were extensively rinsed with toluene and ethanol (3 times each) to remove residual reagent and then dried under nitrogen flow.

Bromide group was then replaced with azido group by nucleophilic substitution  $S_N2$  reaction. Azide substitution were performed on bromo-silanized glass coverslips using sodium azide saturated solution in DMF (~ 50 mM, ~ 1 mL for each coverslip) and let to react under stirring for 24 hours at RT. Afterwards, treated glass coverslips were washed with DMF, ethanol and acetone and then dried under vacuum for 2 h.

### **2.1.8 Water contact angle**

Surface modification of glass slides, starting with NaOH activation, followed by silane immobilization and subsequent bromide-azido substitution, was analyzed by water contact angle measurements of water in air at room temperature under static conditions. An Attention Theta optical tensiometer (Biolin Scientific, Stockholm, Sweden) was used to analyze the different wettability of modified substrates in order to verify to the occurrence of chemical modification. A 4  $\mu$ L droplet of MilliQ water was laid on chemically modified glass surfaces and the picture was taken with a digital camera. Contact angle was recorded as the angle between the point of contact of the droplet with the solid surface and a tangent with the droplet profile. The contact angle measurement was estimated from a picture and calculated as the mean value of 5 separate measurements on 3 different glass coverslips.

### **2.1.9 Binding of PEGylated complexes to modified glass substrate**

Through the activation of glass slides with BPTMS, followed by the bromide-azido substitution, azido groups were exposed at surface in order to allow the linking of gH625-PEG-PEI/DNA complexes. With the purpose of accomplish the covalent bond between complexes and activated glass slides, azido-alkyne click chemistry reaction were carried out. Some considerations elucidated in paragraph 2.1.16 have led us to choose the following reaction conditions: 0.01 eq of copper sulfate and 0.2 eq of sodium ascorbate with respect of total gH625-PEG-PEI used in polyplexes synthesis. After reaction between

exposed azido groups, unbound complexes were removed and the substrates were washed 3 times with PBS and then used for characterization or transection studies.

In order to evaluate the reaction final yield, we exploited the rhodamine functionalization of the gH625-Cys peptide that was monitored by fluorescence measurement before and after the reaction. Rhodamine concentration of the unbound complexes was detected *via* a standard curve, by measuring the fluorescence of gH625-PEG-PEI (ex/em 550/570 nm) in a multi-well plate spectrofluorometer (Enspire 2300, Perkin Elmer, USA). The polyplexes covalent binding efficiency ( $P_{Cov}$ ) was expressed as the difference between the complexes concentration initially incubated on the substrate and the concentration of unbound complexes after the reaction, normalized on initial concentration, in percentage.

$$P_{Cov} = \frac{[P]_i - [P]_f}{[P]_i}$$

Where  $[P]_i$  and  $[P]_f$  are the initial and final concentrations of polyplexes solutions measured before and after process, respectively. The experiments were repeated in triplicate with different samples, for each N/P ratio tested. The density of DNA complexes immobilized to each sample was determined by normalizing the complexes amount bound to area of substrate. After some preliminary tests, the reaction conditions were adjusted in order to obtain the same DNA coverage density in both covalent and adsorbed samples.

### 2.1.10 Complexes adsorption on glass substrates

After preparation gH625-PEG-PEI/DNA and PEI/DNA complexes were adsorbed by 2 h incubation on glass substrates. Different polyplexes solutions (N/P = 10, 15, 20 and 30) at known gH625-PEG-PEI and jetPEI-R concentrations were adsorbed on Ø 23 mm Fluorodish (World Precision Instruments Ltd) for 2 h at room temperature. As for the binding reaction, the final adsorption efficiency ( $P_{Ads}$ ) was determined by rhodamine fluorimetric assay as described in the previous paragraph.

The experiments were repeated in triplicate with different samples, for each N/P ratio and the reactant amount and the deposition time were optimized in order to obtain the desired DNA coverage density.

### **2.1.11 Characterization of substrates**

Substrates and complexes morphology was investigated by scanning electron (SEM) and confocal (CLSM) microscopy. Images of adsorbed and covalent bonded polyplexes were collected using the same instrument configuration described in paragraph 2.1.6.

### **2.1.12 Transfection and cytotoxicity studies**

Transfection efficiency and cell toxicity of the DNA complexes, generated according to the different formulations, were tested performing 2D transfection analysis in three different ways: bolus delivery and substrate mediate gene delivery of adsorbed and bonded complexes. Control studies were performed using un-functionalized PEI/DNA complexes.

For bolus delivery transfection experiments, NIH3T3 cells were seeded in Ø 23 mm Fluorodish (World Precision Instruments Ltd) at density of 70,000 cells/dish and incubated at 37 °C and 5 % CO<sub>2</sub>. After 24 h, polymer/DNA complexes (N/P ratio from 5 up to 30; 1 µg of total plasmid DNA), were added to each separate dishes. Conversely, for reverse transfection studies of adsorbed polyplexes, the same cell amount was seeded in Ø 23 mm Fluorodish already containing adsorbed polyplexes (1 µg of total DNA). Finally, for reverse transfection studies of covalent bonded polyplexes, NIH3T3 cell were seeded on polyplexes Ø 12 mm functionalized glass coverslip placed in a 24 well plate. In order to have comparable densities of both cell and plasmid DNA, 19,000 NIH3T3 cells were seeded onto chemical bonded polyplexes (~ 0.27 µg of total DNA).

After 24 h, samples were stained adding 100 µL of 1:10,000 Hoechst 33342 PBS solution in each Fluorodish (50 µL for 24 well plate). Living cells were directly observed by mean of confocal microscopy equipped with an Okolab incubator (Okolab S.r.l., Pozzuoli, Italy) for temperature and CO<sub>2</sub> control. Analyses of the transfection were carried out using a confocal laser scanning microscope using the same condition described in paragraph 2.1.6. In addition, excitation of GFP-actin was achieved using the 488 nm Ar excitation line, with the resulting fluorescent wavelengths observed in 500-530 nm.

The effective gene transfer was monitored by expression of reporter transgene encoding for green fluorescent protein. Transfection efficiency (number of transfected cells

(GFP-expressing cells)/number of cells (Hoechst 33342-stained cells)) were quantified through analysis of images using ImageJ software. Each estimation was repeated in triplicate on different samples. Results were compared by analysis of variance (ANOVA) and a significance level of 95% ( $P = 0.05$ ) was founded in all cases.

The biocompatibility of DNA complexes generated according to different formulations was evaluated by colorimetric Alamar blue assay (Life Technologies, Grand Island, NY) according to the manufacturer's procedure.<sup>38-39</sup> The experimental setup was identical to the one just described for transfection studies; un-treated cells were used as a negative control. After 24 h of exposure with all kind of DNA polyplexes, the metabolic activity of all cell cultures was determined by using standard Alamar Blue assay. Absorbance of Alamar Blue reagent solution was read at 570 nm and 600 nm by a plate reader (Enspire 2300, Perkin-Elmer). All experiments were performed in triplicate and data sets represent the cell viability percentage of treated cells normalized to un-transfected cells.

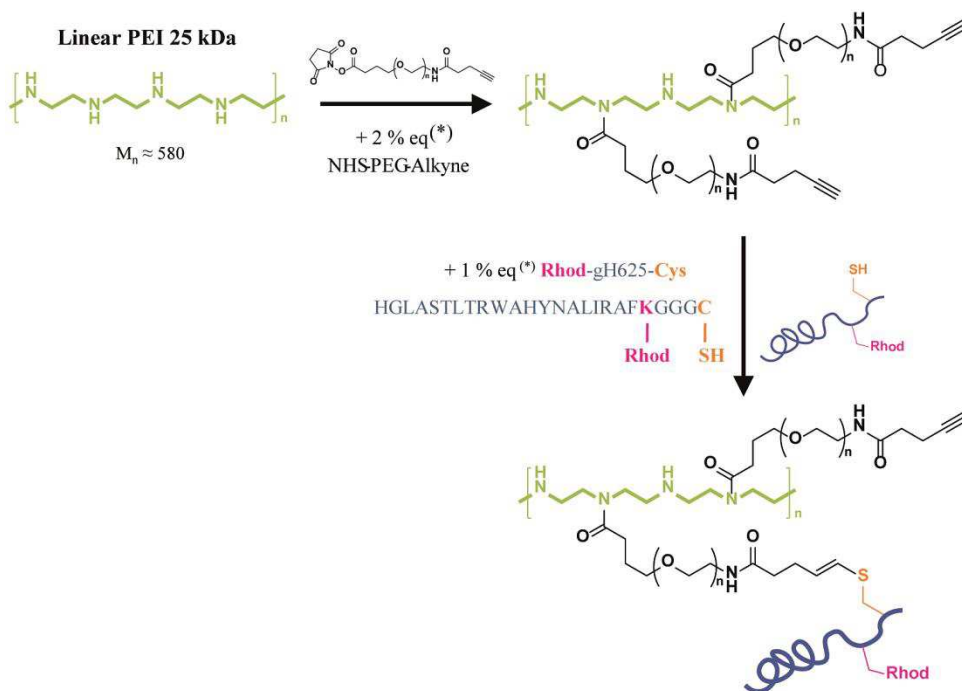
### **2.1.13 Statistical analysis**

All quantitative data were reported as means  $\pm$  standard deviation (SD). Statistical analyses were performed using a one-way analysis of variance (ANOVA); a  $P < 0.05$  was considered statistically significant.

## 1.3 Results and discussion

### 2.1.14 Synthesis and characterization of gH625-PEG-PEI vector

The gH625-PEG-PEI vector was synthesized through a two-step reaction as shown in Scheme 2.1. Hetero-bifunctional NHS-PEG-Alkyne (3.3 kDa) firstly reacted with primary and secondary amine of PEI (25 kDa) obtaining PEG branched PEI. This reaction were carried out in MES buffer at pH 5.5 in order to avoid the competing hydrolysis reaction of the N-hydroxysuccinimide ester that occurred at acidic pH values.<sup>40</sup> The modification of PEI with PEG was assessed by <sup>1</sup>H-NMR spectroscopy in D<sub>2</sub>O (Figure 2.2 A). In particular, in PEI chain region was clearly visible the difference between the peak related to CH<sub>2</sub> protons near to functionalized nitrogen atoms (**a**, 3.13 ppm) and the original CH<sub>2</sub> group of classic PEI (**b**, 3.00 ppm). Results of spectra integration, based on the respective molecular weights, indicated that final PEG/PEI ratio in the copolymer was 12 that corresponded to a functionalization degree of 2.1 % with respect of total amine content of PEI.<sup>41</sup>



**Scheme 2.1.** Reaction outline for the synthesis of gH625-PEG-PEI conjugate: activation of PEI with NHS-PEG-Alkyne followed by the addition of the Rhod-gH625-Cys CPP through thiol-yne “click chemistry” reaction. (\*) Numbers of equivalent are expressed as percentage of the total number of PEG amines (~ 580).

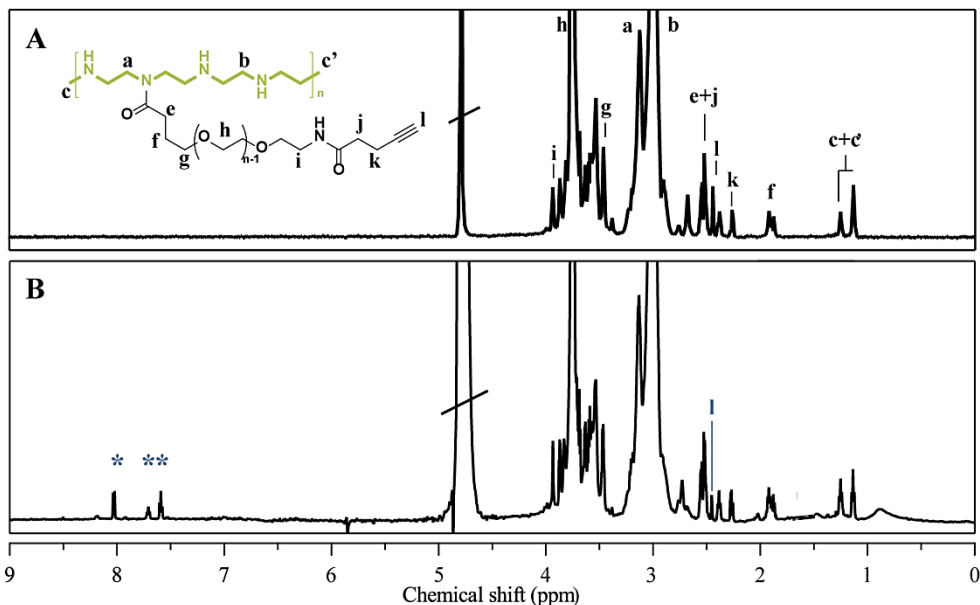


The use of PEG linker offered several advantages in reducing unwanted interactions of the polyplex with proteins, providing enhanced polyplex stability and lowered toxicity.<sup>42</sup> Moreover, it should be useful to overcome restrictions of pure oligopeptide based polyplexes, such as low plasmid complexation ability<sup>43-44</sup> and the decrease of polyplexes efficiency because of a too strong interaction with the complexed DNA.<sup>45</sup> The PEG linker, additionally, provided a steric shielding of the cationic PEI core from the peptide sequence and, thereby, facilitated the coupling reaction with plasmid DNA. Finally, hydrophilic PEG chain divided gH625 peptide from the PEI core promoting a more correct position of the oligopeptide moieties on the surface of the polyplexes.<sup>46</sup>

In the second step of the reaction, gH625 peptide was coupled to the alkyne group through a thiol-yne “click chemistry” photoreaction exploiting the –SH group of Cysteine residue at the C-term of the peptide sequence. Rhod-gH625-Cys peptide was synthesized in good yield (35 %) and characterized using MS and CD analysis demonstrating the effective conjugation of rhodamine to peptide sequence (MW 3167.73 Da) and the correct formation of gH625  $\alpha$ -helical secondary structure, respectively. <sup>1</sup>H-NMR spectrum of the reaction product was shown in Figure 2.2 B.

Generally, as the analogous thiol-ene photoreaction, thiol-yne was used to synthesize highly crosslinked polymer networks.<sup>47-48</sup> Moreover, due to the double unsaturation degree of alkyne group, it was possible to obtain polymer networks with higher crosslinking densities than the equivalent thiol-ene networks.<sup>49</sup> The kinetics of the polymerization process indicated a very fast reaction between thiols and alkynes that, under stoichiometric (2 thiols: 1 yne) conditions, gave rise to the monosubstituted vinyl sulfide moiety was even more reactive with the thiols than the -yne moiety.<sup>47</sup> In this work, in order to avoid double peptide-alkyne linkage, an alkyne stoichiometric excess was used. Using this reaction conditions, only varying amounts of unreacted alkyne and vinyl sulfide product were expected. Even though the interpretation of the NMR spectrum was quite tricky, it was possible to observe the signals of peptide amide bond chain at 7.50-8.10 ppm (\*) and, especially, the drastic reduction of the intensity of the alkyne peak (I).

Finally, the reaction condition were optimized in order to have a final degree of PEI substitution that was calculated to be 2.1 % for PEG and estimated to be almost 1.0 % for gH625 whit respect of all amines present in one PEI 25 kDa chain.



**Figure 2.2.**  $^1\text{H-NMR}$  spectra in  $\text{D}_2\text{O}$  of PEG-PEI (A) and gH625-PEG-PEI (B) copolymers with attribution. In (B) only peaks related to peptide amide bond backbone (\*) and PEG-alkyne proton (l) are highlighted.

### 2.1.15 Polyplexes physicochemical and morphological characterization

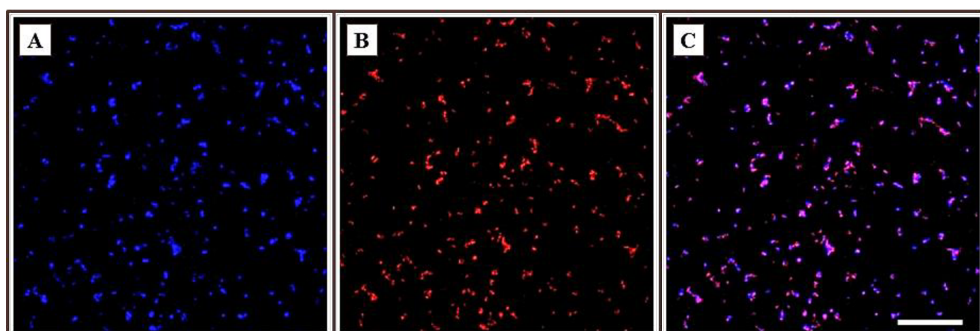
Different N/P ratio formulations of PEI/DNA and gH625-PEG-PEI/DNA complexes were prepared and well characterized in term of size, surface charge and morphology. DLS and  $\zeta$ -potential measurements were carried out using a Zetasizer Nano-ZS. Results indicated that, except for the N/P 5 gH625-PEG-PEI/DNA formulation<sup>(\*)</sup>, the polyplex size ranged from 114 to 160 nm and all of them were positively charged (Table 2.1).

**Table 2.1.** Particle size and  $\zeta$ -potential values for produced polyplexes. Hydrodynamic diameters and surface charges values are reported as means  $\pm$  standard deviation (SD).

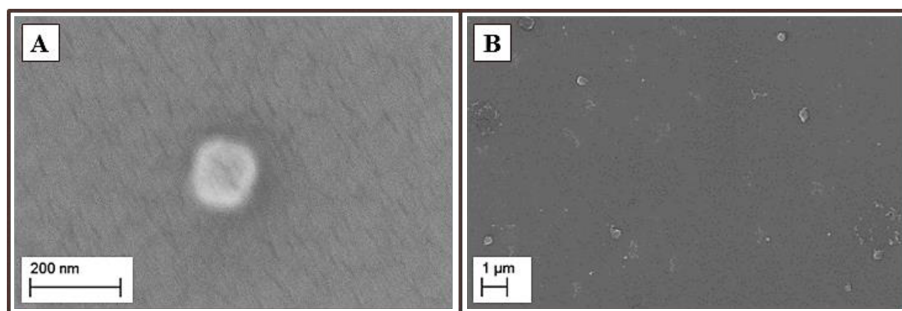
| N/P | <i>PEI only</i> |                         | <i>gH625-PEG-PEI</i>        |                           |
|-----|-----------------|-------------------------|-----------------------------|---------------------------|
|     | Size (nm)       | $\zeta$ -Potential (mV) | Size (nm)                   | $\zeta$ -Potential (mV)   |
| 5   | 146 $\pm$ 12    | 19 $\pm$ 2              | 808 $\pm$ 54 <sup>(*)</sup> | -2 $\pm$ 8 <sup>(*)</sup> |
| 10  | 147 $\pm$ 9     | 27 $\pm$ 3              | 160 $\pm$ 11                | 10 $\pm$ 1                |
| 15  | 114 $\pm$ 8     | 36 $\pm$ 2              | 145 $\pm$ 7                 | 19 $\pm$ 4                |
| 20  | 118 $\pm$ 7     | 38 $\pm$ 2              | 114 $\pm$ 5                 | 25 $\pm$ 2                |
| 30  | 122 $\pm$ 9     | 37 $\pm$ 1              | 118 $\pm$ 3                 | 28 $\pm$ 3                |

However, surface charge of gH625-PEG-PEI/DNA polyplexes was significantly lower than the zeta-potential observed for PEI polyplexes, which was between 30-40 mV for each N/P ratios. It was possible to give an interpretation of these data considering that DNA might involve both PEI and gH625 peptide in the condensation process and also assuming that PEG spacer act as a surface shield as it was described before.<sup>50-51</sup> The lack in surface charge is also the main cause of aggregation of N/P 5 polyplexes that were excluded from further analysis. Polyplexes size and  $\zeta$ -potential are also significant parameters that affect gene transfer efficiency in cells.<sup>52-53</sup> In particular, a high surface charge enhance endocytic uptake of particles but, on the other hand, toxic side effects occurs because of unspecific interactions with cell membranes. However, the reduced zeta-potential and the absence of aggregate formation of gH625-PEG-PEI polyplexes indicate a certain particle surface shielding, ensuring an enhanced stability and lower cytotoxicity.

Additional gH625-PEG-PEI polyplexes morphological characterizations were carried out using confocal and electron microscopy. CLSM images confirmed the polyplexes formation showing both signals of rhodamine labeled gH625-PEG-PEI and DNA-Hoechst on substrates. In particular, Figure 2.3 C showed the merge of Figure 2.3 A and B images and highlighted the correspondence of both signals on substrate after binding process. Furthermore, SEM images (Figure 2.4) confirmed the high uniformity in particle size distribution, circular morphology and the overall homogeneity of the sample.



**Figure 2.3.** Confocal images of N/P 15 gH625-PEG-PEI complexes demonstrate DNA-vector complexation by co-localization (image C) of (A) DNA-Hoechst and (B) Rhodaminated gH625-PEG-PEI vector. Scale bar: 25 $\mu$ m.



**Figure 2.4.** Exemplificative scanning electron microscopy images of gH625-PEG-PEI polyplexes at different magnifications.

### 2.1.16 Modifications of glass substrate and polyplexes covalent attachment

Bind gene complexes to glass substrates for culturing cells requires surface modification. In particular, the covalent attachment of a bioactive compound to a glass surface involves glass pre-treatment and surface activation, commonly using silane.<sup>54</sup> Normally, carboxyl-, amino-, vinyl- or methacrylate- silane were used as coupling agents, ensuring the exposure of a functional moiety which can readily react with the bioactive compound that needs to be anchored to the surface.<sup>55</sup>

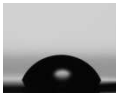

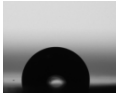

This work aim to develop a glass modified substrate for gene delivery where the presence of gH625 CPP might increase transfection efficiency and reduce cytotoxicity of covalently bonded functionalized polyplexes. In general, it is important that the biomolecules maintain their bioactivity in terms of conformation and chemical stability, once immobilized on a solid surface. For this reason, the gH625-PEG-PEI vector and its own polyplexes were synthesized and grafted with chemoselective, green and biocompatible procedures. Firstly thiol-yne and then Huisgen 1,3-dipolar cycloaddition between azides and terminal alkynes reactions were exploited to this purpose.<sup>47-48, 56-57</sup>

Azide-alkyne click reaction has been largely established as a useful chemical handle for bioconjugation in both non copper-mediated<sup>58</sup> and copper (I) catalyzed<sup>59-60</sup> manners. The unreactive character of azides and alkynes towards other functional groups presented in the synthesized molecules, together with the thermal and hydrolytical stability of their bonding, represented optima features in our specific case, as well as in the general field of bioconjugations.<sup>61-65</sup> The density of polyplexes

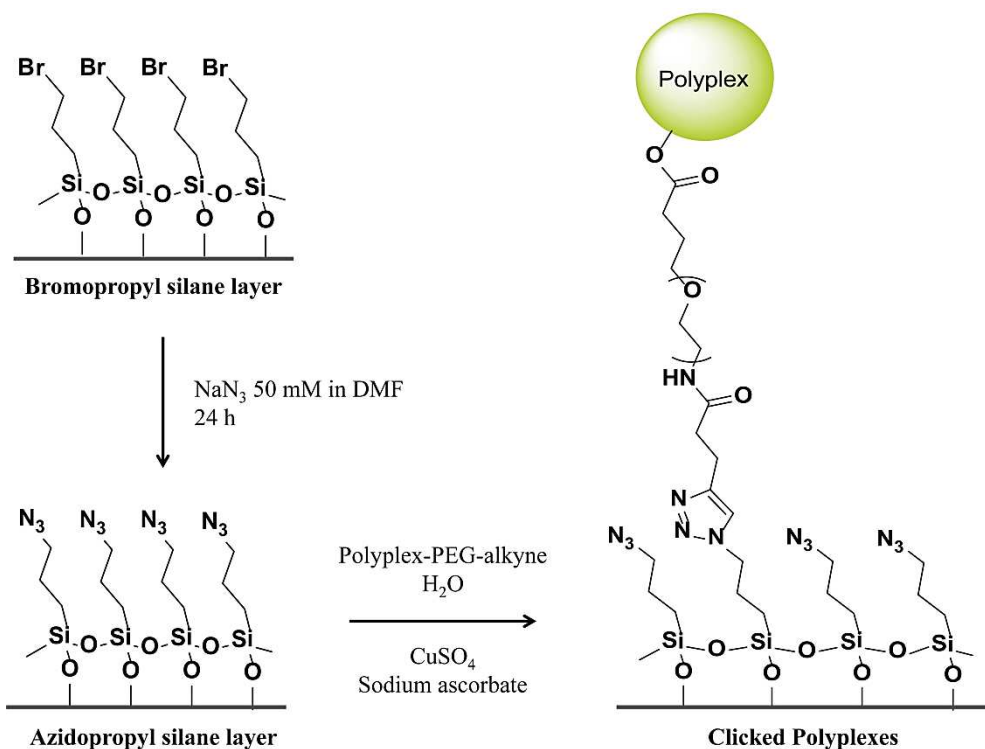
packaging is another important parameter to ponder. Indeed, an adequate free volume for the polyplexes has to be taken into account in order to overcome aggregation phenomena.

Before use, glass slides were washed, activated by NaOH alkaline treatment and then directly modified with a bromo-methoxy silane. After silanization, the bromide atoms were displaced by sodium azide in DMF. Water contact angle (WCA) measurements were carried out on the substrate before the NaOH treatment and after each further modification step. The acquired data were in good agreement with those already reported in literature<sup>66</sup> confirming the occurrence of every reactions (Table 2.2). In particular, for bromo-silanized glass was found a WCA average of 91°, while after azide S<sub>N</sub>2 reaction the average WCA decrease to 77°.

**Table 2.2.** Water contact angle (WCA) values and drop pictures on glass coverslips after each substrate modification step.

| Sample             | WCA        | Drop picture  |
|--------------------|------------|---|
| Glass coverslip    | 68° ± 3°   |   |
| NaOH activation    | 41° ± 0.9° |  |
| BPTMS layer        | 91° ± 3°   |  |
| Azido silane layer | 77° ± 2°   |  |

Finally, gH625-PEG-PEI complexes were linked to modified glass substrates *via* a specific azide-alkyne click reaction. All the synthesis steps were outlined in Scheme 2.2.



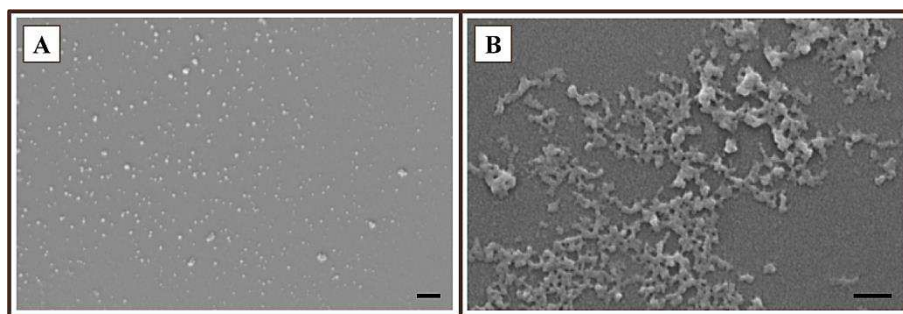
**Scheme 2.2.** Schematic synthesis steps of glass surface functionalization with PEI-PEG-gH625 polyplexes. Once surface exposure of azide moieties has been achieved by  $\text{S}_{\text{N}}2$  nucleophilic substitution, azido-alkyne click chemistry reaction was carried out in order to covalently bind functionalized polyplexes to the substrate.

Generally, for click reaction 0.5 eq of  $\text{CuSO}_4$  and 10 eq of sodium ascorbate were used, based on the amount of alkyne group.<sup>59-60</sup> Considering our final goal that, ideally, was to bind a polyplex through a single PEG linker chain, there are some consideration that influenced the reaction condition adopted: (i) theoretically, a single polyplex is made by 5 up to 10 PEI molecules, (ii) there is an average of  $\sim 6$  free alkyne group for each PEI molecule and (iii) Copper (I) ions and ascorbate attended the reaction as catalytic and not stoichiometric players. Thus, final copper (I) and ascorbate amounts were scaled of 50 times (0.01 eq and 0.2 eq, respectively) with respect of total gH625-PEG-PEI used in polyplexes synthesis. Moreover, in order to avoid multiple anchoring sites and to achieve a layout density control, the reaction was carried out for only 15 minutes. Finally, the DNA coverage density control in both covalent and adsorbed samples was achieved by modifying the reactant amount and the reaction time based on the polyplexes covalent binding efficiency ( $P_{\text{Cov}}$ ).

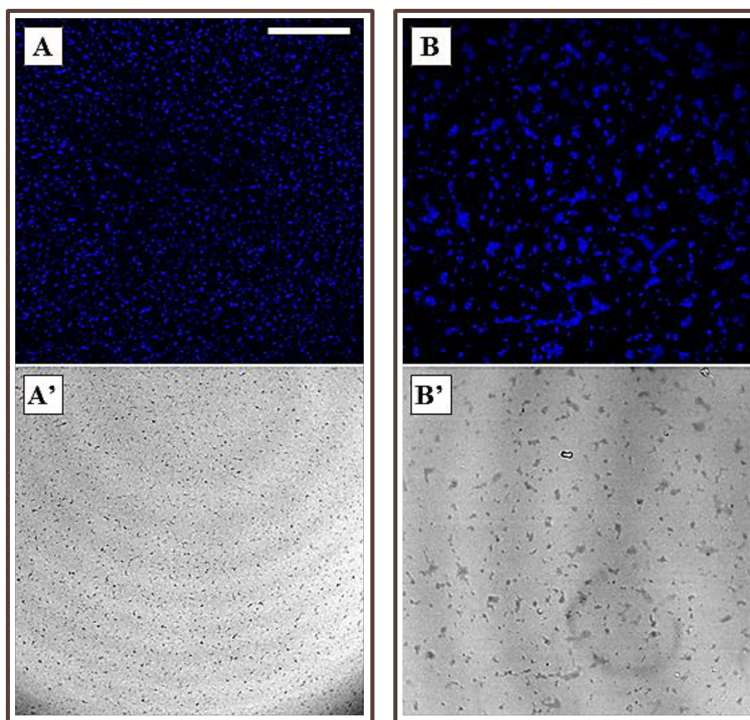
### 2.1.17 Substrates characterization

Morphological features of complexes modified substrates were analyzed by confocal (CLSM) and electronic (SEM) microscopy. Both of them have proven to be an excellent tool for imaging of soft biological structures and can be performed with high resolution after complex deposition on a surface. SEM (Figure 2.5) and CLSM (Figure 2.6) images of covalent bonded (A-A') and adsorbed (B-B') gH625-PEG-PEI polyplexes were obtained by scanning glass slides with immobilized complexes in wet and dry conditions, respectively. Images reveal the typical globular morphology of complexes and their surface distribution on activated substrates.<sup>67-69</sup>

In particular, Figure 2.5 B showed a high density of adsorbed polyplexes on substrate. This demonstrates the expected complexes aggregation, as shown also by the dimensions of fluorescent spots presented on substrates in the related confocal images (Figure 2.6 B-B'). On the other hand, Figure 2.5 A and Figure 2.6 A-A' highlighted the absence of aggregation of complexes on substrates during the covalent binding process. This observation supported and encouraged the synthetic approach and procedures used in this work. This strategy showed several advantages in overcoming problems related to reagent consumption and cell population heterogeneity effect, making these systems attractive for a wide range of assays, from drug discovery to toxicology, stem cell research and therapy. In this way it can be possible to control the spatial distribution and concentration of different polyplexes formulation.



**Figure 2.5.** Scanning electron microscopy images of covalent bonded (A) and adsorbed (B) polyplexes on glass surface. Scale bars: 200 nm.



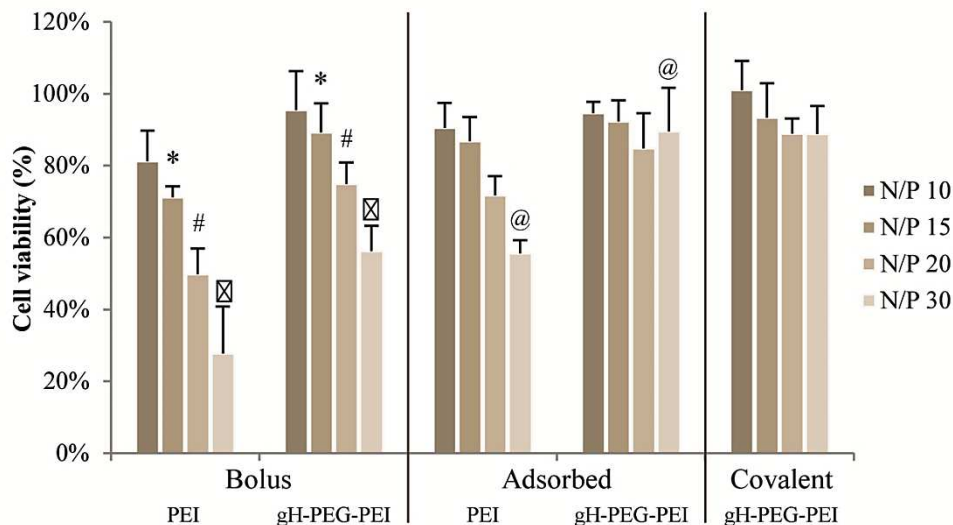
**Figure 2.6.** CLSM and transmission (') images of covalent bonded (A) and adsorbed (B) polyplexes on glass surface. Scale bar: 25  $\mu$ m.

### 2.1.18 Cell viability and transfection studies

Plasmid DNA was complexed with PEI or gH625-PEG-PEI at several N/P ratios (10, 15, 20 and 30). In order to examine the cytotoxicity and transfection efficiency in vitro of polyplexes, 2D analysis on NIH-3T3 cells were carried out. Studies were done through bolus and substrate mediated delivery both with adsorbed than covalently bonded polyplexes.

Cytotoxicity effect of polyplexes was evaluated by Alamar blue assay. Cell viability was expressed as percentage respect to the non-treated control cells after 24 h of incubation. Results in Figure 2.7 indicated that cell viabilities associated with treatment of gH625-PEG-PEI complexes were greater than 90 % even up to N/P ratio of 30 in reverse transfection experiments. Overall, functionalized vectors showed significantly lower cytotoxicity than commercial PEI/DNA complexes.

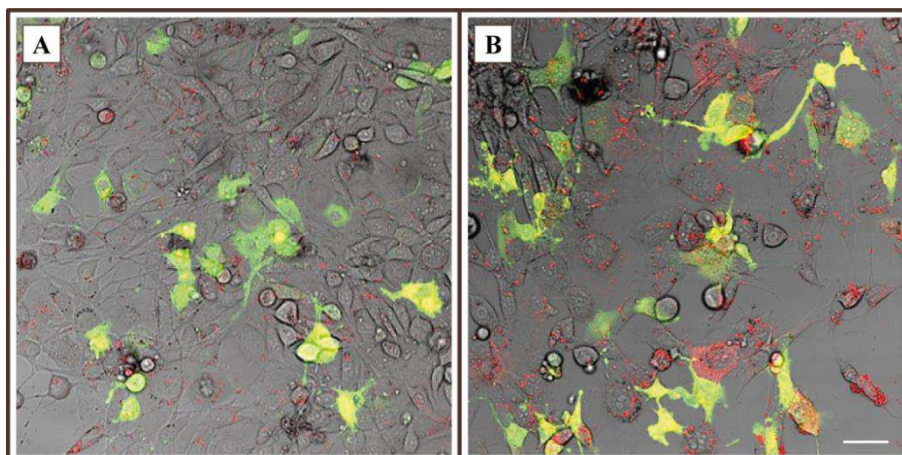




**Figure 2.7.** Cytotoxicity assay of PEI/DNA and gH625-PEG-PEI/DNA polyplexes at different N/P ratios in NIH-3T3 cells after 24 h of incubation. Experiments were carried out in direct (bolus delivery) and reverse (with absorbed or covalent bonded polyplexes) transfection mode. Bars highlighted with symbols are statistically different ( $p < 0.05$ ).

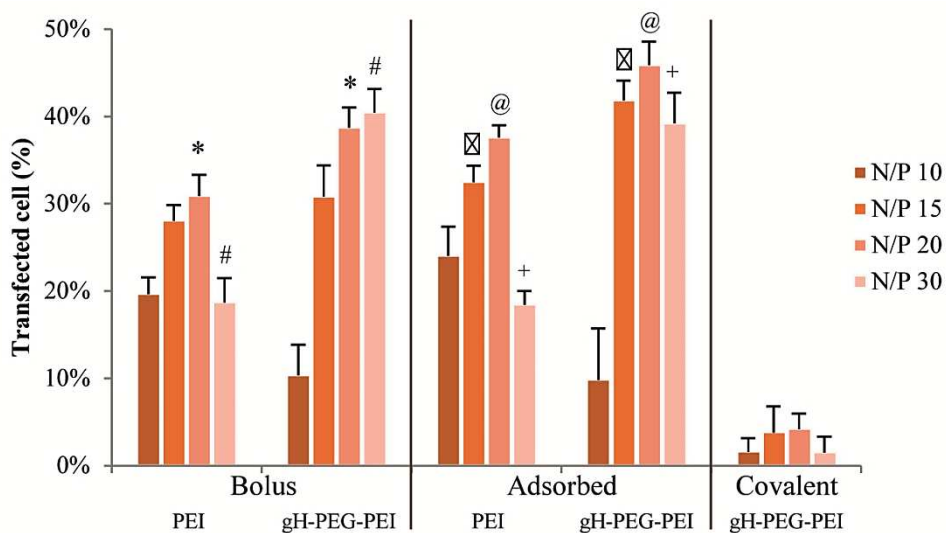
Generally, the polymer toxicity is directly related on the interaction of the PEI/DNA complexes with cell membranes which generally increases with positive charges exposed on the surface, proportionally to N/P ratio.<sup>70</sup> In particular, the polycationic polymers (like PEI) undergo strong electrostatic interaction with plasma membrane proteins, which can lead to destabilization and ultimately rupture of the cell membrane. Fischer *et al.*<sup>71</sup> demonstrated that the cytotoxicity of different types of polycationic polymers depends on the number and arrangement of the cationic charges which determines the degree of interaction with the cell membranes. The cells, exposed to cationic polymers, first show membrane leakage followed by a decrease in the metabolic activity.<sup>70</sup> In our case, the addition of gH625-PEG functionality masks the positive charge of the PEI molecules, reducing the positive charge exposed at the surface and further decrease the complexes toxicity.<sup>67, 72-73</sup>

However, polyplexes cellular uptake was not affected by the adding of the gH625-PEG moiety. In Figure 2.8 was possible to appreciate the distribution of PEI (A) and gH625-PEG-PEI (B) rhodamine-labelled polyplexes where complex (B) exhibited an extremely higher cellular uptake, as well as the good transfection ability, granted by the gH625 CPP.



**Figure 2.8.** Confocal images of NIH-3T3 cells treated with PEI/DNA (A) and gH625-PEG-PEI/DNA (B) polyplexes at N/P = 20 in bolus delivery experiments. Scale bar: 10  $\mu\text{m}$ .

Furthermore, transfection experiments were carried out on NIH-3T3 cells using identical conditions, as described for cytotoxicity studies. Gene-delivery efficiencies were calculated as the number of transfected cells (expressing the green fluorescent protein) normalized on total number of cell. Results clearly indicated an improvement of gene transfection of the gH625-PEG-PEI vector with respect of PEI/DNA complexes almost at every N/P ratio in bolus and substrate adsorbed delivery (Figure 2.9).



**Figure 2.9.** Transfection assay of PEI/DNA and gH625-PEG-PEI/DNA polyplexes at different N/P ratios in NIH-3T3 cells after 24 h of incubation. Experiments were carried out in direct (bolus delivery) and reverse (with adsorbed or covalent bonded polyplexes) transfection mode. Bars highlighted with symbols are statistically different ( $p < 0.05$ ).

The enhancement of transgene expression was well supported by the increased cellular uptake of DNA complexed with gH625. The fusogenic peptide functionalization resulted in a significant increase of the number of transfected cells, also increasing the level of polyplexes uptake by individual cells as showed by fluorescence microscopy images (Figure 2.8). In addition, cytosolic localization of the DNA was substantially improved.

Although the bolus delivery approach showed improvements in transfection efficiency for polyplexes at N/P 20, gene delivery method with adsorbed complexes at N/P 20 and 30 lead to the best results. Altogether, the combination of gene delivery efficiency with a substantial absence of toxicity, makes these formulations the starting point for further experimental investigations.

Unluckily, experiments fulfilled using covalent bonded polyplexes did not give the expected results. While cytotoxic assay of linked polyplexes can be collected as a really good result, transfection efficiency of the functionalized platform was practically negligible. Probably, the covalent linkage represents a too strong connection and, therefore, if the association of gene particles with a substrate is too tight, endocytic uptake and transfection can suffer. As evidence, no significant differences were found on the coverslip surfaces before and after the experimental sessions, sign of much lower complexes internalization.

## 1.4 Conclusions

In this chapter we developed a new non-viral gene delivery vector based on gH625 CPP, by crosslinking 25 kDa PEI with 3.3 kDa PEG, further coupled with the peptide through a thiol-yne click chemistry photoreaction. All the synthesis steps were carried out with good yields and the product were characterized using  $^1\text{H-NMR}$  spectroscopy. We confirmed that gH625-PEG-PEI vector had the ability to form complexes with plasmid DNA at various N/P ratio and showed suitable physico-chemical properties for gene delivery, such as narrow size distribution and positive surface charge. The new vector was able to increasing general polyplexes cellular uptake and cytosolic delivery in NIH-3T3 cells both in direct and reverse transfection methodologies. Furthermore, the new gene delivery vector showed much lower cytotoxicity and higher gene transfection efficiency compared with PEI 25 kDa. The best performances were found in substrate-mediate gene delivery experiments using adsorbed polyplexes at N/P ratio of 20 and 30.

As regards the poor efficiency of the covalent bonded polyplexes, this result should not be discouraged. Numerous advantages coming from the developed strategy can be exploited in order to perform substrate functionalization. This approach represents a promising tool in performing a molecule-substrate linkage with a selective and facile chemistry, without undesired sub-product and achieving a controlled and homogeneous distribution of the linked molecules. Concerning covalent gene delivery, we are optimistic for forthcoming approach based on linker that can assure a very quick release of the polyplexes, such as cleavable peptides or fast biodegradable polymers.

## 1.5 References

1. Niidome, T.; Huang, L., Gene therapy progress and prospects: nonviral vectors. *Gene therapy* **2002**, *9* (24), 1647.
2. Varga, C. M.; Hong, K.; Lauffenburger, D. A., Quantitative analysis of synthetic gene delivery vector design properties. *Molecular Therapy* **2001**, *4* (5), 438-446.
3. Pannier, A. K.; Anderson, B. C.; Shea, L. D., Substrate-mediated delivery from self-assembled monolayers: effect of surface ionization, hydrophilicity, and patterning. *Acta Biomaterialia* **2005**, *1* (5), 511-522.
4. Pannier, A. K.; Shea, L. D., Controlled release systems for DNA delivery. *Molecular Therapy* **2004**, *10* (1), 19-26.
5. Schena, M.; Heller, R. A.; Theriault, T. P.; Konrad, K.; Lachenmeier, E.; Davis, R. W., Microarrays: biotechnology's discovery platform for functional genomics. *Trends in biotechnology* **1998**, *16* (7), 301-306.
6. Silverman, L.; Campbell, R.; Broach, J. R., New assay technologies for high-throughput screening. *Current Opinion in Chemical Biology* **1998**, *2* (3), 397-403.
7. Berthuy, O. I.; Blum, L. J.; Marquette, C. A., Cells on chip for multiplex screening. *Biosensors and Bioelectronics* **2016**, *76*, 29-37.
8. Bailey, S. N.; Wu, R. Z.; Sabatini, D. M., Applications of transfected cell microarrays in high-throughput drug discovery. *Drug discovery today* **2002**, *7* (18), S113-S118.
9. King, K. R.; Wang, S.; Irimia, D.; Jayaraman, A.; Toner, M.; Yarmush, M. L., A high-throughput microfluidic real-time gene expression living cell array. *Lab on a Chip* **2007**, *7* (1), 77-85.
10. Ziauddin, J.; Sabatini, D. M., Microarrays of cells expressing defined cDNAs. *Nature* **2001**, *411* (6833), 107.
11. Bonadio, J., Tissue engineering via local gene delivery:: Update and future prospects for enhancing the technology. *Advanced drug delivery reviews* **2000**, *44* (2), 185-194.
12. Jang, J.-H.; Schaffer, D. V.; Shea, L. D., Engineering biomaterial systems to enhance viral vector gene delivery. *Molecular therapy* **2011**, *19* (8), 1407-1415.
13. Pannier, A. K.; Wieland, J. A.; Shea, L. D., Surface polyethylene glycol enhances substrate-mediated gene delivery by nonspecifically immobilized complexes. *Acta biomaterialia* **2008**, *4* (1), 26-39.
14. Luo, D.; Saltzman, W. M., Enhancement of transfection by physical concentration of DNA at the cell surface. *Nature biotechnology* **2000**, *18* (8), 893.
15. Adler, A. F.; Leong, K. W., Emerging links between surface nanotechnology and endocytosis: impact on nonviral gene delivery. *Nano today* **2010**, *5* (6), 553-569.
16. Bengali, Z.; Pannier, A. K.; Segura, T.; Anderson, B. C.; Jang, J. H.; Mustoe, T. A.; Shea, L. D., Gene delivery through cell culture substrate adsorbed DNA complexes. *Biotechnology and bioengineering* **2005**, *90* (3), 290-302.

17. Segura, T.; Volk, M. J.; Shea, L. D., Substrate-mediated DNA delivery: role of the cationic polymer structure and extent of modification. *Journal of Controlled Release* **2003**, *93* (1), 69-84.
18. Wang, F.; Yu, L.; Monopoli, M. P.; Sandin, P.; Mahon, E.; Salvati, A.; Dawson, K. A., The biomolecular corona is retained during nanoparticle uptake and protects the cells from the damage induced by cationic nanoparticles until degraded in the lysosomes. *Nanomedicine: Nanotechnology, Biology and Medicine* **2013**, *9* (8), 1159-1168.
19. Segura, T.; Shea, L. D., Materials for non-viral gene delivery. *Annual Review of Materials Research* **2001**, *31* (1), 25-46.
20. Boussif, O.; Lezoualc'h, F.; Zanta, M. A.; Mergny, M. D.; Scherman, D.; Demeneix, B.; Behr, J.-P., A versatile vector for gene and oligonucleotide transfer into cells in culture and in vivo: polyethylenimine. *Proceedings of the National Academy of Sciences* **1995**, *92* (16), 7297-7301.
21. Ogris, M.; Steinlein, P.; Kurska, M.; Mechtler, K.; Kircheis, R.; Wagner, E., The size of DNA/transferrin-PEI complexes is an important factor for gene expression in cultured cells. *Gene therapy* **1998**, *5* (10).
22. Zappavigna, S.; Misso, G.; Falanga, A.; Perillo, E.; Novellino, E.; Galdiero, M.; Grieco, P.; Caraglia, M.; Galdiero, S., Nanocarriers conjugated with cell penetrating peptides: new trojan horses by modern ulysses. *Current pharmaceutical biotechnology* **2016**, *17* (8), 700-722.
23. Galdiero, S.; Falanga, A.; Morelli, G.; Galdiero, M., gH625: A milestone in understanding the many roles of membranotropic peptides. *Biochimica et Biophysica Acta (BBA)-Biomembranes* **2015**, *1848* (1), 16-25.
24. Galdiero, S.; Falanga, A.; Vitiello, M.; Raiola, L.; Russo, L.; Pedone, C.; Isernia, C.; Galdiero, M., The presence of a single N-terminal histidine residue enhances the fusogenic properties of a membranotropic peptide derived from herpes simplex virus type 1 glycoprotein H. *Journal of Biological Chemistry* **2010**, *285* (22), 17123-17136.
25. Carberry, T. P.; Tarallo, R.; Falanga, A.; Finamore, E.; Galdiero, M.; Weck, M.; Galdiero, S., Dendrimer Functionalization with a Membrane-Interacting Domain of Herpes Simplex Virus Type 1: Towards Intracellular Delivery. *Chemistry-A European Journal* **2012**, *18* (43), 13678-13685.
26. Tarallo, R.; Accardo, A.; Falanga, A.; Guarnieri, D.; Vitiello, G.; Netti, P.; D'Errico, G.; Morelli, G.; Galdiero, S., Clickable functionalization of liposomes with the gH625 peptide from Herpes simplex virus type I for intracellular drug delivery. *Chemistry-a European Journal* **2011**, *17* (45), 12659-12668.
27. Guarnieri, D.; Falanga, A.; Muscetti, O.; Tarallo, R.; Fusco, S.; Galdiero, M.; Galdiero, S.; Netti, P. A., Shuttle-Mediated Nanoparticle Delivery to the Blood–Brain Barrier. *Small* **2013**, *9* (6), 853-862.
28. Guarnieri, D.; Muscetti, O.; Falanga, A.; Fusco, S.; Belli, V.; Perillo, E.; Battista, E.; Panzetta, V.; Galdiero, S.; Netti, P., Surface decoration with gH625-membranotropic peptides as a method to escape the endo-lysosomal compartment and reduce nanoparticle toxicity. *Nanotechnology* **2015**, *26* (41), 415101.

29. Falanga, A.; Tarallo, R.; Vitiello, G.; Vitiello, M.; Perillo, E.; Cantisani, M.; D'Errico, G.; Galdiero, M.; Galdiero, S., Biophysical characterization and membrane interaction of the two fusion loops of glycoprotein B from herpes simplex type I virus. *PLoS one* **2012**, *7* (2), e32186.
30. Valiante, S.; Falanga, A.; Cigliano, L.; Iachetta, G.; Busiello, R. A.; La Marca, V.; Galdiero, M.; Lombardi, A.; Galdiero, S., Peptide gH625 enters into neuron and astrocyte cell lines and crosses the blood–brain barrier in rats. *International journal of nanomedicine* **2015**, *10*, 1885.
31. Guarnieri, D.; **Melone, P.**; Moglianetti, M.; Marotta, R.; Netti, P. A.; Pompa, P. P., Particle size affects the cytosolic delivery of membranotropic peptide-functionalized platinum nanozymes. *Nanoscale* **2017**, *9* (31), 11288-11296.
32. Galdiero, E.; Falanga, A.; Siciliano, A.; Maselli, V.; Guida, M.; Carotenuto, R.; Tussellino, M.; Lombardi, L.; Benvenuto, G.; Galdiero, S., *Daphnia magna* and *Xenopus laevis* as in vivo models to probe toxicity and uptake of quantum dots functionalized with gh625. *International journal of nanomedicine* **2017**, *12*, 2717.
33. Fitzsimmons, R.; Uludağ, H., Specific effects of PEGylation on gene delivery efficacy of polyethylenimine: interplay between PEG substitution and N/P ratio. *Acta biomaterialia* **2012**, *8* (11), 3941-3955.
34. Kursal, M.; Walker, G. F.; Roessler, V.; Ogris, M.; Roedel, W.; Kircheis, R.; Wagner, E., Novel shielded transferrin– polyethylene glycol– polyethylenimine/DNA complexes for systemic tumor-targeted gene transfer. *Bioconjugate chemistry* **2003**, *14* (1), 222-231.
35. Nguyen, H.; Lemieux, P.; Vinogradov, S.; Gebhart, C.; Guerin, N.; Paradis, G.; Bronich, T.; Alakhov, V.; Kabanov, A., Evaluation of polyether-polyethyleneimine graft copolymers as gene transfer agents. *Gene therapy* **2000**, *7* (2), 126.
36. Dunlap, D. D.; Maggi, A.; Soria, M. R.; Monaco, L., Nanoscopic structure of DNA condensed for gene delivery. *Nucleic acids research* **1997**, *25* (15), 3095-3101.
37. Minagawa, K.; Matsuzawa, Y.; Yoshikawa, K.; Matsumoto, M.; Doi, M., Direct observation of the biphasic conformational change of DNA induced by cationic polymers. *FEBS letters* **1991**, *295* (1-3), 67-69.
38. Nakayama, G. R.; Caton, M. C.; Nova, M. P.; Parandoosh, Z., Assessment of the Alamar Blue assay for cellular growth and viability in vitro. *Journal of immunological methods* **1997**, *204* (2), 205-208.
39. Nociari, M. M.; Shalev, A.; Benias, P.; Russo, C., A novel one-step, highly sensitive fluorometric assay to evaluate cell-mediated cytotoxicity. *Journal of immunological methods* **1998**, *213* (2), 157-167.
40. Lomant, A. J.; Fairbanks, G., Chemical probes of extended biological structures: synthesis and properties of the cleavable protein cross-linking reagent [35S] dithiobis (succinimidyl propionate). *Journal of molecular biology* **1976**, *104* (1), 243-261.
41. Tang, G.; Zeng, J.; Gao, S.; Ma, Y.; Shi, L.; Li, Y.; Too, H.-P.; Wang, S., Polyethylene glycol modified polyethylenimine for improved CNS gene transfer: effects of PEGylation extent. *Biomaterials* **2003**, *24* (13), 2351-2362.

42. Kleemann, E.; Neu, M.; Jekel, N.; Fink, L.; Schmehl, T.; Gessler, T.; Seeger, W.; Kissel, T., Nano-carriers for DNA delivery to the lung based upon a TAT-derived peptide covalently coupled to PEG-PEI. *Journal of Controlled Release* **2005**, *109* (1), 299-316.
43. Reschel, T.; Koňák, Č. r.; Oupický, D.; Seymour, L. W.; Ulbrich, K., Physical properties and in vitro transfection efficiency of gene delivery vectors based on complexes of DNA with synthetic polycations. *Journal of Controlled Release* **2002**, *81* (1), 201-217.
44. McKenzie, D. L.; Kwok, K. Y.; Rice, K. G., A potent new class of reductively activated peptide gene delivery agents. *Journal of Biological Chemistry* **2000**, *275* (14), 9970-9977.
45. Bremner, K. H.; Seymour, L. W.; Logan, A.; Read, M. L., Factors influencing the ability of nuclear localization sequence peptides to enhance nonviral gene delivery. *Bioconjugate chemistry* **2004**, *15* (1), 152-161.
46. Eguchi, A.; Akuta, T.; Okuyama, H.; Senda, T.; Yokoi, H.; Inokuchi, H.; Fujita, S.; Hayakawa, T.; Takeda, K.; Hasegawa, M., Protein transduction domain of HIV-1 Tat protein promotes efficient delivery of DNA into mammalian cells. *Journal of Biological Chemistry* **2001**, *276* (28), 26204-26210.
47. Lowe, A. B.; Hoyle, C. E.; Bowman, C. N., Thiol-yne click chemistry: A powerful and versatile methodology for materials synthesis. *Journal of Materials Chemistry* **2010**, *20* (23), 4745-4750.
48. Concellón, A.; Asín, L.; González-Lana, S.; Jesús, M.; Sánchez-Somolinos, C.; Pinol, M.; Oriol, L., Photopolymers based on ethynyl-functionalized degradable polylactides by thiol-yne 'Click Chemistry'. *Polymer* **2017**, *117*, 259-267.
49. Fairbanks, B. D.; Scott, T. F.; Kloxin, C. J.; Anseth, K. S.; Bowman, C. N., Thiol-Yne photopolymerizations: novel mechanism, kinetics, and step-growth formation of highly cross-linked networks. *Macromolecules* **2008**, *42* (1), 211-217.
50. Petersen, H.; Fechner, P. M.; Fischer, D.; Kissel, T., Synthesis, characterization, and biocompatibility of polyethylenimine-g raft-poly (ethylene glycol) block copolymers. *Macromolecules* **2002**, *35* (18), 6867-6874.
51. Ogris, M.; Walker, G.; Blessing, T.; Kircheis, R.; Wolschek, M.; Wagner, E., Tumor-targeted gene therapy: strategies for the preparation of ligand-polyethylene glycol-polyethylenimine/DNA complexes. *Journal of Controlled Release* **2003**, *91* (1), 173-181.
52. Fischer, D.; von Harpe, A.; Kissel, T., Polyethylenimine: polymer structure influences the physicochemical and biological effects of plasmid/PEI complexes. *Biomaterials* **2000**, 195-211.
53. Kircheis, R.; Blessing, T.; Brunner, S.; Wightman, L.; Wagner, E., Tumor targeting with surface-shielded ligand-polycation DNA complexes. *Journal of controlled release* **2001**, *72* (1), 165-170.
54. Vidič, J.; Podgornik, A.; Štrancar, A., Effect of the glass surface modification on the strength of methacrylate monolith attachment. *Journal of Chromatography A* **2005**, *1065* (1), 51-58.



55. Plueddemann, E. P., Nature of adhesion through silane coupling agents. In *Silane Coupling Agents*, Springer: 1982; pp 111-139.
56. Regitz, M.; Heydt, H., 1, 3-Dipolar cycloaddition chemistry. *Ed. A. Padwa, Wiley Interscience, New York* **1984**, *1*, 393.
57. Huisgen, R., Kinetics and reaction mechanisms: selected examples from the experience of forty years. *Pure and Applied Chemistry* **1989**, *61* (4), 613-628.
58. Jewett, J. C.; Bertozzi, C. R., Cu-free click cycloaddition reactions in chemical biology. *Chemical Society Reviews* **2010**, *39* (4), 1272-1279.
59. Tornøe, C. W.; Christensen, C.; Meldal, M., Peptidotriazoles on solid phase:[1, 2, 3]-triazoles by regiospecific copper (I)-catalyzed 1, 3-dipolar cycloadditions of terminal alkynes to azides. *The Journal of organic chemistry* **2002**, *67* (9), 3057-3064.
60. Rostovtsev, V. V.; Green, L. G.; Fokin, V. V.; Sharpless, K. B., A stepwise huisgen cycloaddition process: copper (I)-catalyzed regioselective "ligation" of azides and terminal alkynes. *Angewandte Chemie* **2002**, *114* (14), 2708-2711.
61. Agard, N. J.; Prescher, J. A.; Bertozzi, C. R., A strain-promoted [3+ 2] azide-alkyne cycloaddition for covalent modification of biomolecules in living systems. *Journal of the American Chemical Society* **2004**, *126* (46), 15046-15047.
62. Prescher, J. A.; Bertozzi, C. R., Chemistry in living systems. *Nature chemical biology* **2005**, *1* (1), 13-21.
63. Cavalli, S.; Overhand, M.; Kros, A., Assembly into  $\beta$ -Sheet Structures upon Peptide-Liposome Conjugation through Copper (I)-Catalyzed [3+ 2] Azide-Alkyne Cycloaddition. *ChemPlusChem* **2014**, *79* (4), 564-568.
64. Cavalli, S.; Tipton, A. R.; Overhand, M.; Kros, A., The chemical modification of liposome surfaces via a copper-mediated [3+ 2] azide-alkyne cycloaddition monitored by a colorimetric assay. *Chemical Communications* **2006**, (30), 3193-3195.
65. Thandu, M.; Rapozzi, V.; Xodo, L.; Albericio, F.; Comuzzi, C.; Cavalli, S., "Clicking" porphyrins to magnetic nanoparticles for photodynamic therapy. *ChemPlusChem* **2014**, *79* (1), 90-98.
66. Balachander, N.; Sukenik, C. N., Monolayer transformation by nucleophilic substitution: Applications to the creation of new monolayer assemblies. *Langmuir* **1990**, *6* (11), 1621-1627.
67. Petersen, H.; Fechner, P. M.; Martin, A. L.; Kunath, K.; Stolnik, S.; Roberts, C. J.; Fischer, D.; Davies, M. C.; Kissel, T., Polyethylenimine-graft-poly (ethylene glycol) copolymers: influence of copolymer block structure on DNA complexation and biological activities as gene delivery system. *Bioconjugate chemistry* **2002**, *13* (4), 845-854.
68. Merdan, T.; Kunath, K.; Petersen, H.; Bakowsky, U.; Voigt, K. H.; Kopecek, J.; Kissel, T., PEGylation of poly (ethylene imine) affects stability of complexes with plasmid DNA under in vivo conditions in a dose-dependent manner after intravenous injection into mice. *Bioconjugate chemistry* **2005**, *16* (4), 785-792.

69. Mao, S.; Neu, M.; Germershaus, O.; Merkel, O.; Sitterberg, J.; Bakowsky, U.; Kissel, T., Influence of polyethylene glycol chain length on the physicochemical and biological properties of poly (ethylene imine)-graft-poly (ethylene glycol) block copolymer/SiRNA polyplexes. *Bioconjugate chemistry* **2006**, *17* (5), 1209-1218.
70. Fisher, J.; Devraj, K.; Ingram, J.; Slagle-Webb, B.; Madhankumar, A.; Liu, X.; Klinger, M.; Simpson, I. A.; Connor, J., Ferritin: a novel mechanism for delivery of iron to the brain and other organs. *American Journal of Physiology-Cell Physiology* **2007**, *293* (2), C641-C649.
71. Fischer, D.; Li, Y.; Ahlemeyer, B.; Krieglstein, J.; Kissel, T., In vitro cytotoxicity testing of polycations: influence of polymer structure on cell viability and hemolysis. *Biomaterials* **2003**, *24* (7), 1121-1131.
72. Malek, A.; Czubayko, F.; Aigner, A., PEG grafting of polyethylenimine (PEI) exerts different effects on DNA transfection and siRNA-induced gene targeting efficacy. *Journal of drug targeting* **2008**, *16* (2), 124-139.
73. Sung, S.-J.; Min, S. H.; Cho, K. Y.; Lee, S.; Min, Y.-J.; Yeom, Y. I.; Park, J.-K., Effect of polyethylene glycol on gene delivery of polyethylenimine. *Biological and Pharmaceutical Bulletin* **2003**, *26* (4), 492-500.

## Chapter 3

# Size and gH625-functionalization affect cytosolic delivery of platinum nanoparticles\*

**Abstract.** The ability of gH625 membranotropic peptide to deliver PtNPs free in the cytosol, by escaping endo-lysosomal pathway, strongly depends on particle size. In particular, peptide functionalization elicits a significant enhancement of NP cellular uptake, though with a prevalent confinement in vesicular structures. Only for the smallest 2.5 nm size, a partial cytosolic localization was observed. Combining the enhanced uptake and partial cytosolic delivery promoted by gH625, a strong improvement of the antioxidant nanozyme function of 2.5 nm PtNPs was achieved.

\* The work described in this Chapter is part of a published manuscript: Guarnieri, D., Melone, P., Moglianetti, M., Marotta, R., Netti, P. A. and Pompa, P. P. (2017). "Particle size affects the cytosolic delivery of membranotropic peptide-functionalized platinum nanozymes." *Nanoscale*, 9(31), 11288-11296. All the figures and table are reproduced or adapted from Ref. <sup>1</sup> with permission from The Royal Society of Chemistry

### 3.1 Introduction

One of the main challenges of nanomedicine is to guide therapeutic agents towards their specific intracellular target, thus improving their efficiency and avoiding side effects. To this aim, drug molecules and nanoparticles (NPs) should cross the highly selective cell membrane to gain access to the interior of the cell and exert their biological functionality. In general, apart from some exceptions (e.g. small non-polar species), molecules and NPs cannot directly overcome the lipid bilayer and are usually internalized by cells according to “classical” endocytosis mechanisms.<sup>2-3</sup> Nevertheless, NPs are typically used as Trojan horses since they allow high intracellular transport of bioactive molecules that cannot otherwise enter the cells, reducing their fast clearance and side effects.<sup>4-6</sup> Following endocytosis, however, nanomaterials become entrapped in vesicular compartments (endosomes/lysosomes), where the very low pH and the presence of specific enzymes generally cause degradation of the internalized material.<sup>7-9</sup> As a consequence, the accumulation of nanomaterials inside endo-lysosomes significantly reduces their therapeutic potential and, sometimes, impairs cellular functions.<sup>7-11</sup> Therefore, shuttling nanoparticles across cell membrane directly into the cytosol by avoiding endocytosis or facilitating endo-lysosomal escape would have a large impact in improving the efficacy of NP-based therapy. To address this issue, several strategies have been explored in recent years, including microinjection, electroporation and endosome lysis through osmotic shock (the so called “proton sponge effect”), but they have shown some limitations due to their invasiveness and cytotoxicity.<sup>2, 12-15</sup>

In this framework, the discovery of cell-penetrating peptides (CPPs), small molecules that can be used as shuttles to deliver bioactive compounds inside cells, has opened new routes for designing effective approaches for intracellular delivery of drugs and nanoparticles.<sup>16-18</sup> Among these, virus-derived peptides, such as the positively charged TAT (derived from HIV-1) and the hydrophobic HA2 (derived from influenza A virus), have been widely employed to functionalize molecules and nanoparticles, in order to enhance their internalization and to avoid lysosomal accumulation at the same time.<sup>16</sup> Several studies have demonstrated that CPPs can improve cellular uptake of nanomaterials.<sup>19-21</sup> However, clear delivery of peptide-functionalized nanomaterials into the cytoplasm has not been fully proved yet, and conflicting findings are reported in the literature.<sup>22-24</sup>

Nativo *et al.* showed that 16 nm gold NPs functionalized with a combination of TAT, penetratin and PEG were partially localized free in the cytosol of HeLa cells.<sup>24</sup> Moreover, Berry *et al.* reported the possibility to deliver TAT-functionalized Au-tiopronin NPs, with an original hydrodynamic diameter of 2.8 nm, to the nucleus of primary human fibroblasts.<sup>22</sup> Oh and co-workers indicated that TAT-functionalized 2.4 nm gold NPs were able to cross nuclear membrane, while 16 nm and larger gold NPs were not able to be taken up by cells.<sup>23</sup> On the other hand, Cesbron *et al.* recently demonstrated that, while endocytosis-mediated uptake significantly increased when the TAT and/or HA2 viral peptides were present on the surface of gold NPs with 5 and 10 nm diameters, no significant cytosolic delivery was observed.<sup>25</sup> Therefore, these results make difficult to formulate a general rule to predict the behavior/fate of CPP-transported NP cargoes. In addition, this scenario includes further complexity, because in many studies CPPs are typically combined with a wide range of surface molecules, including PEG, other stabilizing moieties, tracer elements and targeting agents, which might have a role in cell interaction and uptake.<sup>26-30</sup>

Among other groups, we hypothesized that the size of the NPs linked to the CPP may affect the CPP performance and even modify its uptake mechanism, with consequences in the final intracellular localization of the delivered cargo. In this work, we thus investigated the ability of a membranotropic peptide, namely gH625, to escape the endo-lysosomal compartment and deliver NPs within the cytoplasm, as a function of the NP size. We carried out a systematic assessment of cellular uptake of monodisperse platinum nanoparticles (PtNPs) – with different diameters (2.5, 5 and 20 nm, named Pt2.5, Pt5 and Pt20, respectively) citrate capped or covalently functionalized with the gH625 peptide through a thiol bonding – on human cervix epithelioid carcinoma (HeLa) cells. We combined inductively coupled plasma atomic emission spectroscopy (ICP/AES), scanning transmission electron microscopy (STEM) and electron tomography (ET) analysis to find a correlation between size and surface functionalization of PtNPs with their final intracellular localization. Moreover, ROS generation assays were carried out to investigate the potential effect of gH625 in modifying the cellular interaction of PtNPs and improving their antioxidant properties.

## 3.2 Experimental section

### 3.2.1 Materials

N,N-diisopropylethylamine (DIPEA), O-benzotriazole-N,N,N',N'-tetramethyluronium-hexafluoro-phosphate (HBTU), Ethyl (hydroxyimino)cyanoacetate (OxymaPure®), anhydrous N,N-dimethyl-formamide (DMF), Acetonitrile (ACN), rhodamine B, 4-(dimethylamino) pyridine (DMAP), Dichloromethane (DCM), Methanol, Piperidine, Trifluoroacetic acid (TFA), Triisopropylsilane (TIS), Acetic Anhydride, HPLC-grade water, 2,2,2-trifluoroethanol (TFE) and all buffer solutions were purchased from Sigma-Aldrich (USA). All Fmoc-aminoacids were purchased from IRIS Biotech GmbH (Germany). Distilled and deionized water used Millipore Milli-RO 10 Plus (Millipore, USA) at 18 M $\Omega$  resistance.

### 3.2.2 Platinum nanoparticle synthesis and characterization

Pt5 and Pt20 NPs were synthesized as previously reported.<sup>30</sup> Pt2.5 NPs were synthesized by adding 53  $\mu$ L of 0.5 M H<sub>2</sub>PtCl<sub>6</sub> (BioXtra grade, Sigma Aldrich) to 90 mL of MilliQ water, already heated up to 100 °C. Then, 2.2 mL of a solution containing 1 % sodium citrate and 0.05 % citric acid was added. Under vigorous stirring, 1.1 mL NaBH<sub>4</sub> at 0.08 % was added to the reaction vessel. The vessel was kept under stirring for another 10 minutes. The NP suspension was then extensively purified with 2 mM sodium citrate solution by using 3K Amicon centrifugal filters. The morphology of the produced PtNPs was analyzed by transmission electron microscopy (TEM) (JEOL JEM 1011), operating at an accelerating voltage of 100 kV. Several images were collected to determine the size distribution of the NPs (n = 300) and ICP measurements were made to calculate NP concentrations.

### 3.2.3 Synthesis of Rhodamine-gH625-Cys peptide

The peptide gH625-Cys [Ac-HGLASTLTRWAHYNALIRAFK(Mtt)GGGC-NH<sub>2</sub>] was synthesized using standard solid-phase-9-fluorenyl methoxy carbonyl (Fmoc) method. Mtt

group was then removed from lysine amino group using DCM/TIS/TFA (95/4/1) solution; Kaiser test was used to confirm the complete removal of Mtt groups. Conjugation of rhodamine (rhod) to gH625 peptide was performed on solid-phase by a standard coupling procedure. The mixture of peptide (1 eq), HBTU (3 eq), Oxyma Pure® (3 eq), DIPEA (6 eq) and rhodamine-B (2.5 eq) in anhydrous DMF reacted for 2 h at room temperature under continuous stirring. Then, the resin was washed with DMF, DCM and methanol before cleavage of rhod-gH625 peptide from resin by TFA/TIS/water (95/2.5/2.5) solution and precipitation in cold ethyl ether. The reaction products were verified by analytical LC-MS analysis and then purified by RP-HPLC using a 20/80 (v/v) ACN/ 0.1% v/v TFA. MS for rhod-gH625-Cys peptide: calculated for  $[M+H]^+$  = 3167.73 m/z; found (ESI)  $[M+3H]^{3+}$  = 1056.58 m/z,  $[M+4H]^{4+}$  = 792.68 m/z,  $[M+5H]^{5+}$  = 634.35 m/z,  $[M+6H]^{6+}$  = 528.69 m/z. To verify the secondary structure of rhod-gH625-Cys peptide, circular dichroism (CD) spectra were recorded using a JASCO J1500 CD spectrometer in a 0.1 cm quartz cell at room temperature. The spectra were an average of 15 consecutive scans from 260 to 190 nm, recorded with a band width of 1 nm, a data pitch of 0.2 nm and a scan rate of 100 nm/min. Spectra were recorded and corrected for the blank sample.

### 3.2.4 Peptide conjugation to PtNPs

Peptide-NP functionalization was performed by means of the thiol group in the side chain of the C-terminal cysteine (C) that is able to make a covalent bond with platinum surface.<sup>31</sup> Based on NP size and in order to achieve the same surface functionalization (in terms of number of peptides per surface units), we explored a broad range of peptides/NP ratios trying to accomplish a balance between functionalization efficiency and colloidal stability (Table 3.1).

**Table 3.1.** Theoretical surface densities of gH625 peptide as a function of particle size and peptide/NPs ratios.

| Theoretical surface density (n° peptide/nm <sup>2</sup> ) | Peptide/NP ratio |     |      |
|---|------------------|-----|------|
|   | Pt2.5            | Pt5 | Pt20 |
| <b>0.09</b>   | 2                | 5   | 100  |
| <b>0.18</b>   | 4                | 10  | 200  |
| <b>0.27</b>   | 6                | 15  | 300  |
| <b>0.36</b>   | 8                | 20  | 400  |

NPs were functionalized with rhodamine-gH625 peptide by simply adding proper volumes of NP suspension to peptide water solution, mixing by gently pipetting up and down until suspension was homogenized and let to react for 30 min at room temperature. To evaluate the functionalization efficiency, NPs were centrifuged at  $14.8 \times 10^3$  rpm for 40 min. After centrifugation, the supernatant was collected and the rhodamine fluorescence intensity was measured in order to evaluate the amount of unbound peptide *via* fluorimetric assay (ex/em 550/570 nm). Measurement values were interpolated with the standard curve to obtain peptide concentration. The starting peptide concentration was considered as 100 %.

### **3.2.5 Cell culture**

Human cervix epithelioid carcinoma (HeLa) cells (ATCC) were cultured in Dulbecco's Modified Eagles Medium (DMEM, Invitrogen) supplemented with 10% (v/v) fetal bovine serum (FBS, Hyclone), 100 U/mL penicillin and 100 mg/mL streptomycin (Invitrogen). Cells were maintained in incubator at 37 °C under a humidified controlled atmosphere and 5 % CO<sub>2</sub>.

### **3.2.6 Cell uptake experiments**

The amount of internalized NPs per cell was quantified by Inductively Coupled Plasma Atomic Emission Spectroscopy (ICP-AES).  $5 \times 10^5$  HeLa cells were seeded in 6-well plates and treated with gH625-functionalized and non-functionalized PtNPs with 2.5, 5 and 20 nm diameters at the concentration of 50 µg/ml for 24 hours. The untreated cells were used as a control. After incubation, the cells were washed three times with sterile PBS to remove non-internalized NPs, detached by trypsinization and further washed twice with sterile PBS by centrifugation. The number of cells was determined by using Burker chamber. The samples were digested overnight with 1 mL of aqua regia. The solution was then diluted to 5 mL with MilliQ water and directly analyzed by ICP-AES (iCAP 6300 DUO, ThermoFisher).



### 3.2.7 Transmission electron microscopy

HeLa cells were incubated 24 hours with gH625-functionalized and non-functionalized Pt2.5, Pt5 and Pt20 nanoparticles and processed as previously reported.<sup>30</sup> Briefly, after nanoparticle incubation, the cells were fixed for 1 h in 1.2 % glutaraldehyde in 0.1 M sodium cacodylate buffer (pH 7.4), post fixed in 1 % osmium tetroxide in the same buffer and *en bloc* stained with 1 % uranyl acetate aqueous solution. The cells were then dehydrated in a graded ethanol series and embedded in epoxy resin (Epon 812, TAAB). Semi-thin and thin sections of the embedded cell monolayer were cut with an ultramicrotome (UC6, Leica) equipped with a diamond knife (Diatome). Both projection images and tilt series were acquired in STEM mode working in High Angular Annular Dark Field (HAADF) geometry, using a FEI Tecnai F20 transmission electron microscope operating at 200 kV and equipped with a Schottky field-emission gun. The tilt series were acquired from 400 nm (for the tomography shown in Figure 3.9 A) and 100 nm (for the tomography shown in Figure 3.9 B-D) thick sections tilted over  $\pm 60$  degrees applying the Saxton tilt increment scheme with a 0 tilt step of 3 degrees<sup>32</sup> with a magnification of 75000 and 22500 times corresponding to a final pixel size of 1.30 and 0.46 nm, respectively. Computation of the dual tilt tomogram was carried out with the IMOD software package.<sup>33</sup> Segmentation and 3D visualization were carried out using the Amira package (FEI Visualization Science Group, Bordeaux).

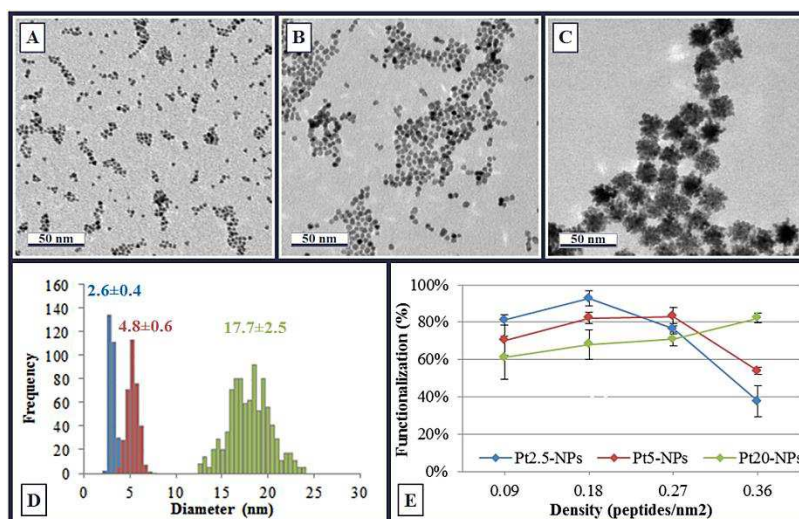
### 3.2.8 DCF assay

$3 \times 10^4$  HeLa cells were seeded in 96-well microplates and treated with functionalized gH625-Pt2.5 NPs at a final concentration of 50  $\mu\text{g}/\text{ml}$ . After 48 hours of cell-NP interaction, the dichlorofluorescein (DCF) assay was performed. Briefly, the cells were washed with HBSS and incubated with 5  $\mu\text{M}$  DCFH-DA in HBSS for 45 min at 37 °C. The cells were washed with HBSS and the DCF fluorescence intensity was measured by using a plate reader (Synergy HT, BioTek – ex/em 480/520 nm). The results were normalized with respect to the negative controls (expressed as 100 %). To verify the ROS scavenging activity of PtNPs, HeLa cells were also treated for 5 min with 1 mM  $\text{H}_2\text{O}_2$  after 48 h incubation with NPs and 45 min staining with 5  $\mu\text{M}$  DCFH-DA.

### 3.3 Results and discussion

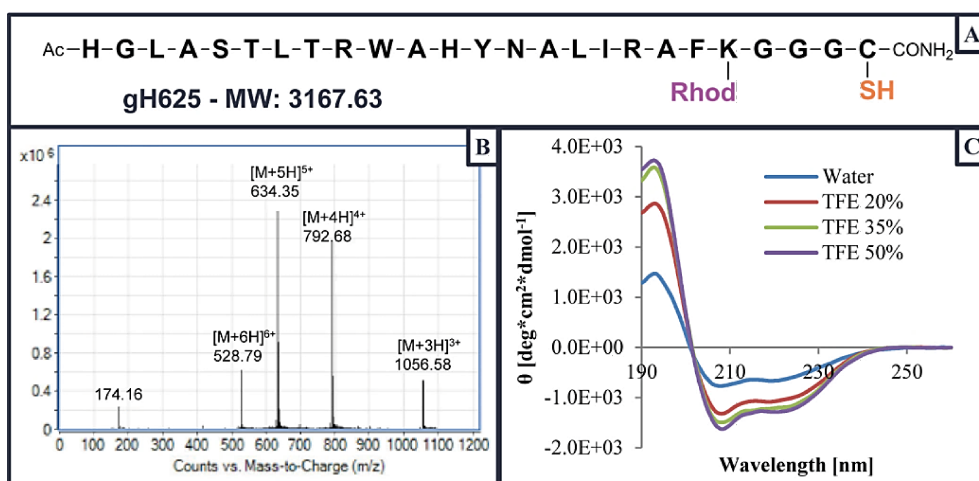
#### 3.3.1 Synthesis and characterization of gH625-functionalized PtNPs

gH625 is a peptide derived from the glycoprotein H (gH) of the *Herpes simplex virus 1* (20-residue). Several studies demonstrated that it is recognized as a membrane perturbing domain,<sup>34</sup> and contribute to their merging interacting with model membranes.<sup>35</sup> Moreover, it is proved that this peptide can transport different kind of cargo, such as NPs, dendrimers, quantum dots and liposomes, both into the cell and across the brain endothelium. In this way, gH625 is able to reduce the accumulation of NPs as large aggregates into the lysosomes and enhance significantly the cell uptake and.<sup>36-42</sup> For these reasons, this peptide could offer several advantages in escaping endo-lysosomal compartments, making gH625 a good candidate for the delivery of free nanoparticles in the cytosol. In particular, platinum nanoparticles with different diameters (2.5, 5 and 20 nm) were synthesized by optimization of a previously reported method.<sup>30</sup> Images obtained by transmission electron microscopy of bare (citrate capped) nanoparticles showed homogeneous distribution of both size and shape for all three preparations (Figure 3.1 A-D).



**Figure 3.1.** TEM images of bare PtNPs with (A) 2.5, (B) 5 and (C) 20 nm diameters. Scale bar 50 nm. (D) Size distribution of Pt2.5, Pt5 and Pt20 NPs calculated by TEM image analysis (n~300) and reported in the chart. (E) Quantification of peptide binding efficiency obtained by using peptide/NP ratios reported in Table 3.1. Functionalization percentages were calculated as difference of initial peptide concentration (100 %) and unbound peptide recovered after the reaction with nanoparticles. Data are reported as mean ± SD.

Similar to other noble metals, such as gold and silver, platinum has high reactivity to thiols.<sup>31</sup> PtNPs were functionalized with rhodamine-conjugated gH625 membranotropic peptide (Figure 3.1 A) through the –SH group of Cysteine residue at the C-term of the peptide sequence (Figure 3.2 A). MS and CD analysis demonstrated the effective conjugation of rhodamine to peptide sequence (MW 3167.73 Da) and the correct formation of gH625  $\alpha$ -helical secondary structure, respectively (Figure 3.2 B-C). Unfortunately, CD spectra of functionalized NP were not conclusive, due to the interference of PtNPs.

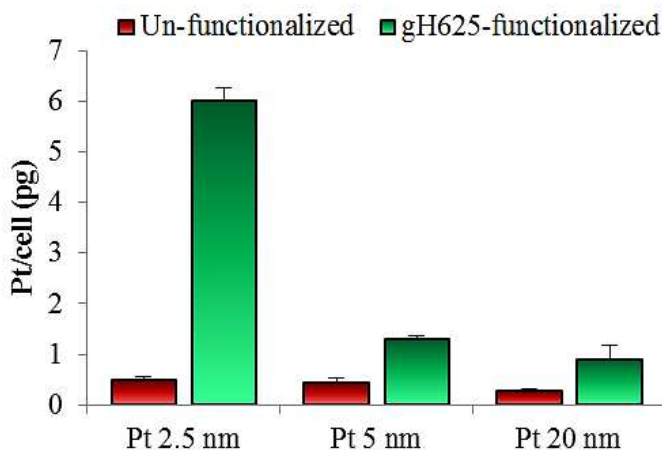


**Figure 3.2.** Characterization of rhodamine-conjugated gH625 peptide. (A) Peptide chemical structure. (B) Mass spectrum shows peaks of multi-charged ions corresponding to 3167.73 Da molecular weight; (C) Circular dichroism (CD) at increasing amounts (up to 50% v/v) of 2,2,2-trifluoroethanol (TFE), used as a structure-inducing co-solvent. The absorption peaks at 194 nm and the negative ellipticity at 208 and 220 nm rise with TFE concentration are indicative of a  $\alpha$ -helix secondary structure.

Then, peptide bio-conjugation was performed with the three NP sizes, to maximize the loading efficiency while guarantying a constant peptide surface density on the particles for biological experiments. Different peptide/NP ratios for each NP were tested, with theoretical values corresponding to 0.09, 0.18, 0.27 and 0.36 peptides/nm<sup>2</sup> (Table 3.1). Results showed that the maximum nominal density of functionalization achievable with all the particle sizes was 0.27 peptides/nm<sup>2</sup> (Figure 3.1 E). Higher density values lead to small particles that lose their functionalization efficiency, partly due to a decrease in NP suspension stability. According to these results, we estimated a real peptide surface density of ca. 0.20 peptides/nm<sup>2</sup> for all NP sizes. Then, the ratios of 6, 15 and 300 peptides/NP were chosen for Pt2.5, Pt5 and Pt20 NPs, respectively.

### 3.3.2 Cell uptake and intracellular localization of gH625-functionalized PtNPs

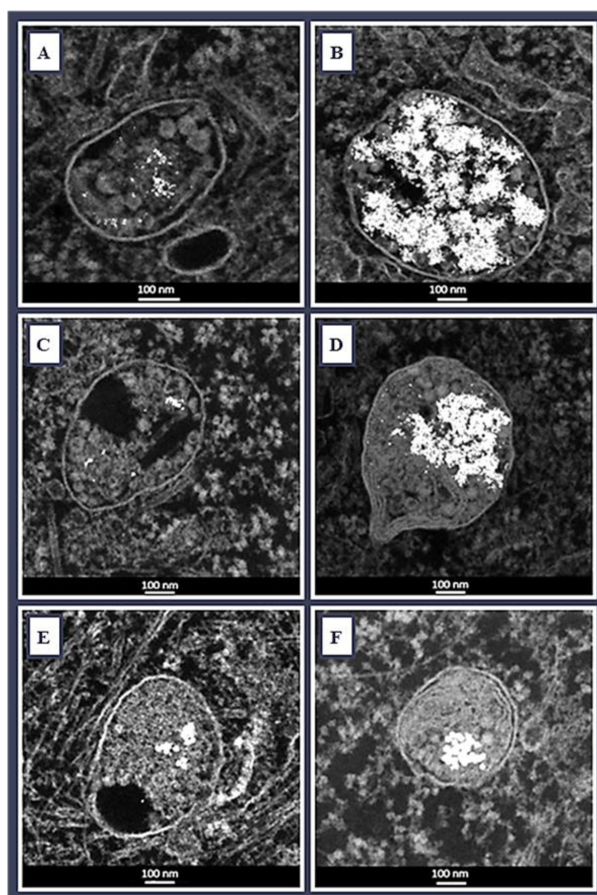
The ability of gH625 to facilitate the intracellular delivery of PtNPs was tested as a function of the particle size. We previously quantified the amount of internalized NPs by ICP/AES. Then we evaluated the uptake by HeLa cells of bare and functionalized PtNPs after 24 h incubation as reported in Figure 3.3.



**Figure 3.3.** Quantification of NP cellular uptake by ICP/AES analysis after 24 h incubation with 50 µg/ml NP suspension in cell culture medium. Data are reported as mean ± SD.

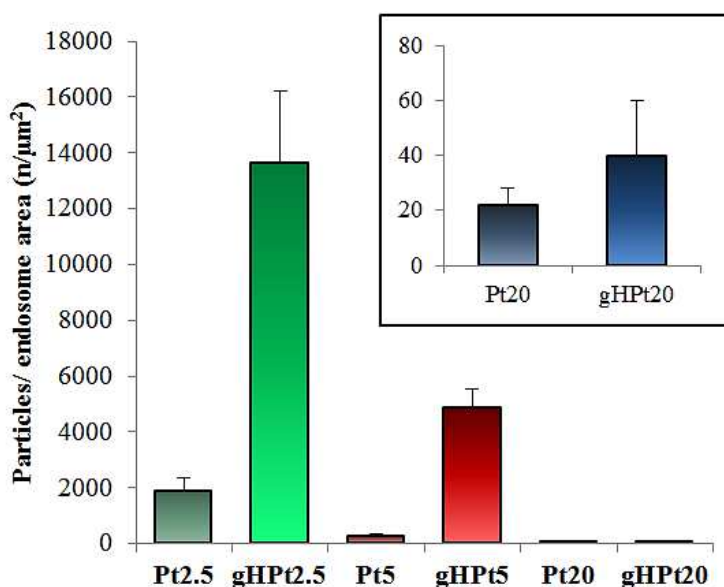
According with literature,<sup>30</sup> bare PtNPs were internalized in cells in a size-dependent manner. Interestingly, functionalized NPs showed a significantly higher cellular uptake than bare NPs, maintaining higher internalization for smaller NPs. The uptake efficiency gain promoted by the peptide was particularly evident for the smallest 2.5 nm particles. Notably, we observed a ca. 4-fold increase for gHPt5 and gHPt20 NPs and a 12-fold increase for gHPt2.5 NPs with respect to pristine particles. These results suggest that the ability of gH625 peptide to enhance NP cellular uptake is strongly limited by the size of the NP cargo. These results confirm previous study, showing that the uptake increase in presence of gH625 peptide was less than 2-fold for 100 nm polystyrene NPs in bEnd.3 cells.<sup>41</sup> Moreover, gH625 is able to fuse with the lipid bilayer through both electrostatic and hydrophobic interactions that work in concert to mediate membrane penetration.<sup>43</sup> In particular, the aromatic residues in the gH625 peptide chain allow its insertion into the membrane interface, while the basic residues stabilize this interaction by linking the negatively charged head-groups, as shown in other systems.<sup>44-46</sup> Therefore the

enhancement of NP cellular uptake observed in presence of gH625 depends on a better peptide-mediated interaction between the functionalized NPs and the cell membrane.<sup>38</sup> Then the intracellular distribution of PtNPs was analyzed by scanning transmission electron microscopy (STEM) and electron tomography (ET), to assess if the ability of gH625 to enhance their delivery was also associated to a different uptake mechanism and, therefore, a different cytoplasmic localization. After 24 h of incubation with HeLa cells, we observed that all bare particles were prevalently confined within vesicular structures, addressable as late endosome/lysosome compartments (Figure 3.4, left), according with the results obtained for 5 and 20 nm PtNPs.<sup>30</sup> Moreover, regarding the cells treated with gH625-PtNPs, we observed a main endo-lysosomal confinement (Figure 3.4, right), with vesicular compartments completely full of particles, especially for the smaller NPs.



**Figure 3.4.** STEM images of endo-lysosomal compartments in HeLa cells after 24 h incubation with bare and gH625-functionalized PtNPs at 50  $\mu\text{g}/\text{ml}$  particle concentration, indicating the intracellular localization of internalized NPs. (A) Pt2.5; (B) gHPt2.5; (C) Pt5; (D) gHPt5; (E) Pt20; (F) gHPt20. Scale bar 100 nm.

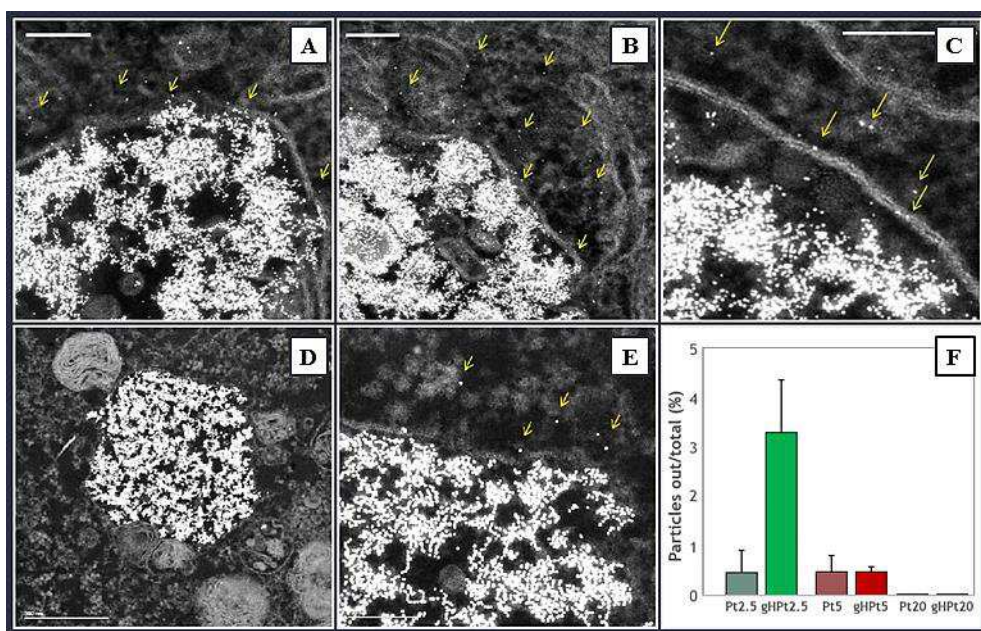
Focusing on the STEM images, we found that there was an increment of NP density per endo-lysosomal unit area (Figure 3.5) that was influenced by both size and peptide functionalization, according with ICP/AES results (Figure 3.3). In particular, gHPt2.5 showed significant internalization efficiency, reaching a density of ca. 14,000 NPs/ $\mu\text{m}^2$  in endo-lysosomes (Figure 3.5).



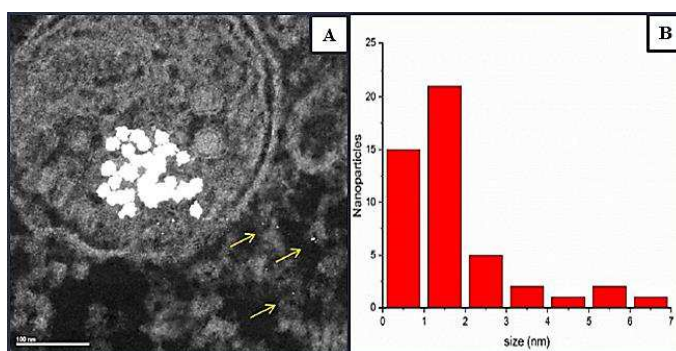
**Figure 3.5.** Semi-quantitative analysis of gH625-functionalized and bare Pt2.5, Pt5 and Pt20 NP density into endo-lysosomal compartments. Inset represents endo-lysosomal density of Pt20 and gHPt20 NPs with a lower scale of y-axis. Data are reported as mean  $\pm$  s.e.m.

A more detailed analysis of these structures revealed the presence of gHPt2.5 NPs in close proximity to the inner part of the endo-lysosomal membrane, some NPs perfectly interposed in the membrane bilayer and some others were found outside the vesicles and free in the cytoplasm (Figure 3.6 A-C). The percentage of the gHPt2.5 NPs found free in the cytoplasm with respect to the total of internalized NPs was calculated to be about 3.3 %, a value almost 7-fold higher than 0.5 % of non-functionalized Pt2.5 NPs (Figure 3.6 F). Larger gHPt5 NPs were also able to escape endo-lysosomal compartments, but with a very low efficiency (ca. 0.5 %), regardless of surface functionalization (Figure 3.6 D-F). Concerning the 20 nm particles, neither Pt20 nor gHPt20 were observed as free in the cytosol (Figure 3.6 F), indicating no effect of gH625 peptide in transporting large ( $\geq 5$  nm) NPs across the endo-lysosomal membrane toward the cytosol. Focusing the attention on 20 nm NPs, we found very few platinum fragments both inside and outside the endo-lysosome

vesicles (Figure 3.7 A). Most of these fragments, deriving from minor lysosomal degradation of the flower-like nanostructures, showed a size ranging from 1 to 2 nm (Figure 3.7 B), thus smaller or comparable to Pt2.5 NPs, which showed some ability to cross the endo-lysosomal membrane. No particles of any size were observed in the cell nucleus.

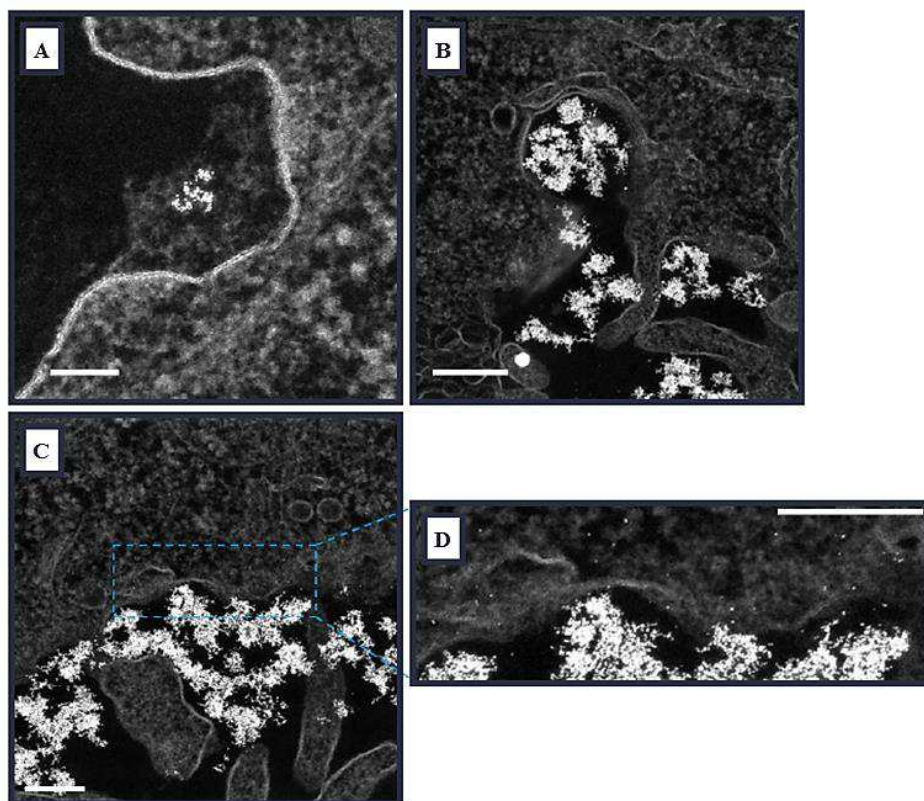


**Figure 3.6.** Representative STEM images of HeLa cells after 24 h of incubation with gH625-functionalized Pt2.5 NPs (A-C) Pt5 NPs (D-E) at 50 µg/ml particle concentration. Worth of note the presence of some endo-lysosomal compartments completely full of particles, NPs crossing the endo-lysosomal membrane and free in the cytoplasm (yellow arrows). Scale bars: 100 nm (A-C), 500 nm (D) and 200 nm (E). (F) Semi-quantitative analysis of Pt2.5 NPs out of endo-lysosomal compartments. Data are reported as mean ± SD.



**Figure 3.7.** (A) STEM image of HeLa cells after 24 h of incubation with gH625-functionalized Pt20 NPs at 50 µg/ml particle concentration, showing some particle fragmentation inside and outside the endo-lysosomal compartment. Scale bar 100 nm. (B) Size range analysis of particle fragments with a peak around 1-2 nm.

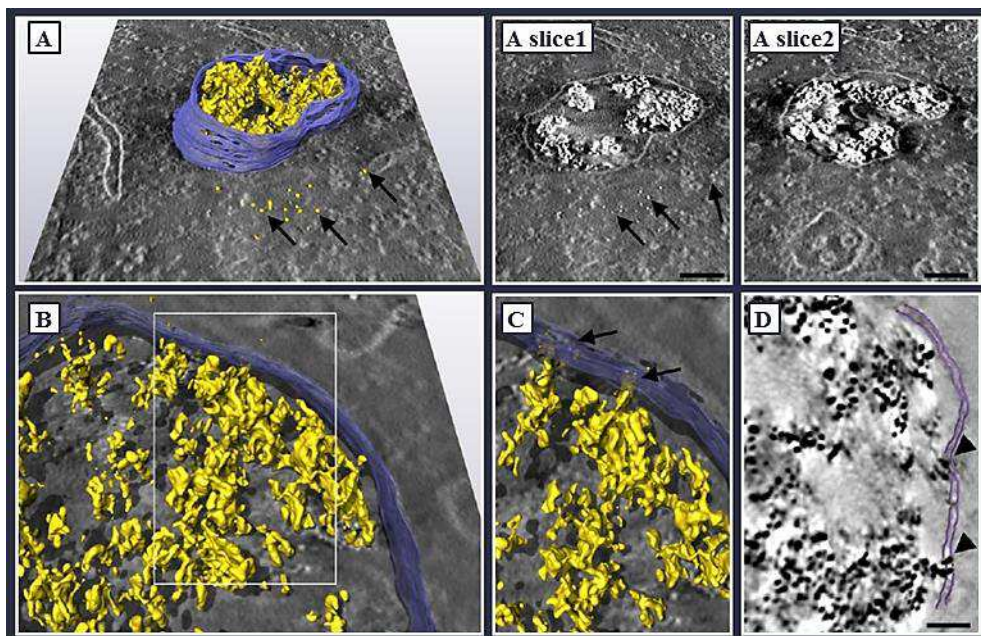
STEM images of cell membrane, revealed that gHPT2.5 NPs went into the cell as small or large aggregates through clathrin-coated pits (Figure 3.8 A) and membrane invaginations (likely macropinosomes) (Figure 3.8 B) and, in a minor fraction, as single particles penetrating lipid bilayer directly (Figure 3.8 C-D).



**Figure 3.8.** STEM images of gHPT2.5 NPs approaching cell membrane. (A) small NP aggregate entering through a large putative clathrin-coated pit; (B) large NP aggregates entering by macropinocytosis; (C) single NPs penetrating cell membrane and reaching directly the cytosol; (D) zoomed image of dashed squared areas in (C). Scale bars: 100 nm (A) and 200 nm (B-D).

STEM HAADF electron tomography (ET), done after 24 h incubation with gHPT2.5 NPs, allowed to obtain a 3D reconstruction of HeLa endolysosomes. With this high-resolution images we were able to confirm the localization of NPs inside these organelles, a small fraction of nanoparticles outside them (Figure 3.9 A), as well as their presence in the lipid bilayer (Figure 3.9 B-D). In particular, focusing on Figure 3.9 C and D, it is possible to note membrane crossing by 2.5 nm functionalized NPs, which seems to occur by diffusion through the lipid bilayer, with no evident membrane damage.





**Figure 3.9.** STEM HAADF electron tomographies (ET) of endosomal compartments in HeLa cells after 24 h incubation with gHPt2.5 NPs indicating particle intracellular distribution. Endosomal membranes and PtNPs are pseudo-colored respectively in violet and yellow. (A-B) 3D reconstruction obtained from tomograms of endosomes containing clusters of gHPt2.5 NPs. (A slices 1-2) Details of single slices extracted from tomogram in (A) indicating NP localization. Black arrowheads indicate particles localized in the cytosol. (C) Zoomed image of the region highlighted by the white square in (B) showing NP diffusion through the lysosomal membrane. (D) Details of a single slice extracted from the tomogram in (B) indicating NPs interposed between the lipid bilayer of endo-lysosomal membrane highlighted in violet (black arrowheads). Scale bars are 100 nm in a slice1-2 and 30 nm in (D). 3D projections in A and B have the same magnification of A slice1 and D, respectively.

The amphipathic nature of gH625<sup>47</sup> let it to transport cargoes across the endolysosomal membrane providing a particular tropism for lipid membranes.<sup>35</sup> Moreover, gH625 is able to fuse with liposomes<sup>36</sup> and to interact prevalently with cholesterol of synthetic lipid membranes.<sup>48</sup> Especially, its shuttling function is drastically reduced upon cholesterol depletion in mouse brain endothelial cells.<sup>41</sup> Our results showed that gH625 improved the interaction with lipid bilayers, facilitating particle uptake. Though, the presence of a differently-sized cargo, covalently bound to the peptide, strongly affects gH625 performance, in terms of membrane penetration and lysosomal escape. It could be explained considering the hindrance of the NPs that limits the interaction of gH625 with the lipid bilayer, especially in terms of its transient destabilization enabling membrane crossing. This is consistent with our findings of undetectable peptide effects with 5 and 20 nm PtNPs, which are too big with respect to ~7 nm thick membrane to preserve the

membranotropic functionality of the conjugated peptide. Our hypothesis are in agreement with Cesbron *et al.* work that showed a significant increase of cellular uptake of 5 and 10 nm AuNPs functionalized with TAT and/or HA2 peptides, with a prevalent vesicular confinement and no cytosolic delivery of NPs.<sup>25</sup>

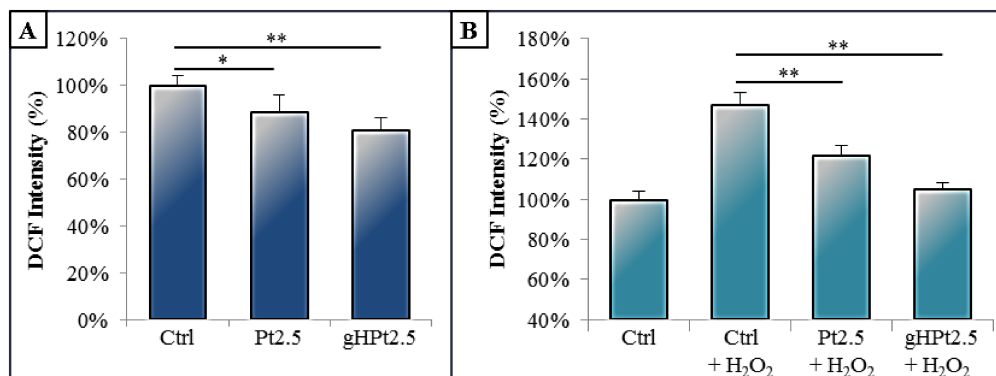
In addition, we observed that for particles of 2-3 nm size, that is ca. 3-fold smaller than cell membrane thickness, part of the gH625 functionality is preserved and some NPs are delivered free in the cytosol following direct membrane penetration. In general, different behaviors could be observed as a function of the specific peptide-NP couple, since several NP properties (e.g. material, size, shape, surface chemistry, stability and protein corona) may affect its interaction with the cell. Peptide surface density and peptide-surface interactions could influence the efficiency of direct membrane crossing. Moreover, the NP dispersion/agglomeration in culture medium can strongly influence the cytosolic delivery mediated by the conjugated peptides, as membranotropic activity can more likely occur at single-particle level (as observed for example in Figure 3.6 and Figure 3.8), while NP agglomerates are likely uptaken through macropinocytosis and confined in endosomes. Therefore, in order to reduce and prevent NP aggregation in cell culture medium we can improve the direct diffusion of single gH625-NPs across the membrane, especially in the case of the smallest particles (2.5 nm).<sup>49</sup>

### **3.3.3 Antioxidant activity of gH625-functionalized PtNPs**

Several works were focused on the properties of PtNPs as efficient catalysts<sup>50-52</sup> and potent antioxidants.<sup>53-55</sup> Kim *et al.* reported the enhancement of the antioxidant activity of 2.4 nm PtNPs functionalized with a TAT fusion peptide in *C. elegans*.<sup>56</sup> In addition, recently It has been demonstrated that Pt5 and Pt20 NPs can act as nanozymes, with strong catalase-, peroxidase- and superoxide dismutase-like activities,<sup>30</sup> and were able to restore physiological reactive oxygen species (ROS) homeostasis in an experimental model of oxidative stress-related disease.<sup>30</sup> Here, we focused on the possibility to use gH625 to improve the ROS scavenging activity of Pt2.5 NPs in HeLa cells, exploiting the highly increased particle uptake and partial cytosolic delivery promoted by the peptide.

Firstly, we evaluated the cellular level of endogenous ROS upon incubation with Pt2.5 and gHPt2.5 NPs, since an increment of ROS generation is often associated to cell-NP

interactions.<sup>57</sup> To this aim, cells were treated for 48 h with 50  $\mu\text{g/ml}$  of Pt2.5 and gHPt2.5 NPs and ROS generation was analyzed by standard DCF assay. As for Pt5 and Pt20 NPs, no increase of oxidative stress was observed. Our experimental results indicated a reduction of ROS basal level in NP-treated cells compared to non-treated control cells (Figure 3.10 A). In particular, the presence of gH625 peptide produced a higher decrease of ROS level (20% of gHPt2.5 vs. 10 % of Pt2.5), in qualitative agreement with the cellular internalization data. The ROS reduction was not observed in cells treated with bigger bare NPs (Pt5 and Pt20),<sup>30</sup> indicating that the higher cellular uptake combined to the smaller size (i.e., larger surface area) increased nanoPt antioxidant activity. Then we studied the ROS scavenging activity of internalized Pt2.5 and gHPt2.5 NPs, after induction of an oxidative stress insult by hydrogen peroxide. Both PtNPs were able to decrease the ROS production. However, the efficacy of gHPt2.5 NPs was significantly stronger, allowing an almost total stress recovery, reaching the same levels of non-treated cells (Figure 3.10 B).



**Figure 3.10.** DCF assay results indicating the ROS scavenging activity of bare and gH625-functionalized Pt2.5 NPs. HeLa cells were treated 48 h with 50  $\mu\text{g/ml}$  NP suspension and stained 45 min with DCF solution. (A) Basal level of ROS; (B) ROS scavenging effect of PtNPs after 5 min treatment with 1 mM H<sub>2</sub>O<sub>2</sub>. Data are reported as mean  $\pm$  SD. Results were analyzed by one-way analysis of variance (ANOVA). Values of  $p < 0.05$  (\*) and  $p < 0.01$  (\*\*) were considered statistically significant.

Therefore, the surface functionalization of PtNPs with the membranotropic peptide is able to enhance their anti-oxidant nanozyme activity. High ROS levels are a common biochemical feature of many diseased tissues, including tumors.<sup>58</sup> The efficacy of gH625-functionalized PtNPs to reduce basal levels of endogenous ROS as well as their overproduction upon an external insult makes this platform very promising for several biomedical applications.

### 3.4 Conclusions

In this chapter, we demonstrated that particle size strongly affects the ability of gH625 to deliver PtNPs free in the cytosol, by escaping endo-lysosomes.

The modulation of peptide functionalization was important to stimulate the efficiency of cellular internalization for all the NP sizes, although such effect is significantly higher for smaller NPs. Regarding larger PtNPs (5 and 20 nm), we did not find any cytosolic localization of the particles, apart from an extremely low fraction (around 0.5 %) of 5 nm NPs, regardless of gH625 functionalization. On the other hand, for particle size of 2.5 nm, we found a population of cytosolic peptide-functionalized NPs, where the presence of gH625 elicited a ca. 7-fold fractional increase in cytosolic localization with respect to bare particles (the overall gain in cytosolic NPs, promoted by the peptide, was thus ca. 80), although single NPs diffusion across cell membrane was partly limited by their aggregation in culture medium. Furthermore, the very small size of gHPt2.5 NPs, combined with the significant enhancement of their cellular uptake due to peptide functionalization, showed great advantage in improving the antioxidant activity of PtNPs. As matter of fact, these results showed the high potential of membranotropic peptides for nanomedicine, as they can provide great benefit to NPs in terms of improved delivery and therapeutic action, yet further studies are needed, both *in vitro* and *in vivo*, to fully understand the size-dependent mechanisms and limitations (including the effects of *in situ* particle agglomeration) of membrane penetration and direct cytosolic delivery.

### 3.5 References

1. Guarnieri, D.; **Melone, P.**; Moglianetti, M.; Marotta, R.; Netti, P. A.; Pompa, P. P., Particle size affects the cytosolic delivery of membranotropic peptide-functionalized platinum nanozymes. *Nanoscale* **2017**, *9* (31), 11288-11296.
2. Iversen, T.-G.; Skotland, T.; Sandvig, K., Endocytosis and intracellular transport of nanoparticles: present knowledge and need for future studies. *Nano Today* **2011**, *6* (2), 176-185.
3. Canton, I.; Battaglia, G., Endocytosis at the nanoscale. *Chemical Society Reviews* **2012**, *41* (7), 2718-2739.
4. Peer, D.; Karp, J. M.; Hong, S.; Farokhzad, O. C.; Margalit, R.; Langer, R., Nanocarriers as an emerging platform for cancer therapy. *Nature nanotechnology* **2007**, *2* (12), 751-760.
5. Blanco, E.; Shen, H.; Ferrari, M., Principles of nanoparticle design for overcoming biological barriers to drug delivery. *Nature biotechnology* **2015**, *33* (9), 941-951.
6. Petros, R. A.; DeSimone, J. M., Strategies in the design of nanoparticles for therapeutic applications. *Nature reviews. Drug discovery* **2010**, *9* (8), 615.
7. Sabella, S.; Carney, R. P.; Brunetti, V.; Malvindi, M. A.; Al-Juffali, N.; Vecchio, G.; Janes, S. M.; Bakr, O. M.; Cingolani, R.; Stellacci, F., A general mechanism for intracellular toxicity of metal-containing nanoparticles. *Nanoscale* **2014**, *6* (12), 7052-7061.
8. De Matteis, V.; Malvindi, M. A.; Galeone, A.; Brunetti, V.; De Luca, E.; Kote, S.; Kshirsagar, P.; Sabella, S.; Bardi, G.; Pompa, P. P., Negligible particle-specific toxicity mechanism of silver nanoparticles: the role of Ag<sup>+</sup> ion release in the cytosol. *Nanomedicine: Nanotechnology, Biology and Medicine* **2015**, *11* (3), 731-739.
9. Wang, F.; Yu, L.; Monopoli, M. P.; Sandin, P.; Mahon, E.; Salvati, A.; Dawson, K. A., The biomolecular corona is retained during nanoparticle uptake and protects the cells from the damage induced by cationic nanoparticles until degraded in the lysosomes. *Nanomedicine: Nanotechnology, Biology and Medicine* **2013**, *9* (8), 1159-1168.
10. Guarnieri, D.; Sabella, S.; Muscetti, O.; Belli, V.; Malvindi, M. A.; Fusco, S.; De Luca, E.; Pompa, P. P.; Netti, P. A., Transport across the cell-membrane dictates nanoparticle fate and toxicity: a new paradigm in nanotoxicology. *Nanoscale* **2014**, *6* (17), 10264-10273.
11. Cheng, H. J.; Wu, T. H.; Chien, C. T.; Tu, H. W.; Cha, T. S.; Lin, S. Y., Corrosion-Activated Chemotherapeutic Function of Nanoparticulate Platinum as a Cisplatin Resistance-Overcoming Prodrug with Limited Autophagy Induction. *Small* **2016**, *12* (44), 6124-6133.
12. Levy, R.; Shaheen, U.; Cesbron, Y.; See, V., Gold nanoparticles delivery in mammalian live cells: a critical review. *Nano reviews* **2010**, *1* (1), 4889.

13. Sandhu, K. K.; McIntosh, C. M.; Simard, J. M.; Smith, S. W.; Rotello, V. M., Gold nanoparticle-mediated transfection of mammalian cells. *Bioconjugate chemistry* **2002**, *13* (1), 3-6.
14. Zhang, Y.; Yu, L.-C., Microinjection as a tool of mechanical delivery. *Current opinion in biotechnology* **2008**, *19* (5), 506-510.
15. Dokka, S.; Rojanasakul, Y., Novel non-endocytic delivery of antisense oligonucleotides. *Advanced drug delivery reviews* **2000**, *44* (1), 35-49.
16. Bechara, C.; Sagan, S., Cell-penetrating peptides: 20 years later, where do we stand? *FEBS letters* **2013**, *587* (12), 1693-1702.
17. Zahid, M.; Robbins, P. D., Cell-type specific penetrating peptides: Therapeutic promises and challenges. *Molecules* **2015**, *20* (7), 13055-13070.
18. Rajendran, L.; Knölker, H.-J.; Simons, K., Subcellular targeting strategies for drug design and delivery. *Nature reviews. Drug discovery* **2010**, *9* (1), 29.
19. Child, H. W.; del Pino, P. A.; De La Fuente, J. M.; Hursthouse, A. S.; Stirling, D.; Mullen, M.; McPhee, G. M.; Nixon, C.; Jayawarna, V.; Berry, C. C., Working together: the combined application of a magnetic field and penetratin for the delivery of magnetic nanoparticles to cells in 3D. *ACS nano* **2011**, *5* (10), 7910-7919.
20. Nakase, I.; Tanaka, G.; Futaki, S., Cell-penetrating peptides (CPPs) as a vector for the delivery of siRNAs into cells. *Molecular BioSystems* **2013**, *9* (5), 855-861.
21. Ding, C.; Wu, K.; Wang, W.; Guan, Z., Synthesis of a cell penetrating peptide modified superparamagnetic iron oxide and MRI detection of bladder cancer. *Oncotarget* **2017**, *8* (3), 4718.
22. de la Fuente, J. M.; Berry, C. C., Tat peptide as an efficient molecule to translocate gold nanoparticles into the cell nucleus. *Bioconjugate chemistry* **2005**, *16* (5), 1176-1180.
23. Oh, E.; Delehanty, J. B.; Sapsford, K. E.; Susumu, K.; Goswami, R.; Blanco-Canosa, J. B.; Dawson, P. E.; Granek, J.; Shoff, M.; Zhang, Q., Cellular uptake and fate of PEGylated gold nanoparticles is dependent on both cell-penetration peptides and particle size. *Acs Nano* **2011**, *5* (8), 6434-6448.
24. Nativo, P.; Prior, I. A.; Brust, M., Uptake and intracellular fate of surface-modified gold nanoparticles. *ACS nano* **2008**, *2* (8), 1639-1644.
25. Cesbron, Y.; Shaheen, U.; Free, P.; Lévy, R., TAT and HA2 facilitate cellular uptake of gold nanoparticles but do not lead to cytosolic localisation. *PLoS One* **2015**, *10* (4), e0121683.
26. Schöttler, S.; Becker, G.; Winzen, S.; Steinbach, T.; Mohr, K.; Landfester, K.; Mailänder, V.; Wurm, F. R., Protein adsorption is required for stealth effect of poly (ethylene glycol)-and poly (phosphoester)-coated nanocarriers. *Nature nanotechnology* **2016**, *11* (4), 372-377.
27. Hirose, H.; Takeuchi, T.; Osakada, H.; Pujals, S.; Katayama, S.; Nakase, I.; Kobayashi, S.; Haraguchi, T.; Futaki, S., Transient focal membrane deformation induced by arginine-rich peptides leads to their direct penetration into cells. *Molecular Therapy* **2012**, *20* (5), 984-993.

28. Liou, J.-S.; Liu, B. R.; Martin, A. L.; Huang, Y.-W.; Chiang, H.-J.; Lee, H.-J., Protein transduction in human cells is enhanced by cell-penetrating peptides fused with an endosomolytic HA2 sequence. *Peptides* **2012**, *37* (2), 273-284.
29. Lee, Y.-J.; Johnson, G.; Peltier, G. C.; Pellois, J.-P., A HA2-Fusion tag limits the endosomal release of its protein cargo despite causing endosomal lysis. *Biochimica et Biophysica Acta (BBA)-General Subjects* **2011**, *1810* (8), 752-758.
30. Moglianetti, M.; De Luca, E.; Pedone, D.; Marotta, R.; Catelani, T.; Sartori, B.; Amenitsch, H.; Retta, S. F.; Pompa, P. P., Platinum nanozymes recover cellular ROS homeostasis in an oxidative stress-mediated disease model. *Nanoscale* **2016**, *8* (6), 3739-3752.
31. Petrovykh, D. Y.; Kimura-Suda, H.; Opdahl, A.; Richter, L. J.; Tarlov, M. J.; Whitman, L. J., Alkanethiols on platinum: multicomponent self-assembled monolayers. *Langmuir* **2006**, *22* (6), 2578-2587.
32. Saxton, W.; Baumeister, W.; Hahn, M., Three-dimensional reconstruction of imperfect two-dimensional crystals. *Ultramicroscopy* **1984**, *13* (1-2), 57-70.
33. Kremer, J. R.; Mastronarde, D. N.; McIntosh, J. R., Computer visualization of three-dimensional image data using IMOD. *Journal of structural biology* **1996**, *116* (1), 71-76.
34. Galdiero, S.; Falanga, A.; Vitiello, M.; Browne, H.; Pedone, C.; Galdiero, M., Fusogenic domains in herpes simplex virus type 1 glycoprotein H. *Journal of Biological Chemistry* **2005**, *280* (31), 28632-28643.
35. Galdiero, S.; Falanga, A.; Vitiello, M.; Raiola, L.; Russo, L.; Pedone, C.; Isernia, C.; Galdiero, M., The presence of a single N-terminal histidine residue enhances the fusogenic properties of a membranotropic peptide derived from herpes simplex virus type 1 glycoprotein H. *Journal of Biological Chemistry* **2010**, *285* (22), 17123-17136.
36. Falanga, A.; Vitiello, M. T.; Cantisani, M.; Tarallo, R.; Guarnieri, D.; Mignogna, E.; Netti, P.; Pedone, C.; Galdiero, M.; Galdiero, S., A peptide derived from herpes simplex virus type 1 glycoprotein H: membrane translocation and applications to the delivery of quantum dots. *Nanomedicine: Nanotechnology, Biology and Medicine* **2011**, *7* (6), 925-934.
37. Tarallo, R.; Accardo, A.; Falanga, A.; Guarnieri, D.; Vitiello, G.; Netti, P.; D'Errico, G.; Morelli, G.; Galdiero, S., Clickable functionalization of liposomes with the gH625 peptide from Herpes simplex virus type I for intracellular drug delivery. *Chemistry-a European Journal* **2011**, *17* (45), 12659-12668.
38. Guarnieri, D.; Falanga, A.; Muscetti, O.; Tarallo, R.; Fusco, S.; Galdiero, M.; Galdiero, S.; Netti, P. A., Shuttle-Mediated Nanoparticle Delivery to the Blood-Brain Barrier. *Small* **2013**, *9* (6), 853-862.
39. Carberry, T. P.; Tarallo, R.; Falanga, A.; Finamore, E.; Galdiero, M.; Weck, M.; Galdiero, S., Dendrimer Functionalization with a Membrane-Interacting Domain of Herpes Simplex Virus Type 1: Towards Intracellular Delivery. *Chemistry-A European Journal* **2012**, *18* (43), 13678-13685.

40. Smaldone, G.; Falanga, A.; Capasso, D.; Guarnieri, D.; Correale, S.; Galdiero, M.; Netti, P. A.; Zollo, M.; Galdiero, S.; Di Gaetano, S., gH625 is a viral derived peptide for effective delivery of intrinsically disordered proteins. *International journal of nanomedicine* **2013**, *8*, 2555.
41. Guarnieri, D.; Muscetti, O.; Falanga, A.; Fusco, S.; Belli, V.; Perillo, E.; Battista, E.; Panzetta, V.; Galdiero, S.; Netti, P., Surface decoration with gH625-membranotropic peptides as a method to escape the endo-lysosomal compartment and reduce nanoparticle toxicity. *Nanotechnology* **2015**, *26* (41), 415101.
42. Valiante, S.; Falanga, A.; Cigliano, L.; Iachetta, G.; Busiello, R. A.; La Marca, V.; Galdiero, M.; Lombardi, A.; Galdiero, S., Peptide gH625 enters into neuron and astrocyte cell lines and crosses the blood–brain barrier in rats. *International journal of nanomedicine* **2015**, *10*, 1885.
43. Galdiero, S.; Russo, L.; Falanga, A.; Cantisani, M.; Vitiello, M.; Fattorusso, R.; Malgieri, G.; Galdiero, M.; Isernia, C., Structure and orientation of the gH625–644 membrane interacting region of herpes simplex virus type 1 in a membrane mimetic system. *Biochemistry* **2012**, *51* (14), 3121-3128.
44. Zhang, W.; Crocker, E.; McLaughlin, S.; Smith, S. O., Binding of Peptides with Basic and Aromatic Residues to Bilayer Membranes. *Journal of Biological Chemistry* **2003**, *278* (24), 21459-21466.
45. Jing, W.; Hunter, H.; Hagel, J.; Vogel, H., The structure of the antimicrobial peptide Ac-RRWWRF-NH<sub>2</sub> bound to micelles and its interactions with phospholipid bilayers. *Chemical Biology & Drug Design* **2003**, *61* (5), 219-229.
46. Rauch, M. E.; Ferguson, C. G.; Prestwich, G. D.; Cafiso, D. S., Myristoylated alanine-rich C kinase substrate (MARCKS) sequesters spin-labeled phosphatidylinositol 4, 5-bisphosphate in lipid bilayers. *Journal of Biological Chemistry* **2002**, *277* (16), 14068-14076.
47. Galdiero, S.; Falanga, A.; Vitiello, M.; Raiola, L.; Fattorusso, R.; Browne, H.; Pedone, C.; Isernia, C.; Galdiero, M., Analysis of a membrane interacting region of herpes simplex virus type 1 glycoprotein H. *Journal of Biological Chemistry* **2008**, *283* (44), 29993-30009.
48. Vitiello, G.; Falanga, A.; Petruk, A. A.; Merlino, A.; Fragneto, G.; Paduano, L.; Galdiero, S.; D'Errico, G., Fusion of raft-like lipid bilayers operated by a membranotropic domain of the HSV-type I glycoprotein gH occurs through a cholesterol-dependent mechanism. *Soft matter* **2015**, *11* (15), 3003-3016.
49. Boselli, L.; Polo, E.; Castagnola, V.; Dawson, K. A., Regimes of biomolecular ultrasmall nanoparticle interactions. *Angewandte Chemie International Edition* **2017**, *56* (15), 4215-4218.
50. Li, Y.; Somorjai, G. A., Nanoscale advances in catalysis and energy applications. *Nano letters* **2010**, *10* (7), 2289-2295.
51. Hosaka, H.; Haruki, R.; Yamada, K.; Böttcher, C.; Komatsu, T., Hemoglobin–Albumin Cluster Incorporating a Pt Nanoparticle: Artificial O<sub>2</sub> Carrier with Antioxidant Activities. *PLoS One* **2014**, *9* (10), e110541.



52. Yoshihisa, Y.; Honda, A.; Zhao, Q. L.; Makino, T.; Abe, R.; Matsui, K.; Shimizu, H.; Miyamoto, Y.; Kondo, T.; Shimizu, T., Protective effects of platinum nanoparticles against UV-light-induced epidermal inflammation. *Experimental dermatology* **2010**, *19* (11), 1000-1006.
53. Kajita, M.; Hikosaka, K.; Iitsuka, M.; Kanayama, A.; Toshima, N.; Miyamoto, Y., Platinum nanoparticle is a useful scavenger of superoxide anion and hydrogen peroxide. *Free radical research* **2007**, *41* (6), 615-626.
54. Hamasaki, T.; Kashiwagi, T.; Imada, T.; Nakamichi, N.; Aramaki, S.; Toh, K.; Morisawa, S.; Shimakoshi, H.; Hisaeda, Y.; Shirahata, S., Kinetic analysis of superoxide anion radical-scavenging and hydroxyl radical-scavenging activities of platinum nanoparticles. *Langmuir* **2008**, *24* (14), 7354-7364.
55. Zhang, L.; Laug, L.; Munchgesang, W.; Pippel, E.; Gösele, U.; Brandsch, M.; Knez, M., Reducing stress on cells with apoferritin-encapsulated platinum nanoparticles. *Nano letters* **2009**, *10* (1), 219-223.
56. Kim, J.; Shirasawa, T.; Miyamoto, Y., The effect of TAT conjugated platinum nanoparticles on lifespan in a nematode *Caenorhabditis elegans* model. *Biomaterials* **2010**, *31* (22), 5849-5854.
57. Nel, A.; Xia, T.; Mädler, L.; Li, N., Toxic potential of materials at the nanolevel. *science* **2006**, *311* (5761), 622-627.
58. Trachootham, D.; Alexandre, J.; Huang, P., Targeting cancer cells by ROS-mediated mechanisms: a radical therapeutic approach? *Nature reviews. Drug discovery* **2009**, *8* (7), 579.



# Double peptide functionalization synergistically enhances PLGA-PEG-NPs crossing of the cerebral endothelium

**Abstract.** The blood-brain barrier (BBB) represents the main obstacle in the treatment of Central-Nervous-System (CNS) diseases. It has already been proven that functionalized PLGA-PEG NPs with the CRTIGPSVC (CRT) peptide, which functionally mimics the endogenous iron, represent a promising brain delivery system due to the high efficacy to translocate across the murine BBB, both in static and dynamic conditions. With these perspectives, in order to enhance nanocarrier performance, we added gH625 peptide in the functionalization setup of NPs. The aim is to investigate the efficacy of this new system in promoting the translocation across the cerebral endothelium: co-localization studies, adhesion and permeation assays across *in vitro* brain endothelial model under dynamic conditions have been investigated. Results establish that the cooperative effect of CRT and gH625 on NPs may change the distribution of NP in the cell and strengthen the BBB crossing of NPs.

## 4.1 Introduction

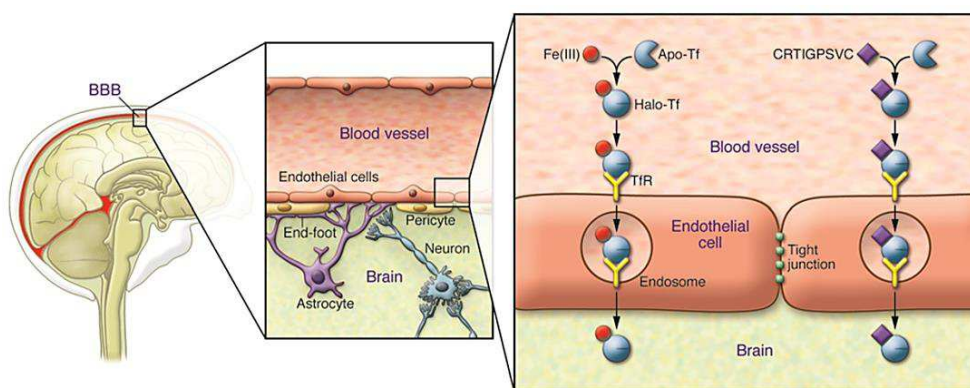
Brain drug delivery systems have been developed to bypass the blood-brain barrier (BBB) in order to therapeutically target central-nervous system (CNS) diseases. To overcome this barrier many delivery, strategies have been attempted, such as local injection, induction of enhanced permeability.<sup>1</sup> Among others, nanotechnologies play an important role in developing strategies for brain drug delivery. In the last decades, several methods have been designed to overcome or exploit the transport systems of the BBB: non-invasive ones involve the systemic application of colloidal drug carriers undergoing a receptor or adsorptive mediated transcytosis mechanism.<sup>2</sup> In particular, direct targeted delivery of a therapeutic cargo to the intended site of action in the brain appears to be one of the most promising non-invasive approaches to overcome the BBB.

By using of nanocarriers, the drug can be transported to the place of action, increasing drug concentration in target tissues; in this way, lower doses of drug are required, minimizing undesirable side effects to healthy tissues. An ideal nanoparticle (NP) should: (i) recognize selectively the targeting tissue, (ii) promote brain drug delivery, (iii) have long circulation time, (iv) protect the cargo from enzymatic degradation, (v) have low immunogenicity and (vi) have good biocompatibility.<sup>3</sup> Usually, NPs enter the cell by endocytic pathway: after, endosomes fuse with lysosomes, in which the acid environment ( $\text{pH} < 5.5$ ) allows the degradation of the content. As a result, the cargo is transferred across the BBB only in few events of transcytosis. For that reason, the design of targeted delivery carriers has garnered significant attention in recent years because of the potential to achieve highly localized delivery to brain endothelium.<sup>4-6</sup> The possibility to modulate physical-chemical properties of NPs such as surface charge, size and specific functionalization moieties, play an important role in mediating their interactions with cell membrane and their intra-cellular fate.

Therefore, the surface functionalization of nanocarriers with specific ligands such as Transferrin (Tf), insulin and low density lipoprotein offers the possibility to recognize and cross the BBB endothelium *via* recognition of specific receptors, overexpressed by the cells, and through mechanism of transcytosis. To do so, the use of Receptor-Mediated Transcytosis (RMT) systems is considered the most useful strategy that has already been proposed for the transport of biologics into the brain.<sup>4, 7-8</sup> However, the

main limitation of RMT is associated with the low efficiency of BBB crossing and the achievement into the CNS. In many cases ligands have high affinity only for specific receptors and often this situation is inefficient to promote an adequate endocytosis.<sup>9</sup>

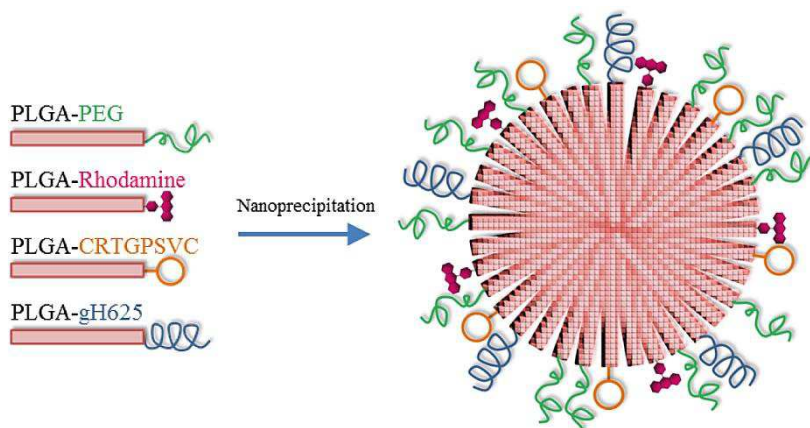
Researchers have been substantially focusing on identifying new BBB RMT targets. Recently, Staquicini *et al.*<sup>10</sup> have identified a new aminoacidic sequence, CRTIGPSVC (named CRT), able to recognize selectively brain endothelium and to enhance brain crossing of viral particles. Transferrin receptor (TfR) is highly expressed on immature erythroid cells, placental tissue and rapidly dividing cells, both normal and malignant. Furthermore it is expressed on hepatocytes and endothelial cells of the BBB.<sup>11</sup> TfR mediates iron delivery to the brain parenchyma *via* binding and intracellular trafficking of the iron-binding protein Tf.<sup>12</sup> Internalization of the Tf-TfR complex leads to the endosomal compartments in which the acidification allows the release of iron from the ligand. Iron is transported into the cytoplasm and is transcytosed, whereas the apo-transferrin (apo-Tf) remains tightly bound to its receptor until it reaches the plasma membrane. Here, the apo-Tf rapidly dissociates from the receptor at neutral pH.<sup>13</sup> The free receptor, on the cell surface, is available for another cycle of RMT. Staquicini *et al.* demonstrated *in vitro* that the BBB targeting peptide CRT, mimicking an iron atom, selectively interacts with apo-transferrin and induce allosteric conformational changes (iron-bound holo-Tf). It finally gains access to the brain side, recognizing TfR, through a non-canonical ligand-directed mechanism (Figure 4.1).



**Figure 4.1.** Transcytosis mechanisms of the Fe(III) ion and the iron-mimicking CRT peptide across the cerebral endothelium. Reprinted with permission of Ref. <sup>14</sup>.

To combine targeting and crossing strategies, some research groups developed dual-functionalized carrier systems for drug delivery across the BBB. For example, these systems can be obtained with Transferrin (Tf) and cell-penetrating peptide (CPP) functionalization, achieving both target and translocation ability through the BBB.<sup>15-16</sup> The aim of this work is to develop a new PLGA-PEG (PELGA) based nanoparticle able to enhance the crossing efficiency through a gH625 and CRT double peptide functionalization. Nanoparticles cellular behavior is tested by using an *in vitro* model of BBB, both in static and dynamic condition.

PELGA based NPs can provide better biocompatibility, higher reproducibility, higher payload properties, easy in functionalization and excellent stability both *in vitro* and *in vivo*.<sup>17</sup> In particular, it has been recently reported the versatility of PELGA nanoparticles as efficient drug delivery systems.<sup>18-22</sup> gH625 is a membranotropic peptide, derived from the glycoprotein H (gH) of the *Herpes simplex* virus type 1. It interacts with model membranes, merging with them and is able to traverse the membrane bilayer carrying a cargo, like quantum dots, liposomes, NPs and dendrimers into the cytosol and enhance BBB crossing.<sup>23-24</sup> It has already been demonstrated that gH625-functionalized polystyrene NPs facilitate the delivery of nanoparticles across the murine BBB, leading to significant higher cell uptake and crossing.<sup>25-26</sup> Therefore, we suppose that the surface modification of NPs with gH625 may change the classical intracellular fate of endocytic pathway, mediating the lysosomal escaping of NPs and enhancing the translocation across the BBB. In this work, we synthesized gH625-functionalized PELGA-NPs, never reported before in a BBB *in vitro* analysis. Because of their non-specific affinity to different cells, gH625-mediated brain delivery systems could show a non-specific distribution in the human body, after systemic administration. For this reason, we exploited the ability of CRT peptide to specifically transport PELGA-NPs across the *in vitro* BBB. It has been previously demonstrated that CRT-PELGA nanoparticles are able to target and cross the cerebral endothelium. Moreover, CRT functionalization enhance uptake, adhesion and crossing ability of the particles.<sup>27</sup> Consequently, in this work, to overcome the CPP lack of targeting specificity, we created a new carrier system, hypothesizing that the coupling of gH625 to CRT may enhance NPs transport across the murine cerebral endothelium (Figure 4.2).



**Figure 4.2.** Schematic synthesis of dual-functionalized NPs with CRT and gH625 peptides for the active targeting and crossing of the cerebral endothelium.

Dual-functionalized NPs, with 3 different ratios of peptides gH625/CRT (33/66, 50/50 and 66/33) were synthesized and the effects of the functionalization on the penetration of PLGA NP through an *in vitro* BBB model based on bEnd.3 cell line were investigated. In order to evaluate the single contribution of both CRT and gH625 peptides in the trans-endothelial ability to cross the *in vitro* BBB, dual-functionalized NP were compared to blank and mono-functionalized nanoparticles: CRT-NPs and gH625-NPs. The main outcome of this work is that gH/CRT<sub>33/66</sub> represent the best formulation to promote the targeting and crossing through an *in vitro* BBB under dynamic condition.

## 4.2 Experimental section

### 4.2.1 Materials

Equimolar uncapped poly(D,L-lactide-co-glycolide) (PLGA) (Resomer RG502H, average Mw 12 kDa) was purchased from Boehringer Ingelheim (Ingelheim, Germany). Polyethylene glycol (PEG, Mw 1500 Da), Ethylenediamine (en), N,N-diisopropylethylamine (DIPEA), O-benzotriazole-N,N,N',N'-tetramethyluronium-hexafluoro-phosphate (HBTU), Ethyl 2-cyano-2-(hydroxyimino)acetate (Oxyma Pure<sup>®</sup>), anhydrous N,N-dimethyl-formamide (DMF), Acetonitrile (ACN), N,N'-Diisopropylcarbodiimide (DIC), N,N'-Dicyclohexylcarbodiimide (DCC), Rhodamine B,

4-(dimethylamino) pyridine (DMAP), Dichloromethane (DCM), Dimethylsulfoxide (DMSO), Sodium carbonate ( $\text{Na}_2\text{CO}_3$ ), Piperidine, Trifluoroacetic acid (TFA), Formic acid, HPLC-grade water and all buffer solutions were purchased from Sigma-Aldrich (USA). All Fmoc-aminoacids were purchased from IRIS Biotech GmbH (Germany). Dialysis bag MWCO 6000-8000 Da were purchased from Spectrum Laboratories, Inc. (Netherlands). Distilled and deionized water used Millipore Milli-RO 10 Plus (Millipore, USA) at 18 M $\Omega$  resistance. Amicon<sup>®</sup> Ultra-4 centrifugal filters were purchased from Millipore Merck.

#### 4.2.2 Synthesis of peptides

CRT ( $\text{Ac-CRTIGPSVC-}\beta\text{AK-CONH}_2$ ) and gH625 ( $\text{Ac-HGLASTLTRWAHYNALIRAFGGG-COOH}$ ) peptides were synthesized using standard solid-phase-9-fluorenyl methoxy carbonyl (Fmoc) procedure and were obtained with good yields (35-40 %). The  $\beta$ -Alanine-Lys (as regards CRT peptide) and the Gly<sub>3</sub> (for gH625 peptide) residues acted as spacer units between polymer and peptide active sequences in order to retain the innate peptide conformation when conjugated to the particle surface.

The syntheses were performed by Biotage Syro Wave peptide synthesizer: Rink Amide and Wang resin was used as a solid-phase support for CRT and gH625 peptide, respectively. Previously, the C-terminal glycine residue (10 eq) of gH625 peptide was manually attached to an equivalent amount of Wang resin using OximaPure<sup>®</sup> (10 eq), DIC (10 eq) and DMAP (0.4 eq). The Fmoc protecting group was removed using piperidine 40 % (v/v) solution in DMF. Peptides were cleaved from resin using TFA/TIS/H<sub>2</sub>O (95/2.5/2.5) solution and precipitated in ice-cold diethyl ether. Purified CRT peptide was obtained by RP-HPLC starting from 5/95 (v/v) acetonitrile (ACN)/water solution containing 0.1 % v/v TFA. For the purification of the gH625 peptide, a 20/80 ACN/water solution with 0.1 % v/v TFA was used. Peptides were lyophilized and then characterized using ESI-LC-MS. These analyses were carried out by injecting aqueous solutions of peptides into Agilent EclipsePlus C18 RRHD (1.8  $\mu\text{m}$ , 2.1 $\times$ 50 mm) eluted with solvent solution of H<sub>2</sub>O and ACN containing 0.1% v/v of formic acid. A linear gradient of 20-80 % of ACN over 8 min at a flow of 150  $\mu\text{l}/\text{min}$  was used.



MS for CRT peptide: calculated for  $[M+H]^+ = 1176.43$  m/z; found (ESI)  $[M+H]^+ = 1176.18$  m/z,  $[M+2H]^{2+} = 588.66$  m/z. MS for gH625 peptide: calculated for  $[M+H]^+ = 2512.79$  m/z; found (ESI)  $[M+2H]^{2+} = 1256.68$  m/z,  $[M+3H]^{3+} = 838.12$  m/z,  $[M+4H]^{4+} = 628.84$  m/z.

#### *Peptide cyclization*

Purified CRT peptide was cyclized by air-oxidation method to allow the formation of the intra-chain disulfide bond between the two cysteine residues. Briefly, cysteinyl peptide (0.1 mg/mL) was dissolved in 0.1 M sodium carbonate (pH 8) and left to stand open to atmosphere under vigorous magnetic stirring until the reaction is complete (48 h). The reaction progress was monitored by LC-MS analysis. MS for CRT-cyclized peptide: calculated for  $[M+H]^+ = 1174.43$  m/z; found (ESI)  $[M+H]^+ = 1173.77$  m/z,  $[M+2H]^{2+} = 587.43$  m/z,  $[M+3H]^{3+} = 391.97$  m/z. Finally, CRT-peptide were purified and lyophilized as described above: the product was obtained with 86 % yield.

### **4.2.3 Synthesis of copolymers and conjugates**

#### *PELGA*

PLGA-PEG copolymer (namely PELGA) was synthesized *via* a coupling reaction between PLGA and PEG.<sup>28</sup> Briefly, the carboxyl group of PLGA were reacted with the terminal hydroxyl group of PEG: 1 eq of PLGA, 4 eq of PEG, 0.4 eq DMAP and 2 eq of DCC were dissolved in 10 mL of anhydrous DCM. After the reaction (2 days, RT, inert atmosphere), the residual DCC was changed into dicyclohexylcarbodiurea (DCU) by adding 10  $\mu$ L of bidistilled water. Then DCM was evaporated and the mixture was dissolved in 10 mL of DMSO, filtrated and dialyzed (MWCO 6-8 kDa) for 1 day against ACN and for 2 days against water.

The pure product was recovered after lyophilization and its identity was confirmed by <sup>1</sup>H-NMR spectroscopy (600 MHz, CDCl<sub>3</sub>):  $\delta$  ppm 5.30-5.13 (PLGA, CH); 4.92-4.60 (PLGA, CH<sub>2</sub>); 3.64 (PEG, CH<sub>2</sub>); 1.59 (PLGA, CH<sub>3</sub>).

### *PLGA-amine*

PLGA was functionalized with ethylenediamine (en) which acts as a bridge between PLGA and rhodamine (or peptide C-terminus) carboxylic groups. Briefly, 30 mg of PLGA 502h, 10.3 mg of DCC, 8.7  $\mu$ l of DIPEA, 10.0  $\mu$ l of ethylenediamine were dissolved in 2.5 mL of anhydrous DCM. After the reaction (1 day, RT, inert atmosphere), the residual DCC was changed into dicyclohexylcarbodiurea (DCU) by adding 10  $\mu$ L of bidistilled water. Then the solution was filtered and precipitated dropwise into cold methanol, centrifuged and then placed under vacuum overnight.

The identity of pure product was confirmed by  $^1\text{H-NMR}$  spectroscopy (600 MHz, DMSO- $d_6$ ):  $\delta$  ppm 8.13 (en, amide); 5.26-5.10 (PLGA, CH); 4.95-4.75 (PLGA, CH<sub>2</sub>); 3.14 (en, CH<sub>2</sub>); 1.44 (PLGA, CH<sub>3</sub>).

### *PLGA-rhodamine*

PLGA-Rhodamine conjugation was performed by a standard coupling procedure: PLGA-amine (1 eq), HBTU (5 eq), DIPEA (10 eq) and rhodamine-B (5 eq) reacted in anhydrous DMSO for 24 h at RT and then purified by dialysis bags (MWCO 6-8 kDa) against water for 3 days.  $^1\text{H NMR}$  (600 MHz, CDCl<sub>3</sub>):  $\delta$  ppm 8.42, 7.85, 7.05 and 6.92 (rhodamine aromatic proton); 5.30-5.13 (PLGA, CH); 4.92-4.60 (PLGA, CH<sub>2</sub>); 4.30, 3.78 (rhodamine CH<sub>2</sub>); 3.42 (en, CH<sub>2</sub>); 1.59 (PLGA, CH<sub>3</sub>).

### *PLGA-peptides conjugate*

PLGA-Peptide conjugates were synthesized using a standard HBTU coupling procedure. Briefly, for CRT peptide, PLGA (1 eq), HBTU (5 eq), Oxima Pure<sup>®</sup> (5 eq), DIPEA (10 eq) and Peptide (1.5 eq) were dissolved in anhydrous DMSO for 48h at room temperature. For gH625 peptide PLGA-amine 2 eq of peptide were used. Adducts were purified from unreacted reagents using dialysis bags (MWCO 6-8 kDa) against pure water and lyophilized. The reaction products were confirmed by  $^1\text{H-NMR}$  spectroscopy.

PLGA-CRT:  $^1\text{H NMR}$  (600 MHz, DMSO- $d_6$ ):  $\delta$  ppm 8.50-6.00 (peptide amide backbone); 5.28-5.14 (PLGA, CH); 4.96-4.84 (PLGA, CH<sub>2</sub>); 1.47 (PLGA, CH<sub>3</sub>). PLGA-gH625:  $^1\text{H NMR}$  (600 MHz, DMSO- $d_6$ ):  $\delta$  ppm 8.50-6.00 (peptide amide backbone); 5.28-5.14 (PLGA, CH); 4.96-4.84 (PLGA, CH<sub>2</sub>); 3.30 (en, CH<sub>2</sub>); 1.47 (PLGA, CH<sub>3</sub>).

### *Nuclear Magnetic Resonance (NMR) analysis*

All Nuclear Magnetic Resonance (NMR) spectra were recorded at 28 °C using an Agilent 600 MHz (14 T) spectrometer equipped with a DD2 console and an OneNMR HX probe. The samples (1 mg) were dissolved in 600  $\mu$ L of 99.9% deuterated solvent (Sigma–Aldrich).  $^1\text{H}$  1D spectra were recorded using 256 scans to obtain a good signal-to-noise ratio for peptides, en and rhodamine. A saturation PRESAT pulse sequence was used to reduce residual peaks of water at 3.33 ppm. Spectra were transformed and analyzed using VNMRJ 4 software and chemical shift scale was referenced to the solvent residual peak signal.

#### **4.2.4 NP preparation**

Rhodaminated PELGA-Peptide nanoparticles were prepared by nanoprecipitation method.<sup>22</sup> In summary, the proper amounts of copolymers and conjugates (Table 4.1) were dissolved in acetone and mixed; the final volume was adjusted to 1.3 mL. Afterwards, the solution was added dropwise (6 mL/h) with a syringe pump into 12.5 mL of distilled water under magnetic stirring (400 rpm). The solution was kept under magnetic stirring until complete evaporation of the organic solvent (3-5 h) and the obtained NP suspension was sterilized with 0.22  $\mu\text{m}$  membrane filter. Finally, the volume of the solution was reduced to 1 mL using Amicon<sup>®</sup> Ultra-4 centrifugal filter. The final NP concentration (mg/mL of polymeric species) was estimated by fluorescence intensity measurements of Rhodamine-PLGA using a spectrofluorometer (Perkin Elmer) that were compared to fluorescence intensity of the initial NP concentration before filtration.

**Table 4.1.** Mass of copolymers used for blank-NPs, CRT-NPs, gH625-NPs, gH/CRT\_33/66-NPs, gH/CRT\_50/50-NPs and gH/CRT\_66/33-NPs preparations.

| NP Sample    | PELGA (mg) | PLGA-Rhod (mg) | PLGA-gH (mg) | PLGA-CRT (mg) | PLGA (mg) | Total (mg) |
|--------------|------------|----------------|--------------|---------------|-----------|------------|
| Blank        | 1.0        | 0.4            | -            | -             | 0.8       | 2.2        |
| CRT          | 1.0        | 0.4            | -            | 0.4           | 0.4       | 2.2        |
| gH625        | 1.0        | 0.4            | 0.4          | -             | 0.4       | 2.2        |
| gH/CRT_33/66 | 1.0        | 0.4            | 0.2          | 0.4           | 0.2       | 2.2        |
| gH/CRT_50/50 | 1.0        | 0.4            | 0.4          | 0.4           | -         | 2.2        |
| gH/CRT_66/33 | 1.0        | 0.4            | 0.4          | 0.2           | 0.2       | 2.2        |

#### **4.2.5 NP characterization**

Mean size, size distribution and  $\zeta$ -potential of NPs were determined by dynamic light scattering (DLS) measurements (Zetasizer Nano ZS, Malvern Instruments, UK) on a 0.1 mg/mL water suspension of each kind of NPs (Table 4.1).

#### **4.2.6 Cell culture**

Immortalized mouse cerebral endothelial cells, (bEnd.3; American Type Culture Collection, Manassas, VA) were grown in DMEM with 4.5 g/L glucose, 10 % Fetal Bovine Serum (FBS), 3.7 g/L sodium bicarbonate, 4 mM glutamine, 1 % non-essential amino acids, 100 U/mL penicillin and 0.1 mg/mL streptomycin in 100 mm diameter cell culture dish, in a humidified atmosphere at 37 °C and 5 % CO<sub>2</sub>. Cells used in all experiments were at passage 22-30.

#### **4.2.7 Co-localization studies**

Indirect immunofluorescence against endocytic markers may give information about the endocytic mechanisms underlying nanoparticle cellular uptake. The co-localization experiments were carried out on 70% confluent cells seeded on glass coverslips.

All the reagents and solutions were prepared as follows. For co-localization experiments with lysosomes, about  $1 \times 10^4$  bEnd.3 were seeded on the round 12 mm-diameter glass coverslips placed in 24 well plates. Cells were incubated for 24 h with all kind of NPs made. After, bEnd.3 were first rinsed twice with PBS to remove non-internalized NPs and fixed with 400  $\mu$ L of 4% paraformaldehyde at room for 10 min. For lysosomes staining, cells fixed were permeabilized with 0.05% saponin-PBS for 10 min and incubated with FBS-PBS 10% for 20 min at room temperature to block unspecific sites. Lysosomes were localized with rabbit 1:150 anti-LAMP-2 polyclonal (Abcam, 1 mg/mL) primary antibody for 1 hour at room temperature in a humidified chamber and with 1:200 AlexaFluor 488 anti-rabbit secondary (1  $\mu$ g/mL) antibody for 30 min. After mounted the coverslips on glass slides with PBS/glycerol (1:1) solution, immunofluorescence analyses were performed by means of confocal laser scanning microscope.

#### 4.2.8 Permeability assay to NPs in Transwell system

bEnd.3 were seeded at a density of  $3 \times 10^4$  cells/cm<sup>2</sup> on Transwell permeable inserts (6.5mm diameter, 3  $\mu$ m pores size; Corning Incorporated, Corning, NY). Permeability experiments were performed after 7 days from the seeding, allowing sufficient time for the cells to develop the junctions between cells. On the day of experiment, Transwell insert filter was washed with PBS and then the media of the donor chamber was filled with 150  $\mu$ L cell culture medium w/o phenol red containing 0.1 mg/mL of all NPs samples, while the acceptor chamber was filled with 400  $\mu$ L cell culture medium without phenol red. The samples of 400  $\mu$ L were drawn every 30 min for 2 h from the acceptor chamber and were then replaced with the same amount of fresh medium.

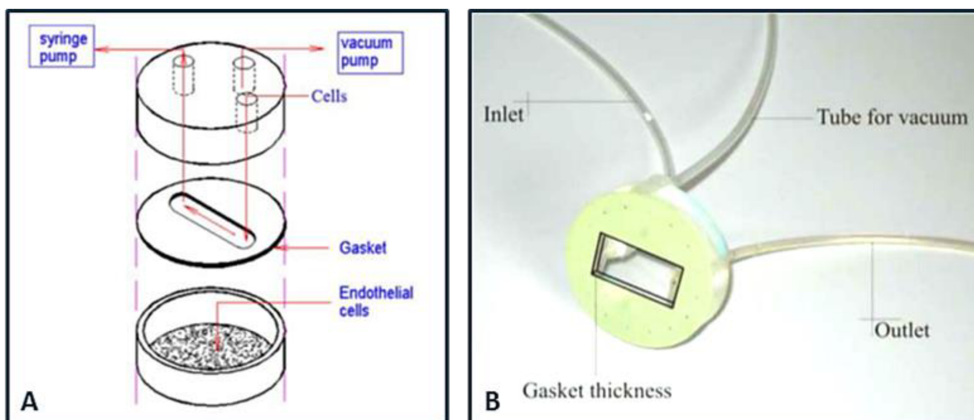
The fluorescence tracer concentration in the samples was determined by a spectrofluorometer (Victor, Wallac, PerkinElmer) with excitation and emission wavelengths of 557 and 578 nm, respectively. The permeability ( $P$ ) to NPs of the bEnd.3 monolayer was calculated according to the following equation:

$$P = \frac{\Delta C_A}{\Delta t} \times \frac{V_A}{C_D \times S}$$

Where  $\Delta C_A$  is the increase in fluorescence concentration in the acceptor chamber during the time interval  $\Delta t$ ,  $C_D$  is the fluorescence concentration in the donor chamber (assumed to be constant during the experiment),  $V_A$  is the volume of the acceptor chamber and  $S$  is the surface area of the filter.<sup>29</sup> The experiments were performed in triplicate.

#### 4.2.9 NP adhesion assay to BBB by using Glycotech system

To perform NP adhesion assays,  $4 \times 10^5$  bEnd.3 were seeded on round glasses ( $\varnothing = 60$  mm) placed in Petri dishes ( $\varnothing = 100$  mm). The experiments were performed after 3 days from the seeding. Adhesion assay to an *in vitro* model of BBB grown on the glass coverslip was performed by using Glycotech system. The system consists of a PMMA flow deck with inlet and outlet bores, a silicon gasket and a glass coverslip (Figure 4.3). The silicon gasket separates the acrylic flow deck and the glass and defines the flow area.



**Figure 4.3.** A) Schematic representation of the Glycotech flow chamber for cellular interaction studies. B) Picture of Glycotech system.

The gasket used in the present experiments had a thickness ( $h$ ) of 0.01 cm in and a width ( $w$ ) of 1 cm. The inlet bore is connected to a syringe-pump through a silastic tube and the outlet bore to a reservoir. The volumetric flow rate  $Q$  ( $10 \mu\text{L}/\text{min}$ ) was fixed to be equal for all the experiments. Based on these data, the mean velocity has been calculated with the following equation  $U = Q/wh$  within the chamber and the shear rate  $S = 6Q/h^2w$  and the shear stress at the wall  $\tau_w = \mu S$  being the viscosity of the medium  $\mu = 1.2 \times 10^{-2} \text{ dyn s}/\text{cm}^2$ . NP solutions at the final concentration of 0.2 mg/mL in cell culture medium supplemented with 40 mM HEPES buffer were flushed by using a 5 mL syringe allocated on a syringe pump. Flow is driven through the parallel plate flow chamber for 1 h at 37 °C in a Plexiglas incubator. At the end of the experiment, cells were washed with PBS to remove non adherent NPs and then fixed. The percentage of mean gray value was analyzed by using imageJ software.

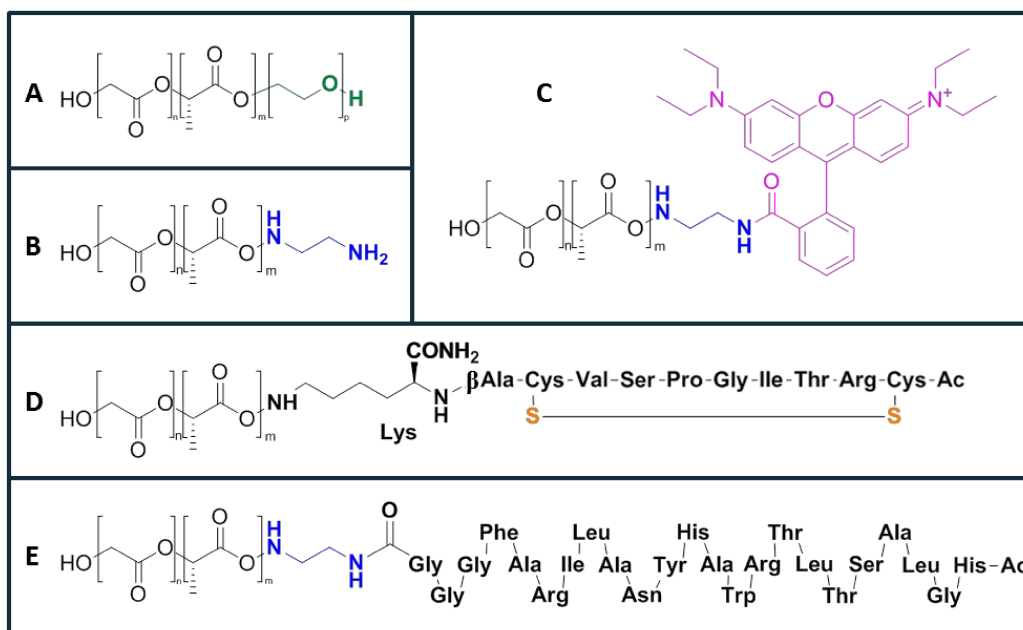
#### 4.2.10 Statistical analysis

Results were expressed as mean  $\pm$  standard deviation (SD). Statistical analyses were performed using a one-way analysis of variance (ANOVA). Results repeats were compared by analysis of variance (ANOVA) and a  $P$  value  $< 0.05$  were considered statistically significant.

## 4.3 Results and discussion

### 4.3.1 NPs precursors synthesis and characterization

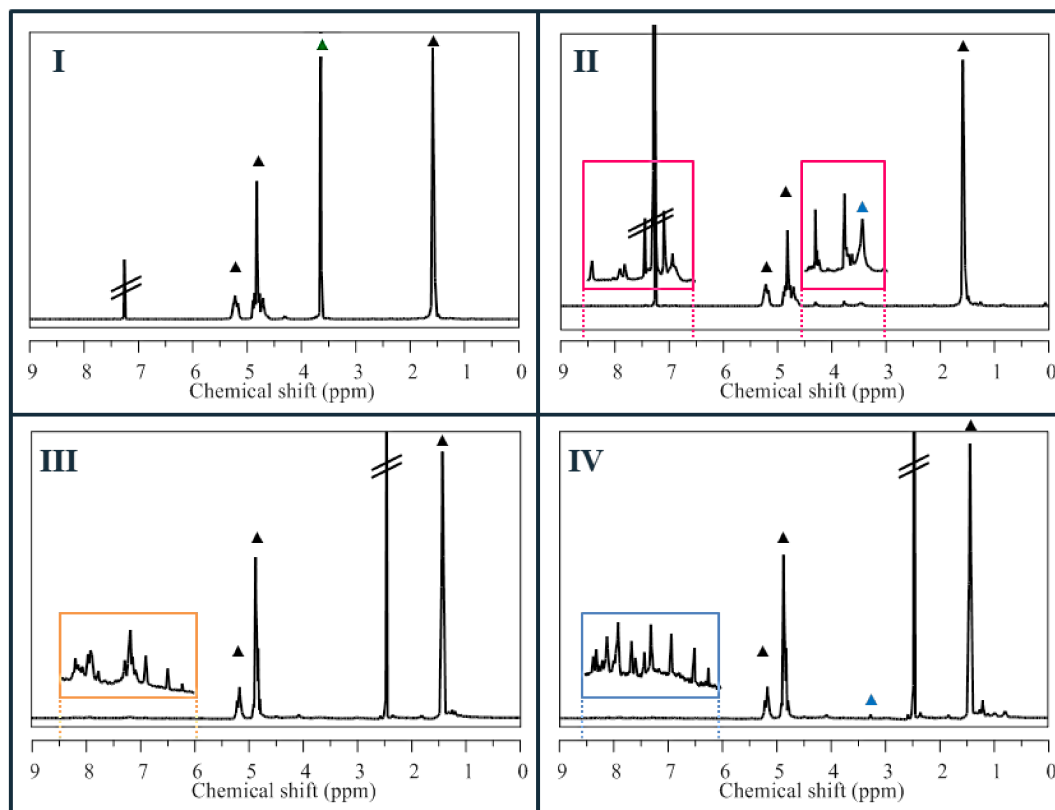
Pure PLGA copolymers and conjugates (Scheme 4.1) were obtained in good yield (80 % to 85 %). NPs precursors were prepared through ester or amide linkage to the carboxylic group of PLGA, optimizing a previously reported synthesis.<sup>28</sup> In particular, Oxima Pure<sup>®</sup> was used as additive instead of 1-hydroxybenzotriazole (HOBt) both in peptide synthesis as in conjugation coupling reaction. It showed clear superiority to HOBt (which have been reported to exhibit explosive properties)<sup>30</sup> in terms of suppression of racemization, coupling efficiency and safety.<sup>31</sup> As regards PLGA-rhodamine (Scheme 4.1 C) and PLGA-gH625 (Scheme 4.1 E), an ethylenediamine linker (blue colored) between the two carboxylic groups of conjugates was previously added (PLGA-amine – Scheme 4.1 B).



**Scheme 4.1.** PLGA copolymers and conjugates: (A) PLGA-PEG (PELGA) copolymer, (B) PLGA-amine, (C) PLGA-rhodamine, (D) PLGA-CRT and (E) PLGA-gH625.

The chemical characterization of synthesized NPs precursors was carried out using two powerful techniques. First of all, peptides synthesis step and CRT cyclization reaction were followed by LC-MS in order to confirm peptide sequences and disulfide bond formation.

Then,  $^1\text{H-NMR}$  spectroscopy was used after dialysis purification of the copolymers in order to assess products purity. NMR spectra (Figure 4.4) confirm structures of all the conjugates and show that it was not found a significant amount of unreacted reagents in any PLGA samples.



**Figure 4.4.**  $^1\text{H-NMR}$  spectra of synthesized PLGA conjugates showed in Scheme 4.1. In every spectrum, peaks related to PLGA were marked with black triangles (▲). Furthermore, peaks of conjugates molecules to PLGA are assigned in order to confirm products structures. (I) PELGA copolymer with PEG signal 3.64 ppm (▲); (II) PLGA-rhodamine with rhodamine signals highlighted in purplish red expansion squares; (III) PLGA-CRT and (IV) PLGA-gH625 with peptide amide backbone signals highlighted in orange and blue expansion squares, respectively. Blue triangles (▲) indicate ethylenediamine  $\text{CH}_2$ .

### 4.3.2 NPs characterization

All NPs were synthesized by nanoprecipitation method. To investigate the effect of the peptide functionalization on the size and  $\zeta$ -potential of NPs, dynamic light scattering (DLS) measurements in aqueous medium were performed. Hydrodynamic diameters, polydispersity indexes (PDI) and the surface charges values of NPs, after filtration,



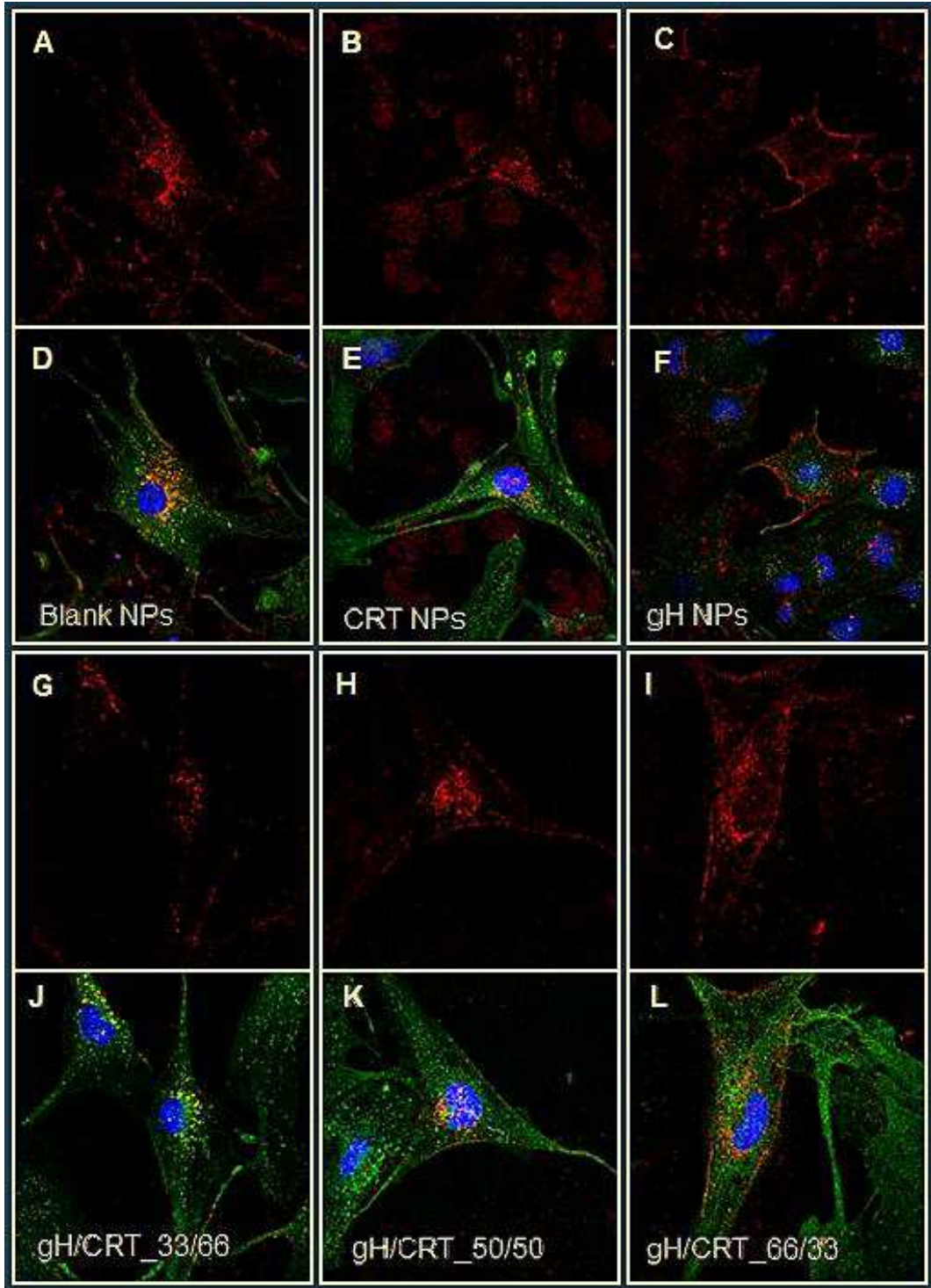
are shown in Table 4.2. Data indicate that the particle used for all the experiments are almost of the same size, narrowly distributed and substantially different in surface charge with respect of the functionalization. In particular, less negative charges were shown with the increase of gH625 surface fraction; this trend is probably due to the net positive charge of the protonated amino-acid side chains at physiological condition.

**Table 4.2.** Size, polydispersity and  $\zeta$ -potential measurements of PELGA-NPs at each functionalization degrees.

| <b>NPs Samples</b> | <b>Size<br/>(<math>\varnothing</math>, nm)</b> | <b>PDI</b> | <b><math>\zeta</math>-Potential<br/>(mV)</b> |
|--------------------|--|------------|--|
| Blank              | 88 $\pm$ 2                                     | 0.15       | -27.4 $\pm$ 0.7                              |
| CRT                | 92 $\pm$ 2                                     | 0.15       | -26 $\pm$ 1                                  |
| gH625              | 84.5 $\pm$ 0.8                                 | 0.14       | -13.8 $\pm$ 0.2                              |
| gH/CRT_33/66       | 76.7 $\pm$ 0.9                                 | 0.13       | -22.1 $\pm$ 0.5                              |
| gH/CRT_50/50       | 78 $\pm$ 1                                     | 0.14       | -20.8 $\pm$ 0.6                              |
| gH/CRT_66/33       | 84.1 $\pm$ 0.7                                 | 0.14       | -19.4 $\pm$ 0.7                              |

### 4.3.3 Co-localization studies

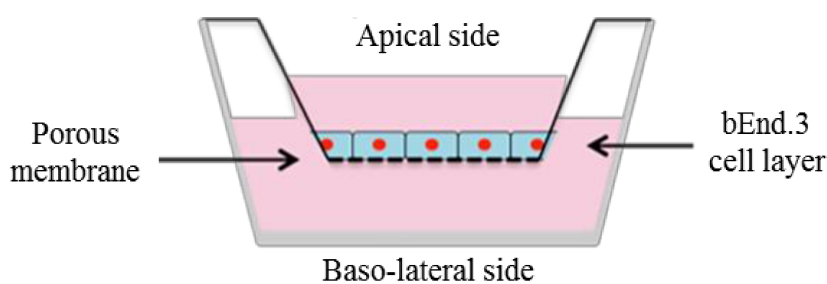
To further investigate the fate of NPs, intracellular distribution and co-localization experiments within endocytic compartments (lysosomes) were carried out. After 24 h of incubation, the samples were fixed with paraformaldehyde 4 % for 10 min and observed by confocal microscope after lysosomes staining with LAMP-2. As shown in Figure 4.5, all kind of nanoparticles are internalized by the cells and display different intracellular localizations. Blank-NPs and CRT-NPs are distributed as spots mainly localized in the perinuclear region of the cell and are partially co-localized with lysosomes. On the other hand, gH625-NPs have a more cytoplasmic distribution with no significant lysosomes co-localization. Furthermore, localization of dual-functionalized NPs changes as a function of the formulation, since lysosomal or cytoplasmic distribution is increasing with the CRT or gH625 amount, respectively.



**Figure 4.5.** Colocalization of blank-NPs (A,D), CRT-NPs (B,E), gH625-NPs (C,F), gH/CRT\_33/66-NPs (G,J), gH/CRT\_50/50-NPs (H,K) and gH/CRT\_66/33-NPs (I,L) with lysosomes after 24 h incubation in bEnd.3 cells. Red: NPs; green: LAMP-2. Scale bar 50  $\mu$ m.

#### 4.3.4 NPs transport across *in vitro* model of the BBB

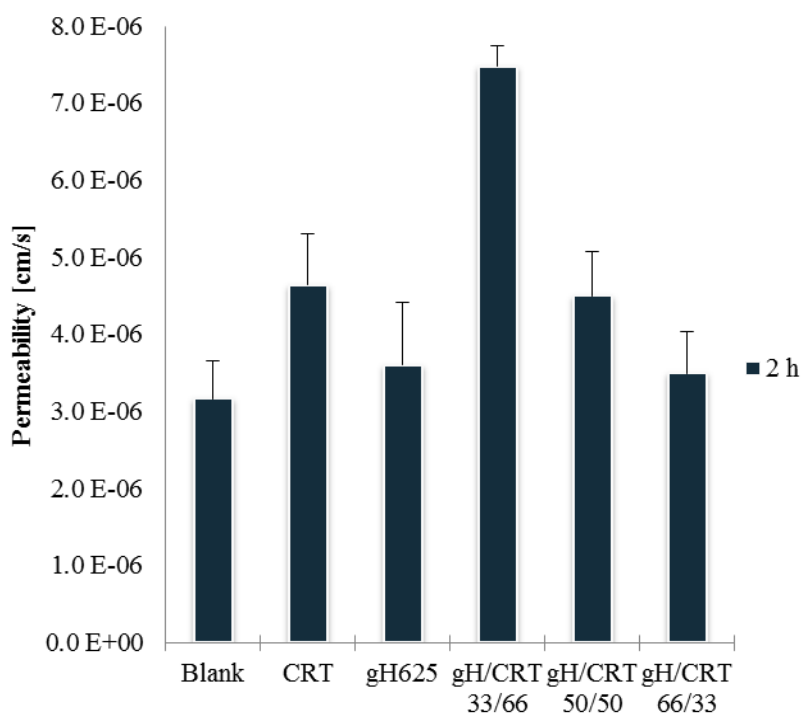
Transwell® cell culture inserts are an easy-to-use permeable support devices (Figure 4.6) for the study of both anchorage-dependent and anchorage-independent cell lines. Transwell *in vitro* BBB models consist of two compartments separated by endothelial cell layer, grown on a microporous membrane, which allows the exchange of molecules between the apical side and the baso-lateral compartments. Several pore sizes of membranes are available, depending on the solute to be investigated. Generally, upper chamber of Transwell insert represents the vascular side while the bottom one acts as the parenchymal side.



**Figure 4.6.** Schematic representation of Transwell® cell culture inserts. Note the porous membrane of the insert that provides independent access to both sides of a cell monolayer

The ability of the two peptides to promote NPs crossing of the bEnd.3 monolayer was investigated in Transwell system (Corning). After 7 days of culture bEnd.3 cells were able to form a confluent cell layer that mimics the permeability properties of the BBB.<sup>32</sup> Data reported in Figure 4.7 show that CRT-NPs and gH/CRT\_33/66 NPs are able to cross more efficiently the endothelial layer compared to blank-NP. In particular, among mono-functionalized NPs, CRT has the highest ability in NPs transport across the *in vitro* model of the BBB with a permeability of  $4.64 \times 10^{-6}$  cm/s. No substantial difference was found for gH625 functionalization ( $3.60 \times 10^{-6}$  cm/s) compared to blank-NPs ( $3.17 \times 10^{-6}$  cm/s). As regards bi-functionalized NPs, permeability values were  $7.48 \times 10^{-6}$  cm/s,  $4.50 \times 10^{-6}$  cm/s and  $3.50 \times 10^{-6}$  cm/s for gH625/CRT ratio of 33/66, 50/50 and 66/33, respectively. Data demonstrated that NPs transport is strictly affected by the CRT presence, both in mono- and bi-functionalized samples. Moreover, it is possible to appreciate the synergic behavior of the gH625 cell-penetrating peptide

in assisting the trans-endothelial crossing, in particular for lower gH625/CRT peptide ratio. Thus, gH/CRT\_33/66-NPs have the highest value for trans-endothelial crossing ability.



**Figure 4.7.** Permeability of bEnd.3 cell monolayer to blank, CRT, gH625, gH/CRT\_33/66, gH/CRT\_50/50 and gH/CRT\_66/33 functionalized NPs.

Burdo *et al.*<sup>33</sup> demonstrated that iron is transported across endothelial cells both bound to Tf (holo-transferrin) and not bound to Tf (apo-transferrin). Several works reported that after endocytosis in brain endothelium, the complex Tf-TfR-iron is transported in coated vesicles to lysosomes, in which the presence of the iron chelating component desferrioxamine removes the iron from the complex. Then, the iron is transported across the membrane of the vesicle into the cytoplasm and is transcytosed, by still unclear mechanism. Fisher *et al.*<sup>34</sup> identified iron transport proteins such as ferritin for iron transcytosis, Mc Carthy *et al.* identified ferroportin.<sup>35</sup> On the other hand, apoTf-receptor complex is sorted into recycling endosomes to the blood on the luminal membrane.<sup>36-37</sup>

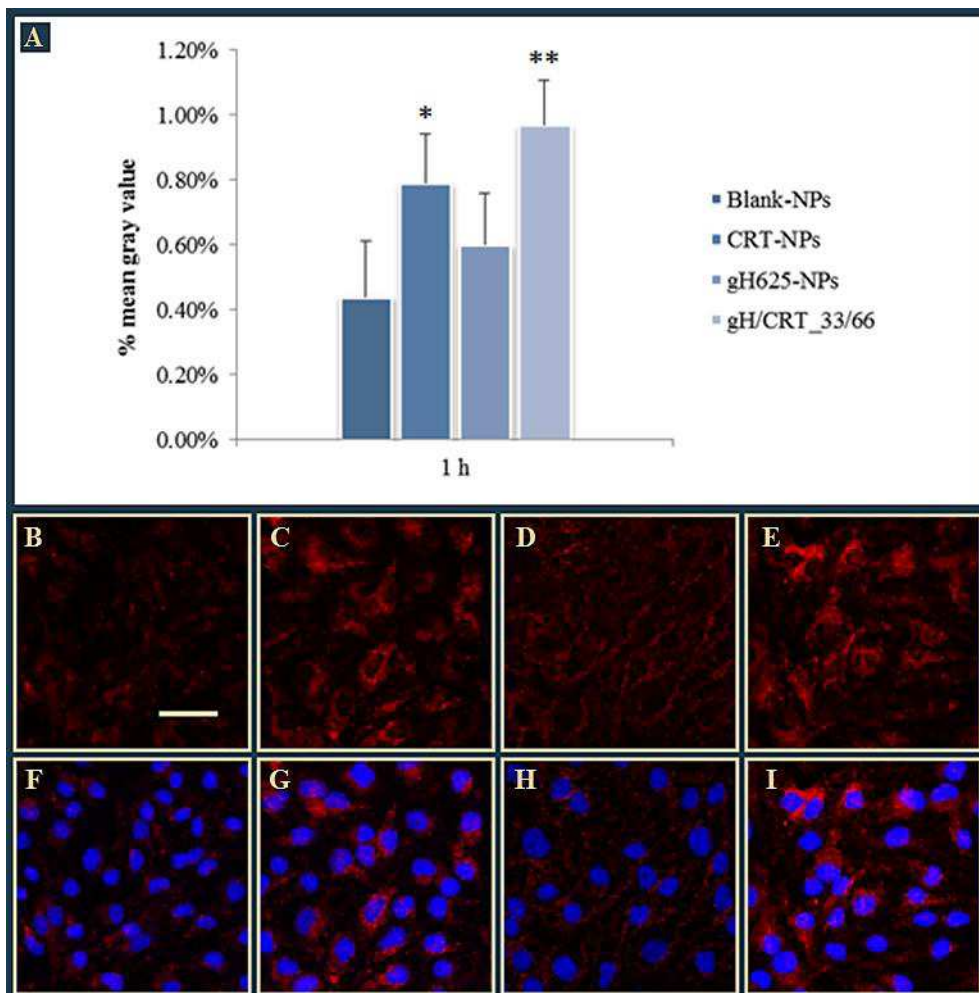
Co-localization studies according with NP transport results, suggest that after the internalization, the complex CRT iron mimicking peptide-Tf-TfR is transported to lysosomes at pH 5-5.5 and then CRT-NP is removed from Tf/TfR complex.

At that point, CRT-NP is transported into the basal compartment separately. On the contrary, the cytoplasmic distribution of gH625-NPs is probably due to the working mechanism of gH625 peptide that promotes lipid membrane-reorganizing processes, through fusion, involving temporary destabilization and subsequent reorganization of the membrane.<sup>23</sup> However, no significant crossing ability was observed when gH625 was exposed on PELGA-NP. Probably, peptide on NP is not able to assume the correct conformation and thus it is able to recognize lipid membrane of cells but does not exert its activity.

#### 4.3.5 Adhesion assay in flow condition

Parallel plate flow chamber Glycotech system is a commercial device that mimics the hydrodynamic conditions at microcirculation level. This assay were performed in order to investigate in what way the surface functionalization could affects the *in vitro* targeting ability of the NPs to a cerebral endothelium under flow conditions. The volumetric flow rate  $Q$  (10  $\mu\text{L}/\text{min}$ ) was fixed to be equal for all the experiments. Based on this and on the other structural parameters ( $w$ ,  $h$ ), we calculated the mean velocity within the chamber ( $U = Q/wh = 0.066$  mm/s), the shear rate ( $S = 6Q/h^2w = 1.55$  s<sup>-1</sup>) and the shear stress at the wall ( $\tau_w = \mu S = 1.86 \times 10^{-3}$  Pa). The mean velocity used for the experiments was comparable with the blood velocity in the human capillary vessel (between 0.01 and 0.1 mm/s)<sup>38</sup> and the shear rate and stress values at the wall were sufficiently small to allow adhesion of nanoparticles to endothelial cells.<sup>39</sup>

Among dual functionalized NP formulations, gH/CRT\_33/66-NPs have the highest of trans-endothelial crossing ability and were chosen to assess whether these NPs could adhere to the BBB also under dynamic conditions. Confocal images for each NP type were acquired and analyzed by imageJ software. Figure 4.8 compares the adhesion ability (Figure 4.8 A) and localization (Figure 4.8 B-I) of blank-NPs, CRT-NPs, gH625-NPs and gH/CRT\_33/66-NPs. Data are reported as the percentage of mean gray value. As shown, CRT-NPs and gH/CRT\_33/66-NPs display the highest targeting ability at 10  $\mu\text{L}/\text{min}$  flow rate (0.79 % and 0.97 %, respectively) compared to blank-NPs (0.44 %). Percentage of mean gray value for gH625-NP was found equal to 0.60 %.



**Figure 4.8.** (A) NP adhesion ability to bEnd.3 under flow condition,  $Q = 10 \mu\text{L}/\text{min}$ .  $P^* = < 0.05$ ;  $P^{**} = < 0.005$ . (B-I) confocal images of NPs in bEnd.3 after the experiments: (B,F) blank-NPs, (C,G) CRT-NPs, (D,H) gH625-NPs and (E,I) gH/CRT\_33/66-NPs. Red: NPs; blue: nuclei. Bar 50  $\mu\text{m}$ .

## 4.4 Conclusions

The aim of this work was to characterize the effect of functionalization of biodegradable nanoparticles with two synthetic peptides in enhancing targeting and transport across the cerebral endothelium. Sub-100nm PELGA NPs were successfully synthesized with three different ratios of CRT and gH625 peptides by using nanoprecipitation method. Results clearly indicate that NPs are internalized by the cells. NPs also show different intracellular localization, strongly guided by peptide functionalization. As a matter of fact, gH625 lead the NPs to a more cytoplasmic distribution while CRT peptide induces lysosomal accumulation. Similar behavior is shown also for blank NPs. NPs transport results in Transwell system demonstrated that the permeability of the cerebral endothelium to gH/CRT\_33/66 and CRT-NPs is about 2.5 and 1.5 times higher than blank NPs, respectively. Further investigations about NPs targeting ability in flow condition were performed using Glycotech system assays. The experiments were carried out using a flow rate of 10  $\mu$ L/min in order to simulate the blood velocity in human capillaries. Data reported as the percentage of mean gray value indicates that gH/CRT\_33/66 formulation has the highest targeting ability to the BBB under flow conditions. More precisely, the percentage of gH/CRT\_33/66 and CRT-NPs is about 2.2 and 1.8 times higher than blank NPs, respectively. No significant adhesion ability was found for gH625-NPs and this can be ascribed to the lacks of specificity to the BBB of gH625. Taken all together, these findings demonstrated a cooperative effect of gH625 and CRT peptides when exposed on dual functionalized NPs in percentage 33/66, respectively. Probably peptides in gH/CRT\_33/66-NPs formulation are able to assume the correct conformation and to exert their activity, promoting NP transport across the BBB in a synergic manner. The new nanocarrier, made up of FDA-approved materials, could be regarded as a promising strategy for administration of therapeutical compounds to the brain.

## 4.5 References

1. De Boer, A.; Gaillard, P., Drug targeting to the brain. *Annu. Rev. Pharmacol. Toxicol.* **2007**, *47*, 323-355.
2. Kreuter, J., Nanoparticulate systems for brain delivery of drugs. *Advanced drug delivery reviews* **2001**, *47* (1), 65-81.
3. Mc Carthy, D. J.; Malhotra, M.; O'Mahony, A. M.; Cryan, J. F.; O'Driscoll, C. M., Nanoparticles and the blood-brain barrier: advancing from in-vitro models towards therapeutic significance. *Pharmaceutical research* **2015**, *32* (4), 1161-1185.
4. van Rooy, I.; Mastrobattista, E.; Storm, G.; Hennink, W. E.; Schiffelers, R. M., Comparison of five different targeting ligands to enhance accumulation of liposomes into the brain. *Journal of controlled release* **2011**, *150* (1), 30-36.
5. Lajoie, J. M.; Shusta, E. V., Targeting receptor-mediated transport for delivery of biologics across the blood-brain barrier. *Annual review of pharmacology and toxicology* **2015**, *55*, 613-631.
6. Van Rooy, I.; Cakir-Tascioglu, S.; Couraud, P.-O.; Romero, I. A.; Weksler, B.; Storm, G.; Hennink, W. E.; Schiffelers, R. M.; Mastrobattista, E., Identification of peptide ligands for targeting to the blood-brain barrier. *Pharmaceutical research* **2010**, *27* (4), 673-682.
7. Jones, A. R.; Shusta, E. V., Blood-brain barrier transport of therapeutics via receptor-mediation. *Pharmaceutical research* **2007**, *24* (9), 1759-1771.
8. Wong, H. L.; Wu, X. Y.; Bendayan, R., Nanotechnological advances for the delivery of CNS therapeutics. *Advanced drug delivery reviews* **2012**, *64* (7), 686-700.
9. Huile, G.; Shuaiqi, P.; Zhi, Y.; Shijie, C.; Chen, C.; Xinguo, J.; Shun, S.; Zhiqing, P.; Yu, H., A cascade targeting strategy for brain neuroglial cells employing nanoparticles modified with angiopep-2 peptide and EGFP-EGF1 protein. *Biomaterials* **2011**, *32* (33), 8669-8675.
10. Staquicini, F. I.; Ozawa, M. G.; Moya, C. A.; Driessen, W. H.; Barbu, E. M.; Nishimori, H.; Soghomonyan, S.; Flores 2nd, L. G.; Liang, X.; Paolillo, V., Systemic combinatorial peptide selection yields a non-canonical iron-mimicry mechanism for targeting tumors in a mouse model of human glioblastoma. *The Journal of clinical investigation* **2011**, *121* (1), 161.
11. Ponka, P.; Lok, C. N., The transferrin receptor: role in health and disease. *The international journal of biochemistry & cell biology* **1999**, *31* (10), 1111-1137.
12. Moos, T.; Morgan, E. H., Transferrin and transferrin receptor function in brain barrier systems. *Cellular and molecular neurobiology* **2000**, *20* (1), 77-95.
13. Sade, H.; Baumgartner, C.; Hugenmatter, A.; Moessner, E.; Freskgård, P.-O.; Niewoehner, J., A human blood-brain barrier transcytosis assay reveals antibody transcytosis influenced by pH-dependent receptor binding. *PloS one* **2014**, *9* (4), e96340.
14. Nathanson, D.; Mischel, P. S., Charting the course across the blood-brain barrier. *The Journal of clinical investigation* **2011**, *121* (1), 31.



15. Zheng, C.; Ma, C.; Bai, E.; Yang, K.; Xu, R., Transferrin and cell-penetrating peptide dual-functioned liposome for targeted drug delivery to glioma. *International journal of clinical and experimental medicine* **2015**, *8* (2), 1658.
16. Salvati, E.; Re, F.; Sesana, S.; Cambianica, I.; Sancini, G.; Masserini, M.; Gregori, M., Liposomes functionalized to overcome the blood–brain barrier and to target amyloid- $\beta$  peptide: the chemical design affects the permeability across an in vitro model. *International journal of nanomedicine* **2013**, *8*, 1749.
17. Bao, G.; Mitragotri, S.; Tong, S., Multifunctional nanoparticles for drug delivery and molecular imaging. *Annual review of biomedical engineering* **2013**, *15*, 253-282.
18. Brancato, V.; Gioiella, F.; Profeta, M.; Imparato, G.; Guarnieri, D.; Urciuolo, F.; **Melone, P.**; Netti, P. A., 3D tumor microtissues as an in vitro testing platform for microenvironmentally-triggered drug delivery systems. *Acta Biomaterialia* **2017**.
19. Biondi, M.; Guarnieri, D.; Yu, H.; Belli, V.; Netti, P. A., Sub-100 nm biodegradable nanoparticles: in vitro release features and toxicity testing in 2D and 3D cell cultures. *Nanotechnology* **2013**, *24* (4), 045101.
20. Graf, N.; Bielenberg, D. R.; Kolishetti, N.; Muus, C.; Banyard, J.; Farokhzad, O. C.; Lippard, S. J.,  $\alpha$ V $\beta$ 3 integrin-targeted PLGA-PEG nanoparticles for enhanced anti-tumor efficacy of a Pt (IV) prodrug. *ACS nano* **2012**, *6* (5), 4530-4539.
21. Nance, E.; Zhang, C.; Shih, T.-Y.; Xu, Q.; Schuster, B. S.; Hanes, J., Brain-penetrating nanoparticles improve paclitaxel efficacy in malignant glioma following local administration. *ACS nano* **2014**, *8* (10), 10655-10664.
22. Cantisani, M.; Guarnieri, D.; Biondi, M.; Belli, V.; Profeta, M.; Raiola, L.; Netti, P. A., Biocompatible nanoparticles sensing the matrix metallo-proteinase 2 for the on-demand release of anticancer drugs in 3D tumor spheroids. *Colloids and Surfaces B: Biointerfaces* **2015**, *135*, 707-716.
23. Galdiero, S.; Falanga, A.; Vitiello, M.; D'Isanto, M.; Cantisani, M.; Kampanaraki, A.; Benedetti, E.; Browne, H.; Galdiero, M., Peptides containing membrane-interacting motifs inhibit herpes simplex virus type 1 infectivity. *Peptides* **2008**, *29* (9), 1461-1471.
24. Galdiero, S.; Vitiello, M.; Falanga, A.; Cantisani, M.; Incoronato, N.; Galdiero, M., Intracellular delivery: exploiting viral membranotropic peptides. *Current drug metabolism* **2012**, *13* (1), 93-104.
25. Guarnieri, D.; Falanga, A.; Muscetti, O.; Tarallo, R.; Fusco, S.; Galdiero, M.; Galdiero, S.; Netti, P. A., Shuttle-Mediated Nanoparticle Delivery to the Blood–Brain Barrier. *Small* **2013**, *9* (6), 853-862.
26. Guarnieri, D.; Muscetti, O.; Falanga, A.; Fusco, S.; Belli, V.; Perillo, E.; Battista, E.; Panzetta, V.; Galdiero, S.; Netti, P., Surface decoration with gH625-membranotropic peptides as a method to escape the endo-lysosomal compartment and reduce nanoparticle toxicity. *Nanotechnology* **2015**, *26* (41), 415101.
27. Falanga, A. P., Effect of peptide functionalization on nanoparticle transport across brain endothelium in a microfluidic chip. **2016**.

28. Lee, S. J.; Han, B. R.; Park, S. Y.; Han, D. K.; Kim, S. C., Sol–gel transition behavior of biodegradable three-arm and four-arm star-shaped PLGA–PEG block copolymer aqueous solution. *Journal of Polymer Science Part A: Polymer Chemistry* **2006**, *44* (2), 888-899.
29. Booth, R.; Kim, H., Characterization of a microfluidic in vitro model of the blood-brain barrier ( $\mu$ BBB). *Lab on a chip* **2012**, *12* (10), 1784-1792.
30. Wehrstedt, K.-D.; Wandrey, P.-A.; Heitkamp, D., Explosive properties of 1-hydroxybenzotriazoles. *Journal of hazardous materials* **2005**, *126* (1), 1-7.
31. Subirós-Funosas, R.; Prohens, R.; Barbas, R.; El-Faham, A.; Albericio, F., Oxyma: An Efficient Additive for Peptide Synthesis to Replace the Benzotriazole-Based HOBt and HOAt with a Lower Risk of Explosion [1]. *Chemistry-a European Journal* **2009**, *15* (37), 9394-9403.
32. Zhang, W.; Smith, S. O., Mechanism of penetration of Antp (43– 58) into membrane bilayers. *Biochemistry* **2005**, *44* (30), 10110-10118.
33. Burdo, J.; Antonetti, D.; Wolpert, E.; Connor, J., Mechanisms and regulation of transferrin and iron transport in a model blood–brain barrier system. *Neuroscience* **2003**, *121* (4), 883-890.
34. Fisher, J.; Devraj, K.; Ingram, J.; Slagle-Webb, B.; Madhankumar, A.; Liu, X.; Klinger, M.; Simpson, I. A.; Connor, J., Ferritin: a novel mechanism for delivery of iron to the brain and other organs. *American Journal of Physiology-Cell Physiology* **2007**, *293* (2), C641-C649.
35. McCarthy, R. C.; Kosman, D. J., Ferroportin and exocytosomal ferroxidase activity are required for brain microvascular endothelial cell iron efflux. *Journal of Biological Chemistry* **2013**, *288* (24), 17932-17940.
36. Dautry-Varsat, A.; Ciechanover, A.; Lodish, H. F., pH and the recycling of transferrin during receptor-mediated endocytosis. *Proceedings of the National Academy of Sciences* **1983**, *80* (8), 2258-2262.
37. Roberts, R. L.; Fine, R. E.; Sandra, A., Receptor-mediated endocytosis of transferrin at the blood-brain barrier. *Journal of Cell Science* **1993**, *104* (2), 521-532.
38. Ganong, W. F., Dynamics of blood and lymph flow. *Review of medical physiology* **2005**, *22*.
39. Decuzzi, P.; Ferrari, M., The role of specific and non-specific interactions in receptor-mediated endocytosis of nanoparticles. *Biomaterials* **2007**, *28* (18), 2915-2922.

## Chapter 5

### Conclusions and future prospective

The work described in this thesis intends to exploit the remarkable properties and applications of gH625 cell-penetrating peptide.

Up to now, cell-penetrating peptides have been widely used in improving cellular translocation of covalently or electrostatic attached cargoes. Based on the scientific reports in the literature, it seems that the CPPs are finally starting to catch up with the alternative non-viral systems, as more efficient and comprehensive applications are described.

It has become increasingly clear that CPPs translocate the cell membrane through different mechanism, which depends on the CPP itself but, in principal, on the cargo physico-chemical nature. More important is that endosomal entrapment represents the major bottleneck in many cellular delivery methodologies, including CPP-mediated delivery. Despite many studies, mechanisms responsible for the extravasation and for the cellular trafficking of these CPP–drug conjugates or complexes are still poorly understood. Overcome these limitations will obviously help in engineering of new CPP generations with a superior potential to target various tissues and to deliver their payload within the appropriate cellular compartment.

For this purpose, our study was definitely pointed in those directions, exploring new targeting and delivery applications of gH625 CPP and evaluating its behavior as

engineering transport agent. In more details, in **Chapter 1** an introduction to the topic is given. In **Chapter 2**, it is shown how CPP functionalization and reverse transfection approach leads to a highly efficient vector transport for intracellular delivery of nucleic acids. Results demonstrate that the PEI/gH625 construct successfully achieve an increase of the transfection efficiency of non-viral polymeric carriers. Furthermore, we were able to reduce their own cytotoxicity and mediate an efficient gene transfer with respect to un-functionalized vectors. Despite of the unsuccessful covalent approach, we effectively developed a facile and clear method for the building up of modified PEI vector and functionalized glass substrate.

In **Chapter 3**, we analyze the behavior in cell culture of gH625 functionalized PtNPs of different size (2.5, 5 and 20 nm). The presence of the CPP significantly increased the amount of internalized NPs in human cervix epithelioid carcinoma cells, as a function of particle size. However, scanning transmission electron microscopy (STEM) and electron tomography (ET) revealed a predominant confinement of PtNPs within vesicular structures, regardless of particle size and surface functionalization. Only in the case of the smallest 2.5 nm particles, the membranotropic peptide was able to partly maintain its functionality, enabling cytosolic delivery of a small fraction of internalized PtNPs. Single-particle transport across the cell membrane is strongly hampered by particle agglomeration in culture medium. Interestingly, membrane crossing seemed to occur by diffusion through the lipid bilayer, with no apparent membrane damage. For larger particle sizes ( $\geq 5$  nm), their hindrance likely blocked the membranotropic mechanism. Combining the enhanced uptake and partial cytosolic delivery promoted by gH625, we were able to achieve a strong improvement of the antioxidant nanozyme function of 2.5 nm PtNPs, decreasing both the endogenous ROS level and its overproduction following an external oxidative insult.

So far, it has been shown that various types of cargo have been effectively transported through biological barriers, providing most diverse ways of interfering with the cellular biochemical processes. Nevertheless, it is a challenge to target the delivery only to specific cells, tissues or organs. Fusions of various approaches allow combining both active and passive targeting and achieve potentially higher selectivity and efficacy. As a matter of fact, in **Chapter 4**, gH625 was conjugated to PLGA-PEG NPs together with CRT peptide, which functionally mimics the endogenous iron and promotes the BBB

crossing through recognition of the transferrin receptors of the cerebral endothelium. Co-localization studies, adhesion and permeation assays across *in vitro* brain endothelial model under static and dynamic conditions have been investigated. Results establish that the cooperative effect of CRT and gH625 on NPs changes the distribution of NP in the cell, avoiding nanoparticle accumulation inside lysosomal compartments and support the translocation across the blood-brain barrier.

To sum up, in this thesis is shown the key role of the gH625 membranotropic peptide in the construction of novel materials, increasing their capability in the overcome of biological barrier. In this way it was possible to prepare functionalized polyplexes, platinum and PLGA NPs, with less cytotoxic effects and higher transfection, antioxidant and brain targeting and delivery performance, respectively. Overall, this work shows the high potential of gH625-based delivery agents for nanomedicine, providing optimism for a wide range of further therapeutic applications.